AD-750 734

SELECTED MATERIAL FROM SOVIET TECHNICAL LITERATURE, MAY 1972

Stuart G. Hibben

Informatics, Incorporated

Prepared for:

Air Force Office of Scientific Research

7 July 1972

informatics inc

Approved for public release;
distribution unlimited.

Approved for public release;
distribution unlimited.

Approved for public release;
distribution unlimited.

UNCLASSIFIED

Security Classification

DOCUMENT CONTROL DATA - R & D

(Security classification of title, body of abstract and indexing annotation must be entered when the overall report is classified)

1 ORIGINATING ACTIVITY (Corporate author)
Informatics Inc.
6000 Executive Blvd.
Rockville, Md. 20852

2a. REPORT SECURITY CLASSIFICATION
UNCLASSIFIED

2b. GROUP

3 REPORT TITLE
Selected Material from Soviet Technical Literature, May, 1972

4 DESCRIPTIVE NOTES (Type of report and inclusive dates)
Scientific . . . Interim

5 AUTHOR(S) (First name, middle initial, last name)
Stuart G. Hibben

6 REPORT DATE
July 7, 1972

7a. TOTAL NO. OF PAGES
158

7b. NO. OF REFS

8a. CONTRACT OR GRANT NO
F44620-72-C-0053

b. PROJECT NO
AO 1622-3

c.
62701D

d.

9a. ORIGINATOR'S REPORT NUMBER(S)

9b. OTHER REPORT NO(S) (Any other numbers that may be assigned this report)
AFOSR - TR - 72 - 1964

10 DISTRIBUTION STATEMENT
Approved for public release; distribution unlimited.

11 SUPPLEMENTARY NOTES
Tech. Other

12. SPONSORING MILITARY ACTIVITY
Air Force Office of Scientific Research
1400 Wilson Boulevard (NPC)
Arlington, Virginia 22209

13 ABSTRACT

This report includes abstracts and bibliographic lists on major contractual subjects that were completed in May, 1972. The major topics are: laser technology, effects of strong explosions, geosciences, and particle beams. A report on biocybernetic studies, selected as the optional topic for May, will be issued under separate cover. The abstracted material includes some selections prior to 1972 that have not otherwise been reported.

To avoid duplication in reporting, only laser entries concerning high-power effects have been included, since all current laser material will appear routinely in the quarterly bibliographies. . .

An index identifying source abbreviations and an author index to the abstracts are appended.

DD FORM 1 NOV 68 1473

UNCLASSIFIED

Security Classification

SELECTED MATERIAL FROM SOVIET TECHNICAL LITERATURE

May 1972

Sponsored by
Advanced Research Projects Agency

ARPA Order No. 1622-3

July 7, 1972

ARPA Order No. 1622-3
Program Code No: 62701D2F10
Name of Contractor:
Informatics Inc.
Effective Date of Contract:
January 3, 1972
Contract Expiration Date:
December 31, 1972
Amount of Contract: $250,000

Contract No. F44620-72-C-0053
Principal Investigator:
Stuart G. Hibben
Tel: (301) 779-2850 or
(301) 770-3000
Short Title of Work:
"Soviet Technical Selections"

This research was supported by the Advanced Research Projects Agency of the Department of Defense and was monitored by the Air Force Office of Scientific Research under Contract No. F44620-72-0053. The publication of this report does not constitute approval by any government organization or Informatics Inc. of the inferences, findings, and conclusions contained herein. It is published solely for the exchange and stimulation of ideas.

informatics inc
Systems and Services Company
6000 Executive Boulevard
Rockville, Maryland 20852
(301) 770-3000 Telex: 89-521

ib

INTRODUCTION

This report includes abstracts and bibliographic lists on major contractual subjects that were completed in May, 1972. The major topics are: laser technology, effects of strong explosions, geosciences, and particle beams. A report on biocybernetic studies, selected as the optional topic for May, will be issued under separate cover. The abstracted material includes some selections prior to 1972 that have not otherwise been reported.

To avoid duplication in reporting, only laser entries concerning high-power effects have been included, since all current laser material will appear routinely in the quarterly bibliographies.

An index identifying source abbreviations and an author index to the abstracts are appended.

TABLE OF CONTENTS

1. Laser Technology

A. Abstracts

Ashmarin, I. I., Yu. A. Bykovskiy, V. A. Gridin, V. F. Yelesin, A. I. Larkin, and I. P. Sipaylo. Shock waves generated by the action of laser radiation on transparent bodies. IN: Sbornik. Kvantovaya elektronika. Moskva, Izd-vo Sovetskoye radio, no. 6, 1971, 126-128.

A set of experiments is described on interaction of powerful laser radiation with type K-8 glass, with the object of determining the criteria for shock wave generation at the focal point. A Q-switched ruby was used generating 50 Mw pulses, focused to a 0.2 mm spot both internally and on the glass surface. A holographic plus high-speed framing method was used to determine wave propagation velocity. Results confirmed that the transition from a longitudinal sonic wave to a shock wave generally occurred near the damage threshold. Wave velocity was observed to be a function of pulse intensity, as well as of delay time in pulse application, as seen in Fig. 1. In theory the sonic wave converts to a shock wave when

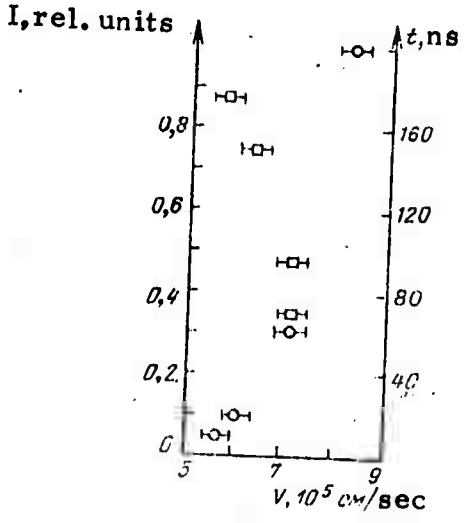

Fig. 1. Wave velocity vs. delay (squares) and laser pulse intensity (circles).

pressure p in the focal region attains a value of $\rho_o C_o^2$, where ρ_o is glass density and C_o is the sonic velocity in the glass. A sample calculation based

on actual parameters was made on this assumption, showing that shock wave velocity should be 1.3 times sonic; this agreed closely with measured results. With the beam focused on the surface a dual spherical wave was typically generated, as shown in Fig. 2. Their characteristics were essentially the same as for the internally focused pulse.

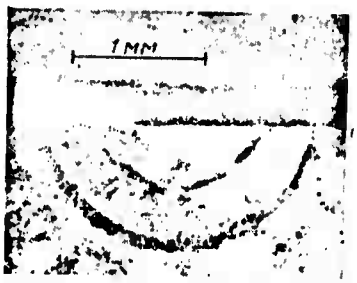

Fig. 2. Dual wave generation from surface irradiation.

Cherkun, Yu. P., and I. N. Konopel'ko.
Current status of experimental and theoretical studies in the field of combined heat exchange.
I-FZh, v. 22, no. 4, 1972, 757-758.

A brief summary is given of several papers on the subject of radiation - induced heat exchange, presented at a session of a general conference on mass and heat transfer held on Sept. 15-17, 1971 at the Thermophysics Institute, Siberian Branch AN SSSR. The general theme of the session was phenomena related to combination heat transfer mechanisms, namely radiative - conductive and radiative - convective.

S. S. Kutateladze and D. I. Avaliani reported on experimental findings of laser beam attenuation in liquid media with pulsating turbulence; this work was judged important from a heat transfer viewpoint as well as in regard to beam propagation in a turbulent medium. A related paper by V. M. Kostylev and V. Ya. Belostotskaya dealt with the relation between conductive and radiative heat transfer in optically thin layers of finely-dispersed media; they show that in this case it is incorrect to use the hypothesis of additive fluxes.

A report by N. A. Rubtsova and A. E. Berte covered the thermal state of pure metal surfaces exposed to a constant thermal flux. Results showed anomalies in surface temperature distribution (the Jacques

effect) on metals including Al, Fe, Sn and others; several possible models for this phenomenon are advanced.

V. M. Yeroshenko discussed variants of ablation techniques in which blowoff of dispersed media is used as a protection against radiative flux; this refers to processes at levels of 100 atm and temperatures in the 20,000°C range. Several papers by other authors dealt with heat exchange studies in various types of combustion reactions.

Special mention is given to a paper by A. I. Leont'yev and A. M. Pavlyuchenko which is cited as giving the most complete picture to date on temperature distribution in a turbulent boundary layer and laminar sublayer in a thermal radiation field. As with Kostylev et al, these authors also demonstrate the fallacy of the additive-flux hypothesis under their test conditions.

In closing, S. Kutateladze stressed the need for further experimental data on radiative heat exchange resulting from interaction of e-m waves with materials.

Epshteyn, E. M. Thermal instability of a semiconductor in a laser beam. IVUZ Radiofiz, no. 1, 1972, 33-37.

A theoretical study is presented on a possible mechanism of laser-induced destruction of a semiconductor. The case is limited to photon energies less than the width of the forbidden zone, so that the main exchange mechanism is absorption by free carriers. In the general case a cumulative heating and increase in free carriers will occur, resulting in a stationary temperature field. However, above some laser threshold level the stationary field breaks down and a rapid thermal reaction sets in which is analogous to breakdown in a d-c field, or the thermal explosion from an exothermic chemical reaction. To examine the governing phenomena the author assumes the simplest case of a cylindrical semiconductor target, axially excited by a uniform-intensity laser beam such that $\lambda \ll \rho \ll R$, where λ is laser wavelength, and ρ and R are beam and cylinder radii. Expressions are derived for the limit conditions of the stationary field solution, and the corresponding threshold power of the laser is determined. Finally, it is shown that the elapsed time required to reach threshold under practical conditions will lie in the 1 millisec - 1 sec range - i.e. demanding in effect a c-w laser regime. Therefore the described mechanism cannot account for breakdown observed, for example, in transparent dielectrics under nanosecond pulse exposure.

Frolov, V. V. Temperature fields in multi-layer translucent coatings under conditions of pulsed radiation heating. I-FZh, v. 22, no. 4, 1972, 755-756. (Annotation of deposited paper.)

A summary is given of an analysis of heat transfer in a multi-layer coating system under beamed irradiation. The problem is treated as nonstationary and one-dimensional, with distribution of absorption taken into account. Reflection and concentrated absorption at layer interfaces are treated; the absorption process is considered to be linear.

As an example the temperature distribution is calculated in a two-layer heat shield in which the heat load is assumed to be applied in triangular pulses of a given energy, at durations ranging from 10 to 60 seconds. Owing to changing boundary conditions, it is shown that the system must be solved as a class of piecewise-discontinuous functions. On this basis graphical solutions are obtained showing the time characteristic of heat absorption as a function of absorption coefficient and pulse duration. Instantaneous temperature distributions are also presented for the cases of absolutely opaque as well as semitransparent coating systems.

The analysis shows that failure to account properly for internal heat absorption can lead to significant errors in theoretical temperature fields and level of total absorption; furthermore, the error increases with reduction in pulse width.

Bessarab, Ya. Ya., Yu. B. Tkach, V. P. Zeydlits, N. P. Gadetskiy, and V. V. Dyatlova. Study of collective processes in a plasma using light of stimulated emission. ZhETF, v. 62, no. 2, 1972, 569-572.

The use of coherent light emission to study the collective processes in a plasma-beam discharge is described. It is shown that an effective method of studying these processes is the direct observation of the form of oscillation in the intensity of spontaneous-emission spectral lines, with a subsequent application of Fourier analysis. Study of the oscillation spectrum was performed through investigation of the fluctuation intensity of coherent emission in the Ar II transitions $4p^2D^0_{5/2} \rightarrow 4s^2P_{3/2}$ at a wavelength of 4880 Å, and $4p^4D^0_{5/2} \rightarrow 4s^2P_{3/2}$ at a wavelength of 5145 Å. The maximum frequency excited in the plasma, which depends upon modulation of the

emission intensity, is determined by the relationship $\omega_{max}\tau \lesssim 1$ where τ is the lifetime at the upper level of the observed transition. In this study $\omega_{max} \approx 100\text{-}120$ MHz. In the case of coherent emission, the spectrum of the oscillation being investigated has a lower limit given by

$$\omega_{min} \approx \frac{2\epsilon_0 E^2 c(1-R)}{(N_1-N_2)\hbar\omega_{12}d},$$

where ϵ_0 is the dielectric permeability of the active medium, E is the field intensity of the light wave in the resonator, c is the speed of light, R is the reflection coefficient of the resonator mirrors, d is the distance between mirrors, $\hbar$ is Planck's constant, ω_{12} is the frequency of the observed transition and N_1 and N_2 the corresponding population densities of the upper and lower laser levels, respectively. Fig. 1 compares obtained spectra of coherent and spontaneous emission.

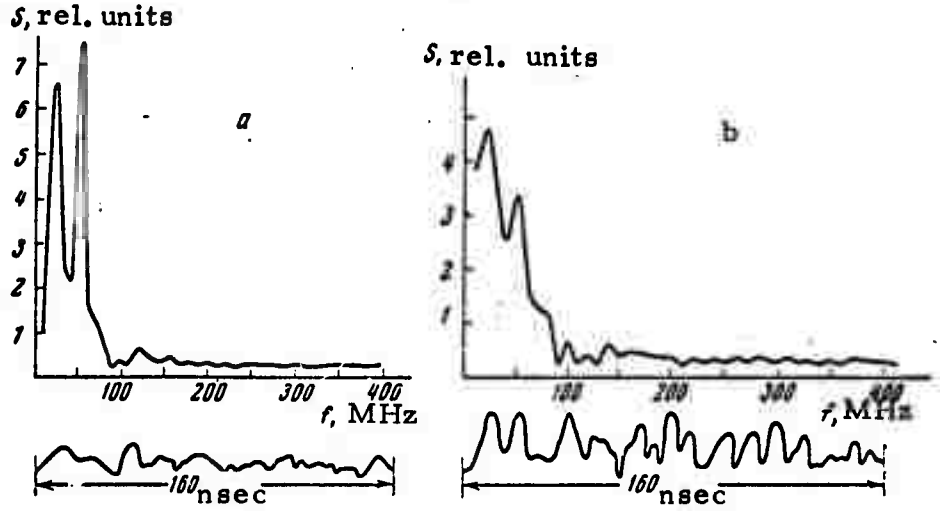

Fig. 1. Realization and type of spectrum obtained. a - by modu ation of coherent emission, b - by modulation of spontaneous emission.

Sultanov, M. A. Destruction of transparent dielectrics under the action of free-running neodymium and ruby lasers. Mekhanika polimerov, no. 2, 1972, 359-360.

The author notes that a variety of theories exist on the basic destruction mechanism of laser interaction with transparent solids; among these are thermal explosion, acoustic phonons from stimulated Brillouin scattering, and photolysis of the target material. Experiments are described which were designed to clarify the predominant mechanism of laser damage in several dielectrics, including polymethyl-methacrylate, polystyrene and several types of glass. Both ruby and neodymium crystal lasers were used, in free-running regimes at energies of 3 to 15 j. Characteristic platelets of cracks at angles up to 90° from the beam axis were observed for both laser types; however in the Nd target specimens the damage area was more extended along the beam axis, whereas the ruby damage was localized near the beam focus. (Repeated reference is made to damage photos, which are unfortunately omitted from the text.)

The test results lead Sultanov to the following concept of the damage process. On focusing a sufficiently powerful beam in the transparent dielectric, a local region is heated to a liquid state in which further energy is absorbed by inhomogeneities, and crack propagation begins. A plasma is generated which expands at high velocity; thus the effect is that of a powerful, instantaneous point explosion. The process is a hydrodynamic one, including shock wave generation which causes further destruction both before and behind the beam focal point. Examples of remote damage regimes in PMMA specimens are cited in added support of the theoretical model.

B. Recent Selections

i. Beam-Target Effects

Agarbiceanu, I. I., I. A. Teodorescu, and M. I. Birjega. Effect of light on stabilization time for thin metal films. Stud. si cerc. fiz., v. 23, no. 9, 1971, 1005-1014 (RZhF, 4/72, #4Ye1624)

Anan'in, O. B., Yu. A. Bykovskiy, A. N. Petrovskiy, and I. S. Rez. Destruction of nonlinear KDP and $LiNbO_3$ crystals by radiation from a ruby laser. ZhTF, no. 4, 1972, 837-840.

Andreyev, S. I., I. V. Verzhikovskiy, Yu. I. Dymshits, V. V. Kulikov, and V. G. Neverov. Determining the formation time for a hole in a metallic film under the action of single-pulsed laser radiation. ZhTF, no. 4, 1972, 893-895.

Bedilov, M. R., K. Khaydarov, and Kh. Babadzhanova. Nature of radiation defects formed on the surface of solids by ruby laser radiation. IAN UzbSSR, ser. fiz-mat. nauk, no. 2, 1972, 66-68.

Belyanskiy, G. G., M. K. Bologa, A. Z. Volynets, and E. Ya. Zafrin. Factors governing the initial stage of sublimation in an shf field. IAN MoldSSR, Ser. fiz-tekh. i mat. nauk, no. 1, 1972, 68-72.

Kaliski, S. Surface wave effect in the wave equation. Biul. WAT J. Dabrowskiego, v. 20, no. 11, 1971, 3-8. (RZhMekh, 4/72, #4V115)

Kostylev, V. M., and N. V. Komarovskaya. Energy transfer in a medium of low optical density. I-FZh, v. 22, no. 5, 1972, 907-912.

Kuznetsov, A. Ye., A. A. Orlov, and P. I. Ulyakov. Pulsed regime for vaporizing optical materials by CO_2 laser radiation. IN: Sbornik. Kvantovaya elektronika. Moskva, Izd-vo Sovetskoye radio, no. 7, 1972, 57-60.

Mezokh, Z. I., L. I. Ivanov, and V. A. Yanushkevich. Change in electrical properties of n-Ge from the effect of a Q-switched pulsed laser at 77°K. IN: Sbornik. Nekotoryye voprosy diffuzii rastvorennykh veshchestv v porakh sorbentov. Krasnodar, 1971, 102-109. (RZhF, 4/72, #4Ye1249)

Osadin, B. A., and G. I. Shapovalov. Pulsed vaporization in a vacuum. TVT, no. 2, 1972, 361-367.

Sultanov, M. A. Destruction of transparent dielectrics under the action of free-running neodymium and ruby lasers. Mekhanika polimerov, no. 2, 1972, 359-360.

Trubyankov, Yu. I., V. B. Bakhmendo, V. A. Krol', and Ye. Z. Diner. Optico-mechanical method for studying changes in molecular structure of polymers under external excitation. Mekhanika polimerov, no. 2, 1972, 209-213.

Zubchaninova, V. N. Temperature fields and stress generated in an elastic half-space as the result of a periodically changing flux of radiant energy. IN: Trudy Kalininskogo politekhnicheskogo instituta. No. 9, 1971, 120-131. (RZhMekh, 3/72, #3V119)

Zubchaninova, V. N. Dynamic temperature stresses generated in a half-space under the action of a radiant flux with pulsed intensity changes. IN: Trudy Kalininskogo politekhnicheskogo instituta. No. 9, 1971, 131-140. (RZhMekh, 3/72, #3V120)

ii. Beam-Plasma Interaction

Arutyunyan, V. M., and G. K. Avetisyan. Reflection and trapping of a charged particle by an e-m wave within the medium. IN: Sbornik. Kvantovaya elektronika. Moskva, Izd-vo Sovetskoye radio, no. 7, 1972, 54-56.

Bunkin, F. V., P. P. Pashinin, and A. M. Prokhorov. A possibility of using infrared lasers for high temperature heating of a superdense plasma. ZhETF P, v. 15, no. 9, 1972, 556-559.

Grechko, L. G., N. Ya. Kotsarenko, and A. M. Fedorchenko. Electromagnetic wave fluctuations in a plasma layer. UFZh, no. 11, 1971, 1771-1776.

Kaliski, S. Description by average value of the phenomenon of cumulation laser heating of D-T plasma for a cylindrical wave. Proc. Vibrat. Probl. Pol. Acad. Sci., v. 12, no. 3, 1971, 231-242. (RZhF, 4/72, #4G262)

Kaliski, S. Heating of plasma by laser radiation, allowing for removal of fusion energy in the case of a spherical thermal wave. II. Biul. WAT J. Dabrowskiego, v. 20, no. 10, 1971, 13-16. (RZhF, 4/72, #4G257)

Kantorovich, I. I. Frequency dependence of optical breakdown in gases. ZhPS, v. 16, no. 4, 1972, 605-610.

Kovpik, O. F., Ye. A. Kornilov, S. M. Krivoruchko, S. S. Moyseyev, and Ya. B. Faynberg. Effect of oscillation type on heating the ions in beam-plasma discharges. ZhETF P, v. 15, no. 9, 1972, 501-504.

Makhlin, A. N., and G. V. Skrotskiy. Behavioral characteristics of intense optical beams in a nonideal gas. IN: Sbornik. Kvantovaya elektronika. Moskva, Izd-vo Sovetskoye radio. No. 7, 1972, 56-57.

Petrun'kin, V. Yu., L. N. Pakhomov, and P. A. Andreyev. Control oscillator for high-voltage nanosecond pulses triggered by laser radiation. PTE, no. 2, 1972, 178-180.

Petrzilka, V. A., and J. Preinhaelter. Propagation and reflection of an electromagnetic wave in a hot inhomogeneous plasma. Czechoslovak Journal of Physics, B21, no. 10, 1971, 1064-1070. (RZhF, 4/72, #4Zh95)

Pyatnitskiy, L. N., G. P. Khaustovich, and V. V. Korobkin. Device for plasma diagnostics by an optical scattering method. Authors' Certificate, USSR, no. 293497, published Dec. 10, 1971. (RZhF, 4/72, #4G275P)

Tarasov, Ye. A. Probing the pre-cathode region of a mercury plasma by laser radiation. IN: Trudy Moskovskogo energeticheskogo instituta, no. 94, 1971, 90-95. (RZhF, 4/72, #4G115)

Zayko, Yu. N., L. I. Kats, N. N. Kireyev, and S. A. Smolyanskiy. Electromagnetic wave propagation in a rarefied plasma located in a variable magnetic field. TVT, no. 2, 1972, 232-242.

2. Effects of Strong Explosions

A. Abstracts

Aslanov, S. K. and I. P. Kopeyka. Generalization of triple discontinuity configurations. IN: Sb. Matematika i mekhanika tezisy dokladov 4-y Kazakhstan mezh.-vuz. nauch. konf. po mat i mekh. Ch. 2. Alma-Ata, 1971, 171-173.

A theoretical generalization of triple discontinuity configurations was undertaken to aid in calculating spin detonation. The generalization consists of introducing into the shock system an additional self-similar rarefaction wave following a Chapman-Jouguet self-sustaining detonation. Three possible variants of the generalization are analyzed. Representing different contact angles between the reflected wave and the incident flow, the variants are extended to the case when the Mach wave is a self-sustaining detonation front and the reflected front is a supercompressed detonation. The calculated pressure values near the triple point agree well with data from experimental oscilloscope traces.

Balakin, V. B. and V. V. Bulanov. A numerical solution of the problem of interaction of a shock wave with a cylindrical body in supersonic flow. PMTF, v. 32, no. 6, 1971, 1033-1039.

A two-dimensional finite difference scheme of the second order accuracy is introduced to compute the process of collision of a nonstationary shock wave with a stationary flow around the nose-end of a cylinder moving at a supersonic speed. The initial set of equations of two-dimensional flow in divergent form is presented in vector notation

$$\frac{\partial f}{\partial t} + \frac{\partial}{\partial x} F(f) + \frac{\partial}{\partial y} G(f) + \frac{\nu}{y} H(f) = 0 \qquad (1)$$

and allowance is made for through computation of shock waves. Eq. (1) is

then approximated in two steps by a finite difference equation which contains artificial viscosity terms in the x and y directions measured along and from the flow axis, respectively. The necessary and sufficient stability criteria of the finite difference scheme

$$\left(\frac{\Delta t}{\Delta x} A\right)^2 \leqslant \frac{1}{2} E, \quad \left(\frac{\Delta t}{\Delta y} B\right)^2 \leqslant \frac{1}{2} E \tag{2}$$

were established by a Fourier method. A = dF/df and B = dG/df in (2) are Jacobians of the F and G vectors in a random point of the flow, Δ x and Δ y are the difference grid pitches along x and y, Δ t is the time pitch, and E is the matrix unit. By use of a through computation method, a common numerical solution is outlined for two corollary problems: the initial supersonic streamline flow around the body, and the oncoming shock wave with establishment of a new regime of supersonic streamline flow. The initial flow parameters are those of the first shock wave. The parameters of the second shock wave are calculated by means of Hugoniot formulas. Numerical solutions of the problem are illustrated graphically.

Limarev, A. Ye. and A. D. Chernyshov. Propagation of shock waves in a reinforced elasto-plastic medium. PMM, no. 6, 1971, 1083-1088.

Propagation and structure of shock waves in a translationally-reinforced elasto-plastic medium is described by the closed set of discontinuity equations

$$[\sigma_{ij}^*] - 2\mu_1 [e_{ij}^*] = 2[\varphi]\{2\mu_1\mu_2 e_{ij}^{*+} - 2\mu_0 \sigma_{ij}^{*+} - \mu_1\mu_2 [e_{ij}^*] + \mu_0 [\sigma_{ij}^*]\} + \ldots \tag{1}$$

$$[\sigma_{kk}] = (3\lambda_1 + 2\mu_1)[e_{kk}] \tag{2}$$

$$\left[\sigma_{ij}^* - \frac{\mu_1\mu_2}{\mu_0} e_{ij}^*\right]\left\{2\left(\sigma_{ij}^* - \frac{\mu_1\mu_2}{\mu_0} e_{ij}^*\right)^+ - \left[\sigma_{ij}^* - \frac{\mu_1\mu_2}{\mu_0} e_{ij}^*\right]\right\} = 0 \tag{3}$$

and

$$[\sigma_{ij}]\nu_j = -\rho^+ G[v_i], \quad [u_{i,j}] = \omega_i \nu_j, \quad [v_i] = -G\omega_i \tag{4}$$

where σ_{ij}, σ_{kk} are stress components, e_{ij} are strain components, λ_1, μ_0, μ_1, μ_2 are elastic coefficients, ν_j is normal to discontinuity surface, G is the propagation velocity of a nonremovable discontinuity surface in a continuous medium, U_i, V_i are the displacement and velocity of a particle, and the asterisk denotes a tensor deviator component. Equations 1-4 were derived assuming a linear dependence between two discontinuous functions within the shock wave transition layer. This linear approximation made possible a common solution to the problems of propagation and structure of shock waves in a plastic noncompressible material.

Using (1) and (4), an expression is derived for the characteristic of irreversible plastic deformation of a continuous medium

$$2[\varphi] = F_1\omega_n(\mu_0\omega_n F_2 - \mu_1 S_{nn}^{p+})^{-1}$$

$$[F_1 = \rho^+G^2 - \lambda_1 - 2\mu_1,\ F_2 = \rho^+G^2 - \lambda_1 - {}^2/_3\mu_1(1 + \mu_2/\mu_0)$$

where S_{nn}^{p+} is the stress component of a plastic element p of the rheological model of the material, the index n and the sign + indicate direction of the normal ν_i and the value ρ ahead of the shock wavefront, respectively. The velocity ρ^+G^2 of discontinuity surface propagation is determined by the roots of the equation of the 4th degree in ρ^+G^2, which was derived from the equations 1-5. The root $\rho^+G^2 = \mu_1$ of the cited equation corresponds to a transverse neutral wave without discontinuity of plastic deformation and satisfies the condition $[\varphi] = 0$. This particular case is illustrated by an example of a rectangular elasto-plastic plate subjected to either a tensile or a shear stress. Two other roots of the 4th degree equation indicated the possibility of generating two plastic shock waves in a three-dimensional reinforced elasto-plastic medium. One of the plastic waves propagates in a medium under spherically symmetric stress, the other in a medium where $S_3^{p*+} = 0$.

Pogorelov, V. I. The impact of an incalculable supersonic jet on a plane. IFZh, v. 21, no. 5, 1971, 941-942.

Shock wave separation occurs in front of a plane positioned normally to the nozzle axis when an incalculable supersonic jet impinges on the plane. The separated wave is convex toward the plane and interacts with the hanging shock of the jet if the nozzle-to-plane spacing is such that the

separated wave interferes with the expansion of a free jet. A flow measurement equation is established for gas flow ahead of and behind the separated shock wave with allowance for a relationship in the shock wave and on assumption that the density and the velocity component parallel to the plane are constant behind the separated wave. This flow equation is used to derive a differential equation which defines the geometry of the generatrix of the separated wave. The boundary condition of this equation is the derivative of the shock wave equation for a triple configuration of shock waves. The coordinate of the triple configuration is determined by a simple algebraic correlation using the numerical value of the derivative. Gasdynamic parameters of subsonic flow behind the shock wave can be also determined, if the relative position versus the plane and the shape of the shock wave are known. The calculated coordinates of the triple point and geometry of the separated shock wave were found to be in good agreement with experimental data obtained from flow shadow photographs.

Kozachenko, L. S. and B. D. Khristoforov. Parameters of a shock wave from explosion at the bottom of a water vessel. FGiV, no. 1, 1971, 127-135.

Measurements are described of the relative pressure profile p/p_1 (τ), duration τ, and specific impulse I of an explosive shock wave in water vessels with three different bottom types. The measurements were prompted by the inadequacy of known formulas, which describe a wave field in water without allowance for significant nonlinear effects. The shock waves were generated by the underwater detonation of a spherical explosive charge. The shock wave parameters were measured with a minimum $\pm$ 10% accuracy by pressure sensors. Data were recorded by PID-9 devices with a 2 Hz - 300 kHz range. The effect of the free surface was eliminated under the experimental conditions. Three series of experiments were carried out in separate vessels with air-water-saturated sand (I), polystyrene (II), or concrete bottoms (III). The three bottom types differed from each other by the nature of their interaction with a shock wave in water. This interaction is defined by the relationship of sound velocity a in water to the velocities C_1 of longitudinal and C_2 of transverse waves in the ground. The inequalities $C_2 < C_1 < a$, $C_1 > a > C_2$, and $C_1 > C_2 > a$ characterize the I, II, and III bottom types. Depth charges of 100 kg cast TNT, 1g compacted TEN, and 0.2 kg compacted TNT were detonated in 3, 1, and 0.5 m deep basins with I, II, and III

bottoms, respectively, at relative distances H = 1-11, 1-12, and 1-4 charge radii from the bottom. The pressure sensors were located at a depth h and at relative distances R = 30-120 for vessel I and 60-120 for vessel III from the blast center, and on the periphery of a hemisphere of 0.45 m radius for vessel II with the center at a point below the charge.

Typical oscilloscope traces of shock waves in water (Fig. 1 and 2) and the experimental $\tau(h)$ and $\tau(\alpha)$ plots (Fig. 3 and 4) are shown. The

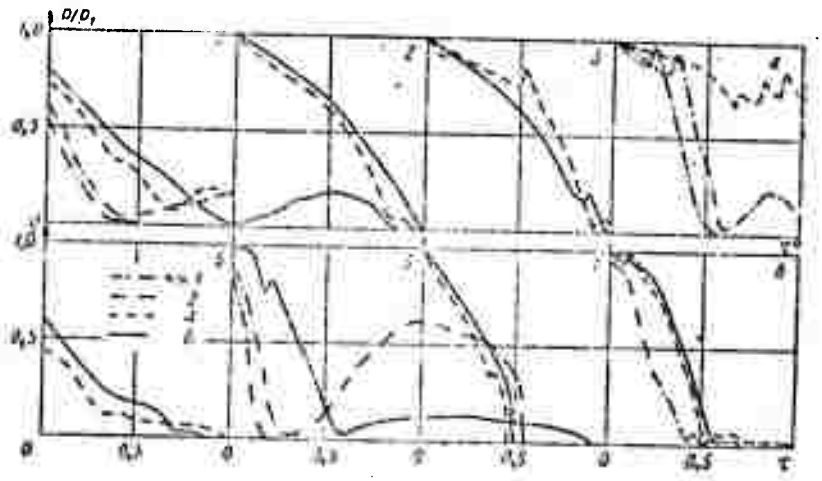

Fig. 1. Relative pressure p/p_1 versus reduced duration τ (μsec/m) of explosive shock waves in a water basin with a sand bottom.

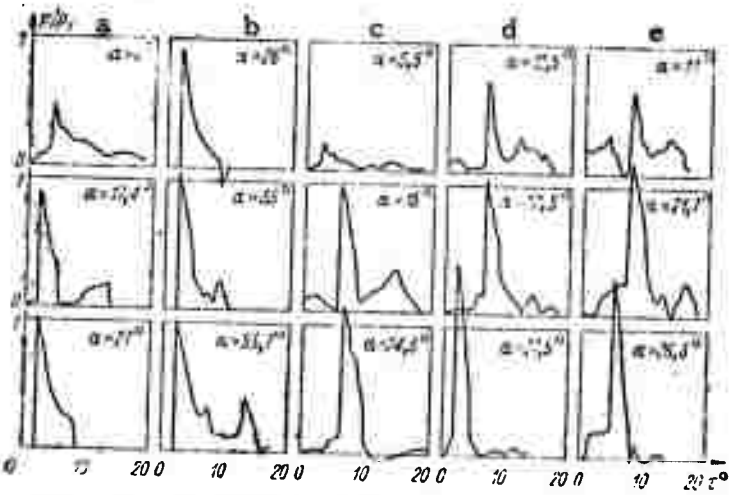

Fig. 2. Relative pressure p/p_1 versus reduced duration τ (msec/m) of explosive shock waves near the polystyrene bottom.

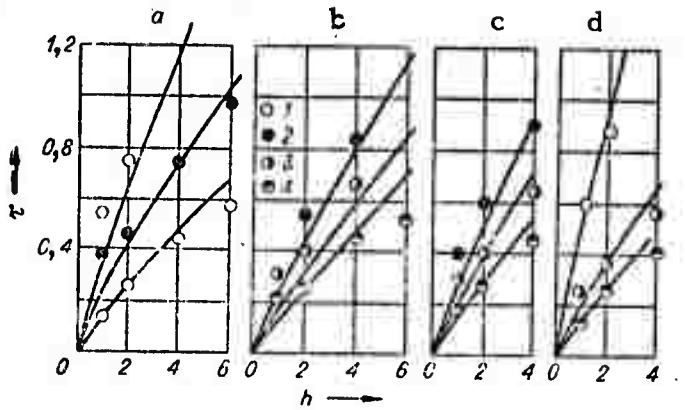

Fig. 3. Duration τ (msec/m) of shock wave versus distance h from the pickup to the sand bottom.

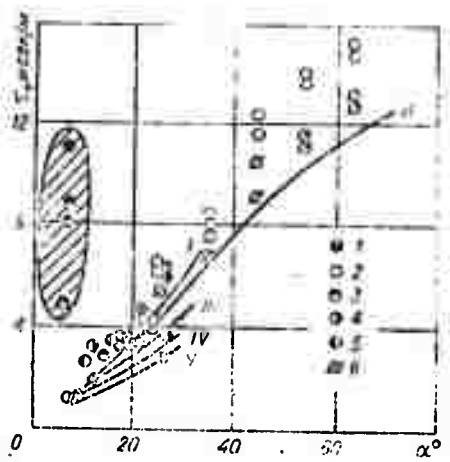

Fig. 4. Reduced duration τ (msec/m) of a shock wave versus angle α for an explosion at a polystyrene bottom.

nearly parabolic shape of the p(τ) curves (Fig. 1) suggests a nonlinear interaction with rarefaction waves propagating from the bottom. The latter decrease the frontal pressure, as shown by the plots of p(h). In the case of the I type bottom, p_{max} of the reflected compression wave, which is observed only at large angles of incidence α of the forward wave to the bottom, attains 30% of p in the leading shock wave. A bottom wave behind and a leading shock wave ahead of the forward wavefront were observed in the case of the II type bottom (Fig. 2). The leading wave is generated only at an angle $\alpha \approx \alpha_0$, which is determined by the intersection of two wavefronts. The p_{max} may exceed by 40% the explosion pressure in an infinite liquid volume due to the

superposition of the leading and forward wave pressures (Fig. 2, d, e). The p_{max} near $\alpha = \alpha_0 \approx 20\text{-}30^\circ$ increases sharply because of the interaction between the forward and leading waves, as shown on the $p(\alpha)$ plot. Interaction of the forward wave with the bottom-reflected rarefaction wave manifests itself in a decrease of τ with a decrease in α (Fig. 4). The shaded area in Fig. 4 d signates the near-bottom zone, where total τ of the wave field is much longer than τ of the forward wave.

Tabulated experimental data (Table 1) show that the parameters

h	$\left(\frac{p}{p_1}\right)_e$	$\left(\frac{p}{p_1}\right)_p$	τ_e, мсек/м	τ_p, мсек/м	$\left(\frac{p}{p_1}\right)_e$	$\left(\frac{p}{p_1}\right)_p$
	$R=90$, $H=4$				$R=90$, $H=3$	
0	0,28	0,45	0,384	0	0,38	0,40
1	0,23	0,64	0,344	0,123	0,70	0,55
2	0,78	0,75	0,376	0,25	0,78	0,64
3	0,73	0,78	0,376	0,37	0,99	0,72
	$R=60$, $H=1$				$R=120$, $H=1$	
0	0,39	0,31	3,5	0	0,33	0,30
4	0,52	0,58	2,1	0,49	0,41	0,51
8	0,57	0,71	0,93	0,87	0,46	0,62

Table 1. Parameters p/p_1 and τ of explosive shock wave in a water basin with concrete bottom. Footnote: The indexes e and p indicate the experimental data and the data calculated from the formulas given in the text, respectively.

of the forward wave for the III type bottom are greatly influenced by the bottom-reflected rarefaction wave. The p_{max} of the forward wave decreases, when the sensor is positioned closer to the bottom, and approaches the p_{max} value calculated using an empirical formula. However, the experimental τ disagrees with the τ calculated from an empirical formula, because of the effect of a strong bottom wave.

The experimental data show that, at great distances from the blast center, the effect on shock wave parameters in water of all three bottom types is analogous to that of a free surface. The empirical formulas proposed can be used to calculate shock wave parameters. The actual τ of the shock wave measured near the bottom is usually longer than the calculated τ, because of bottom wave interference. Pressure in the lateral and leading waves is generally not over 20-30% of that in the forward wave. The maximum pressure

near the intersection of the leading and forward waves is 30-40% higher than the explosion pressure measured in an infinite liquid volume. This paper is an extension of a similar work by the authors reported in Effects of Strong Explosions, no. 2, p. 111.

Dmitriyevskiy, V. A., V. I. Fedulov, and V. F. Nikolayeva. Study of the properties of SF_6 and UF_6 in a shock tube. ZhETF, v. 61, no. 4, 1971, 1427-1433.

Tests are described whose object was to study thermodynamic properties of selected gases under shock heating. The test gases were SF_6 and UF_6, since multiatomic molecules of this type could be expected to exhibit some anon .lous behavior during relaxation. An electrically discharged diaphragm-type shock tube was used, with He as the driver gas. Trace CO_2 and other heavy gases were added on occasion to reduce the velocity of the wave front. One anomaly observed was a drop in thermal capacity of the tested gases with increase in temperature. Results show that both SF_6 and UF_6 have at least two discrete vibrational relaxation modes under the cited test conditions.

Poluboyarinov, A. K. Propagation of a shock front reflected by a blunt body. MZhiG, no. 2, 1971, 70-77.

Shock wave front interaction with a blunt sphere or cylinder is analyzed on the assumption that the front plane is normal to the symmetry axis or plane of the body and, in the case of the cylinder, is parallel to the body generatrix. An exact differential equation is derived to describe nonstationary separation of the symmetry center of the shock reflected by a static body. The equation describes dimensionless axial shock separation ϵ as a function of the independent variable M of the reflected front. The equation also contains two additional unknown quantities: the derivative $(\partial v/\partial x)_1$ of gas velocity immediately behind the shock, and the radius r of the reflected shock front curvature along the symmetry axis. An exact formula was derived for initial $(\partial v/\partial x)_{1*}$ as a function of r_* and M_*. Approximate

formulas define r_* and $(dr/d\tau)_*$ in the initial separation phase of the front from the body. A fairly simple approximate method is introduced to determine nonstationary ϵ for a sphere, on the basis of the derived formulas and the precise equation of ϵ. The method consists of integrating the equation $d\epsilon/dM = \varphi$, where φ is a function of r and $(\partial v/\partial x)_1$. A numerical example shows that the method correctly describes the initial separation phase, and also its final phase if a correction to the φ function is introduced.

Yeliseyev, Yu. B. and A. Ya. Cherkez. The effect of an increase in stagnation temperature in a streamline gas flow past a deep cavity. MZhiG, no. 3, 1971, 8-18.

An earlier observed anomalous increase in temperature of the separated gas flow within a cavity above the stagnation value T_o is discussed, on the basis of a theoretical model of compression and decompression waves in a cylindrical tube. Piston oscillatory movements at the open end of the tube model simulate conditions at the streamline flow-separated gas interface. Characteristics of the nonstationary self-oscillating shock wave process at the interface are formulated and a numerical example is given. A preliminary conclusion was drawn that the observed phenomenon is reproducible with models of different dimensions but is influenced by increased boundary layer thickness. Aerodynamic experiments with different models at $M < 1$ and $M = 1.6$ and 2.0 are described. In agreement with theoretical calculations, the stationary air temperature at the base of a model increased by a minimum of $100^{\circ}K$ above T_o. The experimental data confirmed the hypothesis that the shock wave thermal effect and heat release follow energy dissipation in shock waves. The intensity of the observed effect depends greatly on the shape of the leading edge and the angle formed by the model exit section plane with the axis. The experiments suggest the possibility of reproducing the effects in the surface cavity of an object flying in the atmosphere. Methods for minimizing the undesirable thermal effect are given.

Pustovalov, V. K. Self-similar gas motion behind a shock wave front sustained by radiation. DAN BelSSR, v. 15, no. 12, 1971, 1079-1081.

Adiabatic expansion of a cold perfect gas in vacuum, initiated by a strong shock wave, is analyzed with allowance for radiant energy q supplied to ($q > 0$) or withdrawn from ($q < 0$) the expanding gas. Shock wave propagation through the gas is sustained by radiation which determines the motion pattern of the shock front. The radiation flux density is defined by $q = q_0 t^{\ell}$, where ℓ is an integer. This is a self-similar gasdynamic problem of the first kind, since there are two independent dimensional parameters q_0 and ρ_0. The problem is described by the set of equations

$$\begin{aligned}
&\frac{d\rho_1}{d\xi}(v_1-\xi)+\rho_1\frac{dv_1}{d\xi}=0,\\
&\frac{k}{\alpha}v_1+\frac{dv_1}{d\xi}(v_1-\xi)+\frac{1}{\rho_1}\frac{dp_1}{d\xi}=0,\\
&\frac{m}{\alpha}p_1+\frac{dp_1}{d\xi}(v_1-\xi)-\gamma\frac{p_1}{\rho_1}\frac{d\rho_1}{d\xi}(v_1-\xi)=0
\end{aligned} \qquad (1)$$

where ρ_1, p_1, v_1 are the unknown dimensionless density, pressure, and velocity of the gas, ξ is a self-similar variable, γ is the adiabatic exponent, $\alpha = 1 + \ell/3$ is the self-similarity index, $k = \ell/3$, and $m = 2\ell/3$. The boundary conditions at the shock front and on the vacuum side complete the formulation of the problem.

Solution of (1) with the boundary conditions is given as follows:

$$\begin{aligned}
p_1&=A_1\left(-\frac{1}{2(2-\gamma)}+\frac{\gamma-1}{2-\gamma}\xi\right)^{\frac{\gamma-2}{\gamma-1}},\\
\rho_1&=B\left(-\frac{1}{2(2-\gamma)}+\frac{\gamma-1}{2-\gamma}\xi\right)^{-\frac{1}{\gamma-1}},\\
v_1&=\frac{1}{2-\gamma}\left(-\frac{1}{2}+\xi\right),\\
A_1&=\frac{1}{4-2\gamma}\left(\frac{2\gamma-3}{4-2\gamma}\right)^{\frac{2-\gamma}{\gamma-1}},\quad B=-\left(\frac{2\gamma-3}{4-2\gamma}\right)^{\frac{2-\gamma}{\gamma-1}},
\end{aligned} \qquad (2)$$

$$a = \frac{7 - 5\gamma}{8(2-\gamma)^2(\gamma-1)} \qquad (3)$$

where a is one of the dimensionless constants which define the boundary condition at the shock front. Solution (2) for a = 0 and $\gamma = 7/5$ describes shock wave propagation in the absence of radiation (q = 0). Solution (2) for $a > 0$, i.e., $q > 0$, describes propagation of a shock wave with radiant energy absorption. A numerical solution of (1) with boundary conditions for $a < 0$, i.e., $q < 0$, describes propagation of a shock wave front with self-radiation.

Dremin, A. N., K. K. Shvedov, and V. S. Klapovskiy. Effect of charge shape on detonation parameters of PZhV-20 ammonite. IN: Detonatsiya vzryvchatykh veshchestv i bezopasnost' vzryvnykh rabot. Moskva, Izd-vo Nedra, 1967, 129-135.

This work presents some experimental materials concerning the study of the detonation parameters of spherical, cylindrical and flat charges. The experiments were performed with charges of various diameters and thicknesses. The explosive used was PZhV-20 ammonite, with a density of 1.0 g/cm^3 in all experiments. The experimental data showed that with identical characteristic dimensions of the charge, the shortest wavelength and sharpest drop was observed in spherical charges. The time and wavelength in flat charges is approximately 30% greater than in cylindrical charges. Thus, a flat charge with a thickness equal to the diameter of a cylindrical charge or with equal weight will be more effective from the point of view of generation of shock waves of higher intensity and longer duration in the surrounding medium.

Afanasenkov, A. N., I. M. Voskoboynikov, and A. Ya. Apin. Transmission of detonation through an air gap. IN: Detonatsiya vzryvchatykh veshchestv i bezopasnost' vzryvnykh rabot. Moskva. Izd-vo Nedra, 1967, 101-110.

The purpose of this work was to produce a simple criterion for explosive sensitivity and to study the possible mechanism of transmission

of detonation through an air gap on the basis of available data. Experiments were performed using passive charges 20 mm in diameter and 70 mm long of hexogene of various densities, and active charges of hexogene and TG 50/50 of various weights and shapes. The experiments determined the significance of explosion products and the air shock wave, and produced a quantitative characteristic of the sensitivity of explosives to detonation transmission through an air gap. The dependence of the distance of transmission of detonation on explosive charge density was explained.

Khristoforov, B. D. Small-scale electromagnet for explosion investigations. PTE, no. 1, 1972, 251.

An electromagnet has been built for laboratory measurements of the mass and wave velocities of shock and detonation waves. The field of intensity across a 200 x 200 x 200 mm^3 gap is ~400 Oe; in addition there is a permanent magnetic field which extends over a 50 x 50 x 40 mm^3 region near the gap center. The 70 mm diameter magnetic circuit is made of 900 x 900 mm^2 Armco iron. The corners of the device are strengthened by welding and special straps to increase resistance to explosive loads. Dimensions of the magnet gap and the permanent magnetic field are controlled by specially designed pole shoes made of a 200 mm dia type St. 3 steel. The field intensity across the gap can be increased in inverse ratio to the end-area of a tapered attachment to the pole shoe. Two paralleled magnetic coils, each composed of 2000 turns of 1.8 mm copper wire, are used for superposed magnetization. The 24 volt current supply is supplied by a VSA6 rectifier. The magnetic circuit is installed in a channel welded from channel bars; the channel itself is welded to a table made of angle steel to increase the rigidity of the assembly. Over the past three years, the electromagnet has withstood several hundred detonations of explosive charges up to 0.5 kg without substantial damage. A photograph of the electromagnet assembly is included.

Simonov, I. V. Diffraction of a strong shock wave on a weakly-defined wedge. ZhPMTF, no. 6, 1971, 107-114.

A theoretical study is presented on diffraction of a strong two-dimensional steady shock wave on a wedge whose properties (initial density, behavior under impact load) differ only slightly from those

of the medium in which the shock wave propagates. A linear approximation of diffraction - initiated small perturbations, disregarding differences in strength and sound velocity c in the medium and wedge, is justified under conditions of high pressure ($\sim 10^6$ atm) and temperature behind the strong shock wavefront. The validity of the approximation is supported by the fact that the effect of strength characteristics diminishes with increased shock wave intensity. In this approximation, the unknown perturbation velocity components u' and w' and perturbation pressure p' satisfy the ordinary linear equations for the two-dimensional flow of an ideal compressible fluid. The equations are given in the form

$$Dp = \frac{\partial u}{\partial x} + \frac{\partial w}{\partial y},\ Du = \frac{\partial p}{\partial x},\ Dw = \frac{\partial p}{\partial y}\quad \left(D = x\frac{\partial}{\partial x} + y\frac{\partial}{\partial y}\right) \tag{1}$$

where u, w, and p are dimensionless variables. Conditions in the perturbation region of the shock wavefront are described by

$$p = A\,(f - yf'),\ u = Bp,\ w = -Mf' \text{ at } x = k \tag{2}$$

in the medium, and

$$\begin{gathered} p = A\,(f - yf') + A_1,\ u = Bp + B_1,\ w = -Mf' \text{ at } x = k \\ A = \frac{2\varkappa M}{1-j},\ A_1 = kM\frac{(2\varkappa - 1)\,v' - \varkappa v_0}{(1-j)(1-\varkappa)},\ B = \frac{1+j}{2k} \\ B_1 = M\frac{v' - \varkappa v_0}{2(1-\varkappa)}\quad \left(\varkappa = \frac{V_0}{V},\ M = \frac{U_0}{c},\ k = \frac{D_0 - U_0}{c},\ j = \frac{k^2c^2j_0}{V_0}\right) \end{gathered} \tag{3}$$

in the wedge. Vo and Uo in (3) are specific volume and mass velocity, respectively, behind the shock wavefront, and V is the specific volume of the medium ahead of the front. The problem was reduced to determining the function p(x, y), which is continuous along the discontinuity boundary line. Two possible diffraction wave configurations are examined. At wedge angles $\alpha_1,\ \alpha_2 < \alpha_*$, the limit angle, a triple configuration (Fig. 1) forms near the

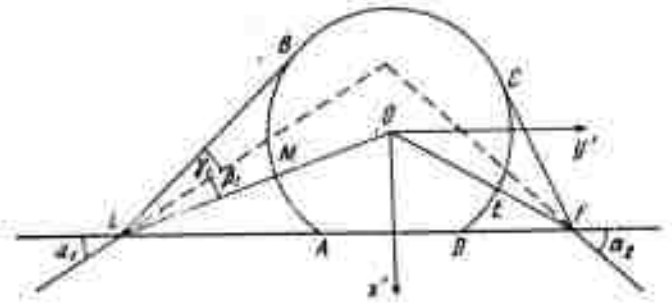

Fig. 1. Diffraction pattern at $\alpha_1,\ \alpha_2 < \alpha_*$.

intersections L and F of the shock wave with the edges of a wedge. The nonstationary perturbation from the shifted wedge center O propagates within the region bounded by the ABCD arc of the Mach circle, the attached reflected acoustic wavefronts, and the AD portion of the shock wave. At $\alpha_{1,2} > \alpha_*$, there is an irregular refraction near L and F and only one region of nonstationary flow, which includes the shock wave sections outside the wedge (Fig. 2).

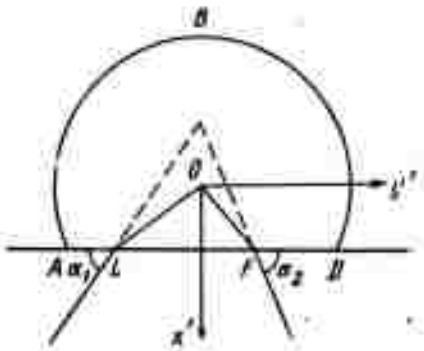

Fig. 2. Diffraction pattern at $\alpha_1, \alpha_2 > \alpha_*$.

The α_* value in the system of x'y' coordinates is determined by

$$\alpha_* = \arcsin\left(k_0 / \sqrt{k_1^2 + k_0^2}\right) \qquad (k_1 = \sqrt{1 - k^2}) \tag{4}$$

where $k_0 = D_0/C_0$, D_0 = shock wave velocity.

In any case, the problem of determining p(x, y) is transferred into the plane $Z = x_1 + iy_1$ (Fig. 3) and the lune is represented conformally

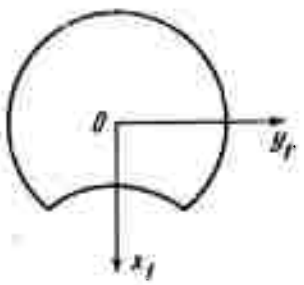

Fig. 3. Region of nonstationary flow in the Z complex plane.

on the upper half-plane ζ by means of the transform

$$\zeta = \xi + i\eta = \frac{i}{k_1}\frac{2z - k(1+z^2)}{z^2-1} \tag{5}$$

The analytical function $F^+(\zeta)$ of ζ half-plane satisfies the condition

$$a\frac{\partial p}{\partial \eta} + b\frac{\partial p}{\partial \xi} = d \tag{6}$$

where

$$\begin{gathered}
a = \xi\sqrt{1-\xi^2}, \quad b = B\xi^2 - B_2 \qquad (|\xi|<1) \\
a = 0, \quad b = B - B_2 \qquad (|\xi|>1) \\
d = (B-B_2)(p_1\delta(\xi-\xi_1) - p_2\delta(\xi-\xi_2)) \qquad (\alpha_{1,2}<\alpha_*) \\
d = (B_1\xi^2 + A_1B_2)(\delta(\xi-\xi_3) - \delta(\xi-\xi_4)) \qquad (\alpha_{1,2}>\alpha_*) \\
\xi_1 = \xi_B = k_1^{-1}(\operatorname{cosec}\theta_1 - k\operatorname{ctg}\theta_1), \quad \xi_2 = \xi_C = k_1^{-1}(\operatorname{cosec}\theta_2 - k\operatorname{ctg}\theta_2) \\
\xi_3 = \xi_L = -\varkappa^{-1}\operatorname{ctg}\alpha_1, \quad \xi_4 = \xi_F = \varkappa^{-1}\operatorname{ctg}\alpha_2
\end{gathered} \tag{7}$$

and

$\delta(\Theta)$ is a Dirac function.

The formulas (6) and (7) represent the inhomogeneous Hilbert problem with continuous parameters. The problem is solved by determining the function having a zero point not lower than second order at infinity. The solution must satisfy the condition

$$0 < k^2(1-j) < \varkappa k_1^2(1+j) \tag{8}$$

which is equivalent to the condition of stability of a two-dimensional stationary shock wave in a homogeneous medium. The boundary $\Phi^+(\xi)$ of the analytical function

$$\Phi^+(\zeta) = \frac{1}{B\zeta^2 - B_2 + i\zeta\sqrt{1-\zeta^2}} \tag{9}$$

satisfies the condition (8), since it does not exhibit singularities in the upper half-plane. The function $F^+(\zeta)/\Phi^+(\zeta)$ must be regular at infinity. It follows that

$$F^+(\zeta) = \Phi^+(\zeta)[\Psi^+(\zeta) + C_0] \tag{10}$$

where

$$\psi^+(\zeta) = \begin{cases} \frac{1}{\pi}\left(\frac{p_1}{\Phi^+(\xi_1)(\xi_1-\zeta)} - \frac{p_2}{\Phi^+(\xi_2)(\xi_2-\zeta)}\right), & \alpha_{1,2}<\alpha_* \\ \frac{1}{\pi}\left(\frac{B_1\xi_4^2 + A_1B_2}{\xi_4-\zeta} - \frac{B_1\xi_3^2 + A_1B_2}{\xi_3-\zeta}\right), & \alpha_{1,2}>\alpha_* \end{cases} \tag{11}$$

The constant C_o in (10) is determined from the condition of smooth conjugation of the wavefront.

Pressure is determined from

$$p(\xi, \eta) = \mathrm{Im} \int_{-1}^{\xi} \left(\frac{\partial p}{\partial \eta} + i \frac{\partial p}{\partial \xi} \right) d\zeta + p_A \qquad (12)$$

where $p_A = p_1$ for $\alpha_{1,2} < \alpha_*$ and $p_A = 0$ for $\alpha_{1,2} > \alpha_*$.

Pressure, as well as f', u, and w, exhibit a logarithmic singularity in L and F. A formula is also derived for p distribution p(y) along the curved section AD of the shock wave. The functions u and w are determined from (1) and expressed in terms of p in a closed system of equations.

It is noted that the results obtained may contribute to the development of a theory of irregular refraction.

Salamandra, G. D. and N. M. Ventsel'. Measurement of gas velocity with the use of the contact discontinuity surface. ZhTF, no. 11, 1971, 2463-2465.

A method is described for gas velocity measurements behind a detonation wave front. The contact discontinuity surface formed in the gas is used as the point of reference for gas motion; the contact discontinuity surface is assumed to be formed by the interaction between shock and detonation waves. The surface is visualized by the Toepler technique. For several experiments, the numerical value of gas velocity measured 16% lower than the theoretical value. Shock tube experiments show that the contact discontinuity surface can give a reasonably accurate value of shock wave velocity, and can furthermore serve as a reference for evaluating other velocity measurement references, e.g. the heat inhomogeneity technique.

Zaydel', R. M. Shock wave passage through a curved boundary interface between two media. MZhiG, no. 1, 1972, 111-121.

Shock wave interaction with a slightly curved boundary surface and shock wave-induced surface motion are analyzed in an x-y coordinate system. The shock wave theoretically propagates with velocity D_o through a light medium ($X > 0$) toward the boundary surface $X = 0$ and interacts with it during the time $\tau = 2\ a_o/D_o$ (Fig. 1). During the interval τ, the A point

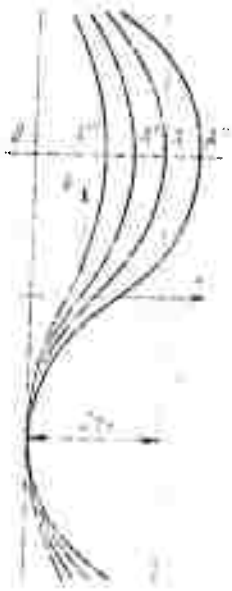

Fig. 1. Shock wave interaction with the free-stream interface X = 0 between two media.

shifts to A' and the points between A and A' are distributed at a time τ along the boundary

$$a = a_0 \exp(ikY) \qquad (1)$$

where $ka_o \leq 1$ is a small perturbation. The free-stream boundary is set in motion after τ at a velocity U relative to an uncompressed heavy medium ($X < 0$). V_1 and V_2 are the relative velocities of the reflected and transmitted shock waves. A set of gas dynamic equations with boundary and initial

conditions is formulated for small perturbations. Introducing polar hyperbolic variables

$$y_s = r_s \operatorname{ch}\theta_s, \quad x_s = r_s \operatorname{sh}\theta_s, \quad r_s = \sqrt{y_s^2 - x_s^2}, \quad \operatorname{th}\theta_s = x_s / y_s \qquad (2)$$

and using a Laplace transform, the author obtains a solution to the equations in the general form

$$w_s''(q_s, \theta_s) = F_s(q_s + \theta_s) + \Phi_s(q_s - \theta_s) \quad (s = 1, 2) \qquad (3)$$

where F and Φ are arbitrary functions, $p_s = \sinh g_s$, s = 1 in the $0 < X < V_1 t$ region, and s = 2 in the $-V_2 t < X < 0$ region. Integration of the original gas dynamic equation in polar hyperbolic coordinates, using (3), gives three finite difference equations which have a unique solution in the form of expansion in an exponential series. In the $\Delta p \to 0$ approximation, where Δp is the shock wave intensity, the solution is

$$\Phi_1(q_1) = -{}^1/_2 v_1^\circ e^{-q_1}, \qquad F_2(q_2) = {}^1/_2 v_2^\circ e^{-q_2} \qquad (4)$$

$$u(t) = k a_0 U \psi(\tau) \qquad (\tau = k c_1 t)$$

$$\psi(\tau) = \frac{1}{2\pi i} \int \Psi(p) e^{p\tau}\, dp = \int_0^\tau \psi_1(x)\, dx + \psi_2(\tau) + \psi_3(\tau) \qquad (5)$$

where

$$\Psi(p) = p^{-1}\Psi_1(p) + \Psi_2(p) + \Psi_3(p)$$

$$\Psi_1(p) = (1 - \mu)\,[\mu / r + 1/R]^{-1}, \quad \Psi_2(p) = (\mu - 1/\alpha)\,[\mu + r/R]^{-1}$$

$$\Psi_3(p) = (1 - \alpha)\,[1 + \mu R / r]^{-1}, \quad r = \sqrt{p^2 + 1}, \quad R = \sqrt{\alpha^2 p^2 + 1} \qquad (6)$$

is the transform of $\Psi_1(p)$, c_1 is the sound velocity in the s = 1 region, $\mu = \rho_1 / \rho_2$, and $\alpha = c_1 / c_2$. Expression (6) is simplified in the cases of $\alpha = 1$ ($c_1 = c_2$), $\rho_1 = \rho_2$ ($\mu = 1$), or the acoustic impedance ρ_1, $c_1 = \rho_2 c_2$ ($\lambda = \alpha\mu = 1$). Integration of (5) gives the asymptotic value

$$\psi(\tau \to \infty) = \text{const} = \frac{1 - \mu}{1 + \mu} = \frac{\rho_2 - \rho_1}{\rho_2 + \rho_1} \qquad (7)$$

i.e. $\Psi(\tau)$ depends on the ρ_1 / ρ_2 ratio only. A generalization of the conclusion led to an equation of motion for the free-stream boundary

$$\frac{d^2 a}{dt^2} = \frac{\rho_2 - \rho_1}{\rho_2 + \rho_1} kga \qquad (8)$$

where the acceleration $g = NU$, and N is the number of incident shock waves, each imparting ΔU acceleration to the boundary interface. This equation is identical to the equation of Rayleigh-Taylor for gravitational instability of noncompressible fluids. It is concluded that the effect of compressibility is insignificant when the wavelength of boundary perturbations is sufficiently small.

Bezhanov, K. A. Diffraction of a shock wave on a wedge moving at supersonic velocity. Prikladnaya matematika i mekhanika, no. 4, 1969, 631-637.

A theoretical study is made of the diffraction of an arbitrarily strong shock wave on the surface of a wedge, moving with supersonic velocity. Using the notations of Fig. 1, the author assumes that the incident angle δ of

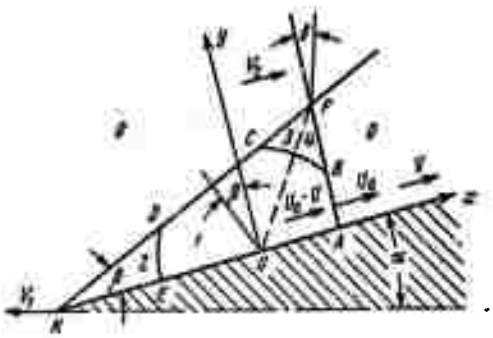

Fig. 1. Flow model.

the shock wave is approximately the same as the wedge angle α. In this notation U_o defines absolute shock wave velocity, while U is its velocity relative to adjacent flow. With the use of some simplifying assumptions the analysis is made with a linearized equation for planar gas flow, using dimensionless parameters. The work is an extension of some cited earlier treatments of a similar problem in which diffraction of the shock wave was assumed not to take place.

Borovoy, V. Ya. and M. V. Ryzhkova. Heat transfer on a semi-conic surface at high hypersonic velocities. MZhiG, no. 4, 1969, 137-142.

Formation of narrow bands of intensive heat transfer on the flat surface near the edges of a streamlined spherically-blunted semi-cone (Fig. 1) was studied experimentally at a Reynolds number Re in the 1.5×10^5 - 2.4×10^6 range. At a sufficiently high Re, the boundary layer separates

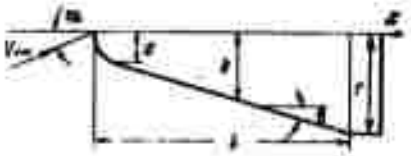

Fig. 1. Spherically blunted semi-cone.

from the flat surface and two separate vortex formations appear near the edges as boundary lines along the surface. Most of the heating occurs along the boundary lines where heat transfer coefficient h^o may be several times higher than h^o on the remaining part of the flat surface. The experiments show that Re is the most important factor in formation of the boundary lines of intensive heat transfer. At $Re = 2.5 \times 10^4 - 10 \times 10^4$, h^o_{max} increases nearly proportionally to Re, while at $Re > 10 \times 10^4$ the rate of h^o_{max} increase is somewhat slower. The strong effect of Re confirmed the assumption that the laminar flow changes to turbulent at the boundary of the separation zone. Boundary layer separation occurs because of an overflow of gas from the conic to the flat surface. This was confirmed by an experiment with a barrier. Experiments with a reduced thickness boundary layer and increased conic surface roughness did not contradict the proposed flow pattern.

Myshenkov, V. I. Subsonic and transonic viscous gas flow in the wake of a two-dimensional body. MZhiG, no. 2, 1970, 73-79.

Viscous gas flow in the wake of a finite thickness plate is analyzed at subsonic and transonic velocities, Prandtl number = 0.71, and Reynolds numbers R in the 1-1,000 range. The problem is formulated by Navier-Stokes equations for given flow parameters at infinity and at a finite distance from the bottom of the plate. Equations of state and motion are solved by approximation of a finite-difference scheme in two steps. A numerical solution which satisfies the condition of a steady flow is presented graphically for different R and M values. The solution shows that at $R \leq 1.7$ gas flows without separation from the bottom, and at $R > 1.7$ a region of reverse flow with separation forms at the stagnation point. The reverse flow region expands with increase in R and the separation point shifts upwards in the

direction of the angular point of the plate. A deformation of the reverse flow region with a decrease in relative velocity of reverse current is observed at R = 100 at increased M (from 0.288 to 1.15). The flow patterns are in agreement with earlier theoretical and experimental data. Pressure variation patterns at the bottom of the plate are also shown in the flow plane and the plane normal to flow.

Stulov, V. P., and L. I. Turchak. Non-equilibrium chemical reactions in a shock layer in a streamline flow of a carbon dioxide -nitrogen-argon mixture around a sphere. MZhiG, no. 5, 1969, 147-150.

A theoretical evaluation of hypersonic (M = 16-20) flow of CO_2-N_2-Ar mixtures around a sphere was made using a known physico-chemical model of a shock-heated gas mixture. The model presumes the existence of nine components in the shock layer, with allowance for five molecular dissociation and five atom exchange reactions which are tabulated. Dissociation rate constants were calculated for collisions with particles of different catalytic activity. The presence of O_2 was disregarded in the establishment of the model, and molecular vibrations at $T \geq 4000^{\circ}K$ were considered to be at equilibrium. It was shown that the flow changes significantly with a change in relative concentrations γ_∞ (CO_2) and γ_∞ (N_2) in the shock layer. Shock wave separation increases by $\sim 50\%$ when γ_∞ (CO_2) is decreased from 0.95 to 0.05, and thermal energy absorbed by the gas simultaneously increases because of a decrease in T and an increase in the fraction of atomic components. The effect of Ar addition is analogous to that of N_2. Most of the heat is absorbed by CO_2 dissociation because of its higher rate.

Shifrin, E. G. Formation of a "hanging" compression shock in the streamline flow past a profile with a broken generator. PMM, no. 6, 1970, 1159-1167.

Uniform supersonic streamline flow past a profile with a convex salient point is analyzed in the case of an oncoming stream with a low supersonic velocity, when entropy changes in the shock wave can be disregarded. The region behind the shock wave is projected on the hodograph

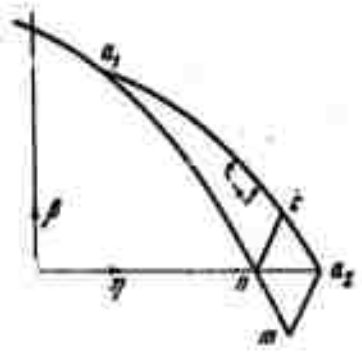

Fig. 1. Projection of the flow behind shock wave on hodograph plane $\eta - \beta$.

plane $\eta - \beta$ (Fig. 1) where $\eta = (k + 1)^{1/3}(\lambda - 1)$, β is the inclination of the velocity vector to the symmetry axis, λ is the velocity factor, and k is the adiabatic exponent. A streamline flow with attached shock wave past a profile formed by straight line intercepts is considered in a first approximation. The equations of the shock polar β and intersecting characteristics, e.g., $a_1 a_2$, are given in a transonic approximation. Proof is offered that a single "hanging" shock is necessarily generated behind the shock wave. The "hanging" shock propagates downstream from its starting or end point which is located at an infinite distance from the profile. The shock at $\beta_0 \leq 0$ is convex in relation to the flow behind it. In addition to the tail shock, there is an internal shock, at $\beta_0 < 0$, which intersects the tail shock and forms a lambda-shaped shock.

Apshteyn, E. Z., L. G. Yefimova, and G. A. Tirsky. Intensive destruction of a vitreous body by [shock] radiation. MZhiG, no. 2, 1971, 131-134.

Destruction of a vitreous body by radiation from a shock layer in hypersonic gas flow is analyzed assuming an optically thin boundary layer at high injection rates and sufficiently intense vaporization. Presence of a liquid film near the stagnation point on the body surface is presumed, to simplify calculations of destruction parameters. Application of an approximation of radiative heat conduction in the body to the liquid film led to a set of transcendental equations which describe ablation, friction, and surface temperature as functions of shock layer parameters. Iterative solution of the

equations is illustrated by diagrams of the destruction rate and gasification Γ of a heat insulating material with thermophysical characteristics of fused quartz under assumed flight conditions. Plots of Γ versus body radius R_B show that Γ decreases with a decrease in R_B due to liquid phase ablation. At great R_B values, coating destruction proceeds by vaporization only. The contribution of liquid phase ablation to the destruction rate becomes significant at small R_B, because of the effect of the radiative heat conductance parameter λ_R (Fig. 1). Since it increases greatly with increase in atmospheric reentry

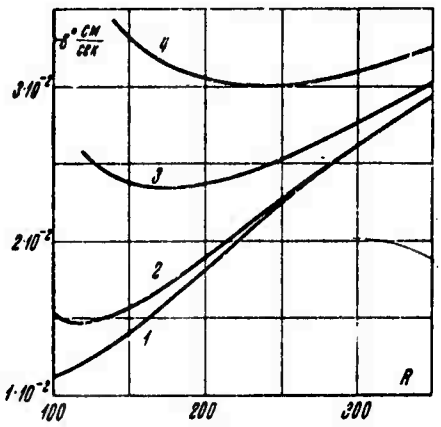

Fig. 1. Destruction rate of heat insulating coating. Curves 1, 2, 3, 4 correspond to $\lambda_R = 0$, 10^4, 5×10^4, 10^5, respectively.

velocity, radiative heat flux is thus a decisive factor in calculation of destruction. A previous study on this problem was reported by Apshteyn in Effects of Strong Explosions, no. 1, 1971, p. 22.

Antonets, A. V. Computation of three dimensional supersonic flow past blunt bodies with generator breaks and allowance for equilibrium and frozen states of the gas in the shock layer. MZhiG, no. 2, 1970, 178-181.

An algorithm is developed for computation of the steady supersonic flow of an inviscid gas past a blunt body with multiple breaks of a generator. The algorithm is based on the principle of separation (behind

each of an arbitrary number of breaks) of the regions of smooth solutions between the body and the characteristic shock wave surfaces, at a positive (expansion) or negative (compression) break. Finite-difference equations in the nodal points of a net are substituted for differential equations in the regions of smooth solution. The unknown velocity components, pressure p, and enthalpy i are determined from the equations by the method of successive calculations. The algorithm accounts for the effect of nonequilibrium physicochemical reactions by computing the flow for either the entire shock layer in a nonequilibrium (frozen) state or for only a partially frozen layer in the area adjacent to the body surface, the other part being occupied by a gas at equilibrium. The effect of the gas equation of state in the shock layer is illustrated by p(x) plots for the flow past a spherically blunted cone with an apex half angle $\theta \leq 10^{\circ}$. The plots show that at $\theta = 10^{\circ}$ p in some points on the surface in a flow at equilibrium can be twice that in the frozen flow. The computation method may be useful in evaluating actual flight effects at altitudes above 60 km and at velocities of 6,500 m/sec or greater.

Antonets, A. V., A. V. Krasil'nikov, and V. I. Lagutin. Experimental determination of the position of pressure center in hypersonic gas flow around a blunted cone at different angles of attack. MZhiG, no. 2, 1971, 142-143.

Following from the previous paper, the relationship between the position of a pressure center C_d and an angle of attack α was determined in a hypersonic wind tunnel at $M_\infty = 6$ and 15 and Reynolds number $Re \cong 10^6$ using a spherically blunted test cone. The cone had a sphere radius R, relative conic length x/R = 5, and apex half-angle $\theta = 11^{\circ}$. The highly accurate method of free aerodynamic balance was applied while varying the distance x_o of the rotational axis from the cone nose. The C_d value for a balanced α coincides with x_o. Plotted experimental C_d data (Fig. 1) agree within a 2%

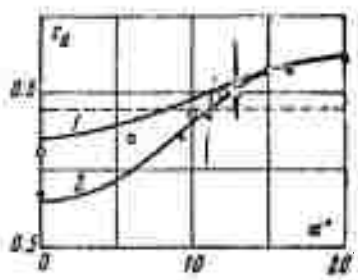

Fig. 1. Pressure center C_d versus angle of attack: curves 1 and 2 - calculated for $M_\infty = 6$ and 15, respectively; small circles - experimental data for $M_\infty = 6$; points - experimental data for $M_\infty = 15$.

maximum discrepancy with theoretical data calculated by the method of Antonets cited in the previous paper [MZhiG, no. 2, 1970, 178], but disagree with the $C_d(\alpha)$ data calculated by the Newton formula (dotted line). Results suggest that physical phenomena on the leeward side of a cone at $\alpha \geq \theta$ do not significantly affect aerodynamic characteristics.

Voronkin, V. G. Nonequilibrium viscous flow of a multicomponent gas near the stagnation point of a blunt body. MZhiG, no. 2, 1971, 144-147.

A theoretical study is made of the effect of shock layer variable parameters on heat transfer, in the case of nonequilibrium-dissociated air at a barrier of finite catalytic activity near the stagnation point of a spherically blunted body. Heat transfer in the nonequilibrium outer flow is compared to that in an equilibrium-dissociated gas flow. Numerical calculation of the nonequilibrium flow was based on the concept of a compressed viscous shock layer. Only free-stream Reynolds numbers R above 1,500 were considered. Under these assumptions, the calculation was reduced to a solution of the boundary layer equations with boundary conditions corresponding to those immediately behind the leading shock wave. Temperature profiles, concentrations of oxygen and nitrogen atoms in the shock layer, and the relative heat flux Q_w were calculated at a 60 km height, 7.4 km/sec free-stream velocity, 700°K wall temperature and 1-100 cm radius of curvature R. It was shown that Q_w in the nonequilibrium shock layer at small R can be significantly increased (by a factor of 3) in relation to the theoretical Q_w in an asymptotically thin nonequilibrium boundary layer with equilibrium parameters at its outer boundary. At increased R the vorticity effect decreases and the effects of nonequilibrium chemical reactions become predominant.

Lunev, V. V., and N. Ye. Khramov. Flow past a blunt body near the stagnation point in a divergent hypersonic stream. MZhiG, no. 3, 1970, 102-105.

The inhomogeneous hypersonic outer stream near the stagnation point past a blunt smooth body is analyzed at a small ratio k of densities ahead of and behind a straight shock wave. Thickness δ of the shock layer at the

forward stagnation point is formulated by

$$\frac{\delta}{kR_*}=\frac{1}{2}\ln\frac{2}{k},\quad \nu=0$$
$$\frac{\delta}{kR_*}=\frac{1}{1+\sqrt{2k}}\quad (\nu=1) \qquad (1)$$

where R_* is the effective curvature radius of the body and $\nu = 0$ and $\nu = 1$ refer to two-dimensional and axisymmetric flows. The formulas in (1) were derived from equations of motion assuming gas density to be constant. It follows from (1) that δ, and hence the profile of the shock layer, depend on k and R_* only. This dependence is illustrated by computed $\delta(k)$ plots for an axisymmetric, strongly underexpanded conic jet around a sphere. The initial flow parameters are tabulated. The data all lie on the same curve which coincides with the theoretical curve calculated for $\nu = 1$ and R_*/R boundary values. Plots of pressure distribution p/p_o' along a barrier versus x/R ratio diverge significantly for different jets, but the same plots of p/p_o' versus x/R_* form a relatively narrow band which is close to the plot for a sphere in a homogeneous stream and the Newtonian plot. The effect of stream divergence is thus accounted for by introduction of R_*. The effects of nonuniform density and velocity of the oncoming stream are taken into account in an analogous manner.

Arutyunyan, G. M. Climb of a shock wave on a wedge moving at supersonic velocity. IN: Volny v neuprugikh sredakh (Waves in nonelastic media). Kishinev, AN Mold SSR, 1970, 7-12.

The flow generated at the upper surface of a moving wedge by an oncoming plane shock wave was analyzed. Conditions are formulated for the flow according to the pattern shown in Fig. 1. It was assumed that intensity of the oncoming shock wave CE was equal to that of the attached compression shock OA, CE is normal to OB, and the interacting shocks CD and DA are weak and reflected at a $\psi/2$ angle by a rigid wall with resulting refraction, but without formation of a third shock wave. It is shown that, under these assumptions, the flow past the wedge upper surface OB can be calculated using linearization theory, if a point, defined by the Mach number M of the oncoming flow and the angle δ of the wedge, lies within certain boundaries in the M-δ plane. All the conditions were verified within an area bound by the curves

f_1 (M, δ) = 0, f_2 (M, δ), f_3 (M, δ), and the abscissa. If the point defined

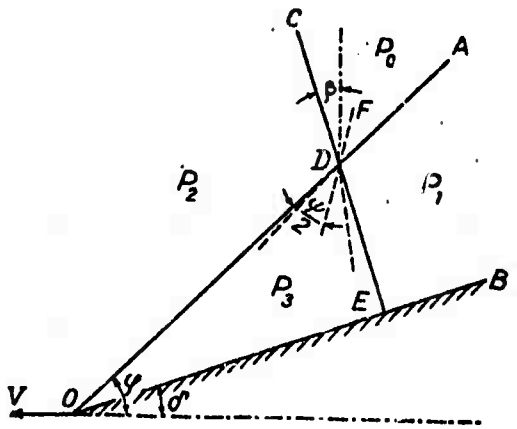

Fig. 1. Flow diagram on the upper surface of a wedge.

by the wedge parameters M and δ lies within this area, the flow will be uniform. Pressure p_3 within the area is then given by

$$\frac{p_3}{p_0} = 1 + \frac{2\gamma M^2}{\sqrt{M^2-1}}\,\delta \qquad (1)$$

where p_0 is the pressure generated by interacting shocks and γ is the adiabatic exponent.

Mamadaliyev, N. A., and Kh. A. Rakhmatufin. Streamline fluid-solid, two-phase flow past a slender profile. IN: Volny v neuprugikh sredakh (Waves in nonelastic media). Kishinev, AN Mold SSR, 1970, 146-152.

A mathematical model of a fluid-solid supersonic flow past a slender profile, e.g., a wedge, is introduced for use in calculations of jet parameters from supersonic nozzles, flight mechanics in a gas-dust medium, etc. The model makes allowance for post-shock reflection of particles from the profile surface. For a specific volume <1, the effects of particles on the

gas flow and friction between particles in the region of a three-velocity flow can be disregarded. Solution of linearized equations of motion for particles impinging on and reflected from a wedge with a given apex angle β_0 thus leads to the conclusion that the boundary between the three-velocity and the two-velocity flows is a straight line with slope $\beta = 2\beta_0$. The boundary condition at $y = 0$ is also a straight line, and formulates the law of mirror reflection. For the case of a two-phase medium with a significant particle concentration, and disregarding the effect of the reflected stream, a solution to the inverse problem is presented in the form of an equation of the profile surface for a given flow separation boundary with a constant inclination β. In contrast to the first analyzed case, the profile surface is weakly concave in relation to the stream, and the three-velocity region II narrows with the increase in X_1, as shown in Fig. 1.

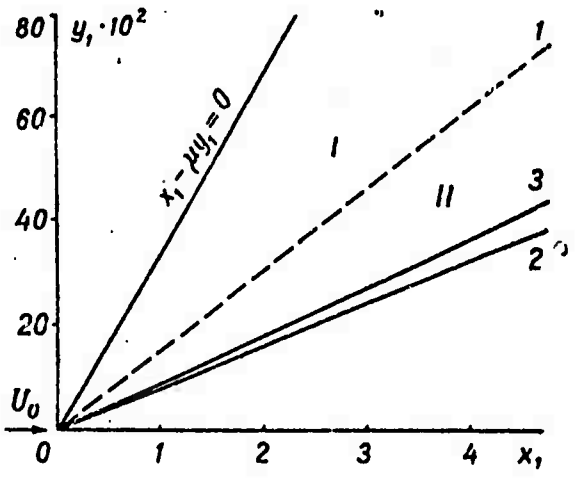

Fig. 1. 1 - separation line, profile surface; 2 - at a small and, 3 - at a significant particle concentration.

Lunev, V. V. Nonviscous flow near the critical point of a blunt body having a variable density along its axis. MZhiG, no. 6, 1971, 56-61.

The flow in a thin compressed layer around a smooth blunt body is described, in the framework of hypersonic theory. A set of conservation equations is derived using an x, y curvilinear coordinate system with the stagnation point as origin. A localized closed solution near the stagnation point is possible when the shape of the shock wave approaches

that of the body and the ratio k of densities ahead and behind the shock wave tends towards zero. A solution in the vicinity of the axis is sought in the form of an expansion in xK powers:

$$v = -v_0(y) + \ldots, \quad u = Kxu_1(y) + \ldots, \quad r = x + \ldots$$
$$p = p_0(y) - K^2x^2\beta(y) + \ldots, \quad k\rho = \rho_0(y) + \ldots \qquad (1)$$

where $K = R^{-1}$ is the body curvature, uV and vV are velocity components along x and y axes of the incident flow, r is the distance from the symmetry axis, and ρ is density. By substitution of variables, conservation equations are derived, which are similar to adiabatic flow equations for a perfect gas with nearly constant ρ. Derivation of the Busemann formula from (1) indicated that universality of pressure distribution can be extended to the entire front surface of a smooth body. The Busemann formula also led to the conclusion that the asymptotic pressure distribution along the body is independent of flow physics. Analysis of boundary conditions revealed two possible boundary flow patterns. According to one pattern, ρ distribution in the vicinity of the wall satisfies the condition

$$\varphi \lesssim \text{const}\, \zeta^{2/(1+\nu)} \lesssim k \qquad (2)$$

i.e., the solution in similar variables ζ, t, including $t\,\delta$, depends only on the body values of ρ distribution and the axial pressure gradient (at $\zeta = 0$), and is the same as the solution in the case of a constant $\rho = k_0^{-1}$ along the thickness δ of a shock layer. The solution of (2) for an axisymmetrical flow is shown to be weakly dependent on k_0, except for a narrow near-wall region of the order $t \sim k_0^{\frac{1}{2}}$. The solid lines in Fig. 1 are plotted for the condition

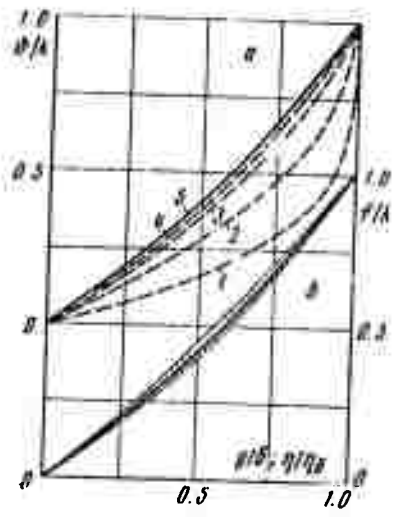

Fig. 1. Axial velocity profiles versus initial coordinate y δ; the numbers 1-5 at the curves correspond to those in Fig. 2.

$k_o = 0.1$. The $t_\delta = \eta_\delta / k = 0.80$ value calculated from the plots in Fig. 2 in effect coincides with the $\delta / kR \simeq 0.78$ value, which was obtained earlier for a streamline flow of dissociated air at an equilibrium within $k = 0.05 - 0.20$ range. But the true thickness δ / kR calculated for curves 1-5 depends significantly on ρ distribution. The solution for a two-dimensional

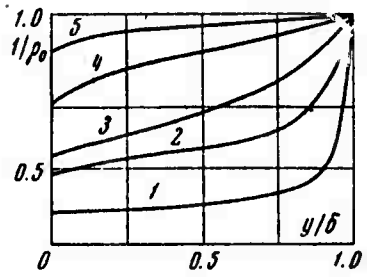

Fig. 2. Density profiles versus initial coordinate y/δ for an axisymmetric flow.

flow ($v = 0$) is seen to be always dependent on k_o; but the dependence on $k_o = 0.05 - 0.2$ is weak as shown in Fig. 3, where the plots 1-4 correspond to $k_o = 0.2$, 0.05, 0.01, and 0.001. A certain degree of universality of the $\zeta(\eta / \eta_\delta)$ function is consequently also to be expected in the case of two-dimensional flow.

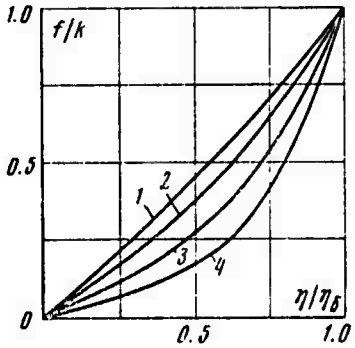

Fig. 3. Axial velocity profiles versus similar coordinates ζ, t, for a two-dimensional flow.

According to the second flow pattern, ρ distribution near the wall exhibits a singularity. A significant variation occurs in the ρ profile which is bound to affect the flow, particularly in the near-wall layer. Even in this case, however, the $\zeta(\eta / \eta_\delta)$ profile is expected to remain universal, because of the weak dependence of the solution on the parameter k_o, i.e., the gas ρ near the wall.

It is concluded that in all except the near-wall sublayer case, the solution should be the same as for a constant ρ equal to the ρ value behind the shock wave. Calculation of the structure of an inviscid shock layer can thus be simplified, given the universality of the axial flow profile in ζ, η variables.

Karasev, A. B., and T. V. Kondranin. The effect of ablation products on heat transfer during destruction of graphite in radiative air plasma. MZhiG, no. 1, 1971, 23-31.

A steady hypersonic flow of viscous, heat-conductive, radiating air around the leading stagnation point of a graphite sphere is analyzed in the region between the separated shock wave and the body surface. The flow is described by a set of equations with self-similar variables and boundary conditions behind the shock wave and on the surface. Heat transfer in the radiant air was calculated by solving the equations by the method of successive approximations. A binary model was adopted for diffusion of ablation products. Chemical reactions were considered to be frozen in the boundary layer and equilibrated at the boundary layer-shock wave interface. Gas state on the ablation surface was determined from the chemical equilibrium condition, assuming equality of vapor pressure with stagnation pressure. Radiative and convective heat transfer were calculated in the presence or absence of ablation. Analysis of plotted data shows that the spectral range of radiant energy transfer is narrow in the streamline flow around an impervious surface at high atmospheric reentry velocities. In the absence of ablation, the total radiant heat flux changes insignificantly by transfer through a cold boundary layer. Thus the presence at the boundary layer of ablation products capable of absorbing or emitting radiation means that heat flow to the surface will increase if the vapor product is opaque in the visible range, but will decrease if opacity extends to $\lambda < 0.115$ micron. Actually, the shielding effect at $\lambda < 0.115\mu$ is to a large degree cancelled by the radiative effect at $\lambda > 0.115\mu$. A previous paper by these authors on graphite ablation was published in Effects of Strong Explosions, no. 1, 1971, p. 41.

Karasev, A. B., and A. N. Lyakh. Study of radiative and convective heat transfer by an emissive mixture of carbon dioxide and nitrogen flowing past the stagnation point. MZhiG, no. 2, 1971, 39-47.

Hypersonic flow characteristics of a viscous thermally conductive mixture (90% CO_2, 10% N_2) around a spherically blunted body were calculated with allowance for radiation energy transfer and reabsorption. Self-similar variables and boundary condition equations describe the gas flow in a compressed thin shock layer, assuming local thermodynamic equilibrium through the entire shock layer. A solution was obtained by iteration and successive computation for flights of the spheres at 9,000 - 12,000°K and 1-10 atm pressure behind the shock wave. The spheres were of 1 m radius and had a 3000°K wall temperature. Analysis of resulting data revealed an insignificant radiation effect on convective heat transfer. The relative contribution of different spectral ranges to the radiative heat flux on the wall was found to be approximately 43, 40, 20, and 15% for the 0.128 - 0.33μ (CO band), 0.33 - 0.66μ (CN bands), 0.80 - 1.15μ and 0.45 - 0.80μ ranges, respectively. The contribution of the UV spectral range decreases while that of the visible range increases with an increase in pressure. Radiation heating is five times greater than convection heating at 10 atm and 12,000°K. Convective and radiative heat fluxes in the CO_2-N_2 mixture exceed the corresponding values in air by 20 and 40%.

Neyland, V. Ya. Upstream propagation of perturbations from interaction of a hypersonic flow with a boundary layer. MZhiG, no. 4, 1970, 40-49.

Hypersonic viscous gas flow past a slender body is analyzed for weak, moderate and strong free interactions. In the case of a weak hypersonic interaction, perturbations generated in the vicinity of a singular point, (e.g., bottom cut or angular point), are seen to propagate upstream a short distance only. Locally nonviscous flow regions may also form with high pressure gradients. Boundary layer separation into sub-regions of different sizes disappears in the presence of a moderate or strong hypersonic interaction. The perturbations in this case propagate up to the leading edge of the body in the process of free interaction along the entire boundary layer. Proof was obtained that localized flow regions of very high pressure gradients are

not generated at the interaction parameters $\chi \geq 1$. The possibility exists, however, of a separation zone formation on the order of magnitude of one body length. The hypersonic boundary layer at $\chi \geq 1$ is described in a first approximation by a set of equations derived from Navier-Stokes equations with boundary conditions. Boundary conditions at the aft end of a body must be satisfied in addition to those near the leading edge. A complete set of boundary conditions was established in the form of a nonsingular solution. The conclusion was drawn that the flow at $M_1 \to \infty$ and $\chi \geq 1$ is described by the same boundary layer equations along the entire separation zone, except for small regions such as those near the angular points.

Bogashchenko, I. A., A. V. Gurevich, R. A. Salimov, and Yu. I. Eydel'man. Flow of a rarefied plasma around a body. ZhETF, v. 59, no. 5, 1970, 1540-1555.

Experimental data are compared with the theory on the structure of a perturbation zone in the vicinity of a disc in a rarefied plasma stream. Quasi-neutral potassium plasma was produced and its streamline flow around a 0.25 cm radius disc was studied in a Q-device (Fig. 1). Plasma parameter

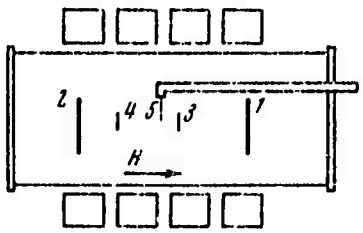

Fig. 1. Experimental Q-device:
1 - tungsten ionizer, 2 - anode, 3 - disc no. 1, 4 - disc no. 2, 5 - probe.

measurements were made using Langmuir probes in both the axial and radial directions. Density and velocity of the plasma, temperature T of the ionizer, surface potential and position of the disc, and magnetic field H were varied. The experimental conditions in the Q-device effectively reproduced those in the ionosphere at ~200-1,000 km height. In the near zone at a distance $Z \leq 1$ cm from the disc, the self-consistent electric field effect on plasma distribution was predominant. This effect was manifested in an increased ion concentration near the axis. The body trace had

an oscillatory structure in the far zone. Oscillation damping is determined by the ionic temperature $T_{i||}$ which tends to equalize with $T_{i\perp}$ as the result of collisions. A change of sign of the relative body potential strongly affects the structure of the perturbation zone between two discs. The experimental data agreed well with the theory of neutral approximation, except in the far zone at increased H values.

Lifshits, Yu. B. and E. G. Shifrin. On the problem of transonic flow over a convex corner. MZhiG, no. 2, 1971, 67-69.

Mathematical analysis of two-dimensional potential flow in the vicinity of the sonic point O shows that a similar solution, satisfying the conditions of Vaglio-Laurin's solution [J. Fluid Mech., 1960, v. 9, no. 1], is possible for equations of transonic flow over a convex corner. A solution to the $\psi(u, v)$ hodograph plane is obtained by analogy with that of Tricomi equations which become equal to zero at the $v = 2/3\ u^{3/2}$ characteristic of the first family of flow lines. A solution $C = |u|^3/v^2$ to the $\psi = 0$ equation was found in the third quadrant of the u, v plane. It is concluded that the profile in the subsonic region must be convex. A one-sheeted plot of the solution in the hodograph plane indicates that the sonic line is convex in relation to the region of subsonic velocities. The surface velocity vector at a transition point from the subsonic region is given by $u = (K^2C)^{1/3} \varphi^{2/3}$, where K is the curvature of profile in the O point. The similar solution derived satisfies a boundary condition in the vicinity of the salient point, as well as the condition of finite curvature in the subsonic region. The solution also describes the principal member of asymptotic expansion in axisymmetric and rotational flow.

Filatov, Ye. I. The optimum shape of a lifting body at hypersonic speeds. MZhiG, no. 1, 1972, 82-86.

Optimization of the aerodynamic characteristics of a horizontally flying hypersonic body is attempted, omitting some previous simplifying assumptions. The body is given a rectilinear coordinate system in which directions of the x and z axes are opposite to the flight direction and vertically downward, respectively. It is assumed that xz is the symmetry plane; that $z = my$ and $z = f(x, y)$ are the upper and lower boundary planes of the semi-body

$y \geq 0$, and that the rectilinear leading edge is formed by intersection of the $z = my$ and $x = ky$ planes. It is further assumed that the bottom section is in the $x = k\ell = \ell_1$ plane, where ℓ is the semi-span; the function $f(x, y)$ can be approximated by a polynomial of a low order in any $x = \text{const}$, $y = \text{const}$ section, and that the thickness of the leading edge is negligibly small in relation to the characteristic dimension of the optimum body in the z direction, i.e. at $x = ky$ and $f(x, y) = mz$. The optimum body shape problem is then formulated in terms of a variational method. Solution of the problem is reduced to finding, within the class $\zeta = \zeta(\xi, \eta)$ of surfaces satisfying the condition $\zeta(0, \eta) = 0$, a surface which would satisfy the maximum value of the functional

$$K = (Y_1 + Y_2)(X_1 + X_2)^{-1} \tag{1}$$

where X_1, X_2 are the drag factors relative to the double velocity head on the semi-body and its leading edge, respectively, and Y_1, Y_2 are the corresponding relative lift forces. The volume of the semi-body must be $V = \text{const}$, and the m, ℓ, and k parameters are assumed to vary with surface geometry. The new coordinates

$$\xi = (x - ky)/l, \quad \eta = y/l, \quad \zeta = (z - my)/l$$
$$p = \frac{\partial \zeta}{\partial \xi}, \quad q = \frac{\partial \zeta}{\partial \eta} - pk + m \tag{2}$$

are introduced in the solution. Using the Ritz method, the unknown optimum surface is described by the equation

$$\begin{aligned} \zeta = \xi\{&6/k^2l^3 + a_{11}(\eta - 0.25) + \\ &+ a_{12}(\eta - 0.1) + \\ &+ a_{20}(\xi - k/2) + a_{21}(\xi\eta - \\ &- k/10) + a_{22}(\xi\eta^2 - \\ &- k/30) + \ldots\} \end{aligned} \tag{3}$$

The problem thus formulated contains two implicit parameters: the coefficient of friction C_f and the relative radius R of leading edge curvature. Numerical calculation of the unknown coefficients a_{11}, a_{12}, etc. in (3) was made by the method of descent. In the zero-th order approximation, equation (3) describes pyramids. For a pyramid with a sharp leading edge, calculations show that the larger the span (21), the higher is the aerodynamic quality. At moderate ℓ_1, the quality K of such pyramids and the slope P of the lower surface toward the x axis only weakly depend on ℓ_1 (Fig. 1 and 2). At moderate ℓ_1, the friction T is one third of the total drag.

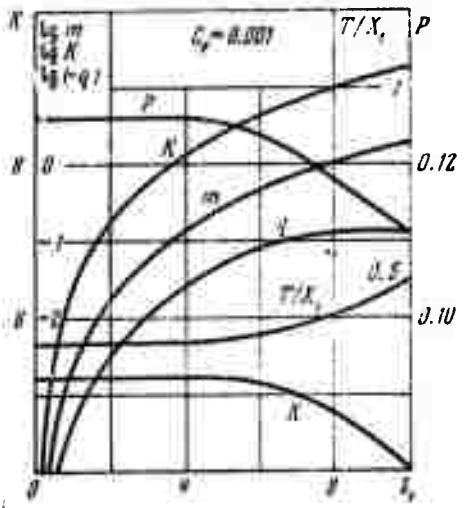

Fig. 1. Maximized parameters of pyramids with sharp leading edges at $C_f = 10^{-3}$.

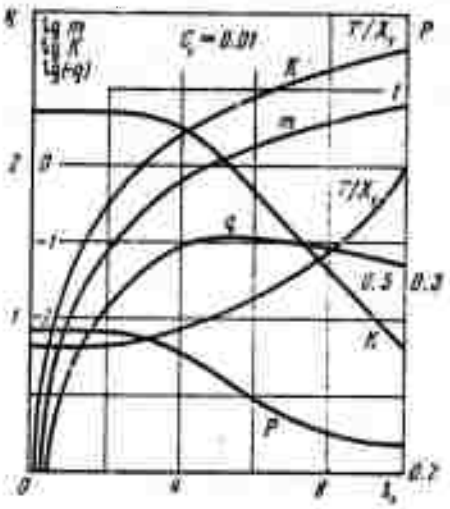

Fig. 2. Maximized parameters of pyramids with sharp leading edges at $C_f = 10^{-2}$.

The effect of bluntness R of the leading edge is primarily evident on l_1 of the optimized pyramids (Fig. 3). The parameter P remains

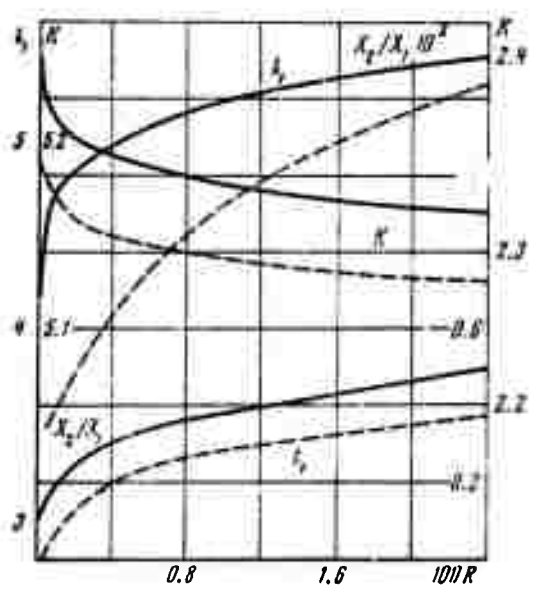

Fig. 3. The parameters of the optimized pyramids versus blunt R. Continuous line - $C_f = 10^{-3}$; broken lines - $C_f = 10^{-2}$.

constant over the entire range of R in contrast to the pyramids with sharp leading edges. The leading edge bluntness does not significantly affect the aerodynamic quality of a lifting body. The values of parameters m, ℓ, k calculated from (3) in the first and second approximation indicate that the aerodynamic quality of optimum bodies differs by less than 0.1% from that of the corresponding pyramids. The data are in qualitative and quantitative agreement with the earlier Western data approximating cone-shaped bodies with sharp leading edges.

It is concluded that the geometry of the body type studied, having a given volume and a maximum aerodynamic quality, is nearly pyramidal and in good agreement with the earlier advanced hypothesis.

Temkin, L. A. Approximate solution to the problem of the ground zone in a rarefied gas. MZhiG, no. 1, 1972, 139-143.

Two-dimensional equilibrium flow in a monatomic rarefied gas around a semi-finite rectangular bar is analyzed, on the basis of the Krook model for collision processes in gases. The Krook equation is given in the form

$$f = Vf_0 \tag{1}$$

where f = f(r, u) is the coordinate and velocity distribution function of gas molecules, f_0(r, u) is the local Maxwellian distribution function, and V is the integral kinetic operator. A set of equations

$$n(\mathbf{r}) = \iiint_{-\infty}^{+\infty} Vf_0(\mathbf{r}, \mathbf{u})\,d\mathbf{u}, \qquad \mathbf{U}(\mathbf{r}) = \frac{1}{n(\mathbf{r})}\iiint_{-\infty}^{+\infty} \mathbf{u}\cdot Vf_0(\mathbf{r}, \mathbf{u})\,d\mathbf{u}$$

$$T(\mathbf{r}) = \frac{m}{3kn(\mathbf{r})}\iiint_{-\infty}^{+\infty} [\mathbf{u} - \mathbf{U}(\mathbf{r})]^2 Vf_0(\mathbf{r}, \mathbf{u})\,d\mathbf{u} \tag{2}$$

was derived from (1) for gas density n, macroscopic velocity U, and temperature T. The set of equations (2), where k is the Boltzmann constant and m is the molecular mass, was solved by iteration in a first-order approximation both with and without allowance for conditions at infinity. Using the M-20 computer, the macroscopic flow parameters n, U, and T were calculated and plotted against coordinates x and y, where the x-axis is the flow direction at infinity. The plots calculated for the Knudsen

number $K_\infty = 1$ and Mach number $M_\infty = 2$, and for $K_\infty = 1$ and $M_\infty = 0.75$, displayed a sharp rise in T in the ground zone of the bar, near the corners, followed by a smooth decrease to the T level at infinity. T on the axis of symmetry is maximum at the points $x_\infty \simeq 1$ and 0.6 at $M_\infty = 2$ and 0.75, respectively. At both M_∞ values, n and pressure p=nT increase monotonically to the levels at infinity. At $M_\infty = 2$, the stream line deviates from the body near the ground zone because of decelerating gas flow. Results are in qualitative agreement with an earlier solution to the ground zone problem obtained within the framework of the Navier-Stokes equations.

Shapiro, Ye. G. Shock layer radiation during hypersonic air flow around a spherical segment. MZhiG, no. 1, 1972, 101-106.

A theoretical analysis is presented of the effect of shock layer radiation on gas dynamic parameters of hypersonic air flow (V_∞ = 10-16 km/sec) around a spherical segment of a base with radius R. The shock layer flow (Fig. 1) is described by a set of integro-differential

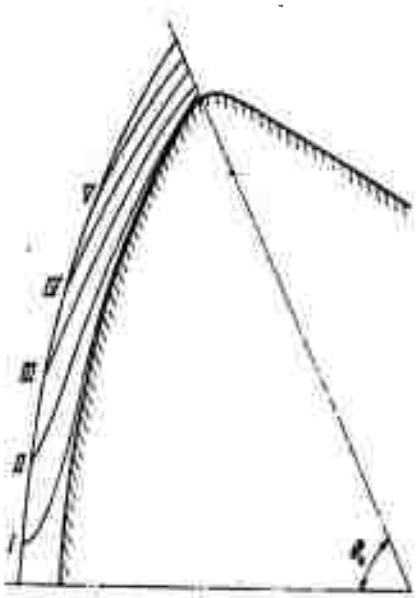

Fig. 1. Shock wave profiles and flow line system for a segment of R = 1 m at V_∞ = 15 km/sec: the flow line numerals I thru V correspond to ϑ = 0.1, 0.3, 0.5, 0.7 and 0.9, respectively.

equations in the spherical coordinate system r, ϑ, whose origin is shifted at a distance l = 0.65 R from the segment center. The term Q or the divergence of the integral radiation flux in the equations was apparently known. The equations were then solved for gas dynamic parameters using an iterative method and an independent variable

$$\xi = (r - r_b)(r_s - r_b)^{-1} \qquad (1)$$

where r_s is the shock wave profile and r_b is the body profile. All gas dynamic parameters and r_s were approximated by Lagrangian polynomials with Hugoniot relations and impermeability as boundary conditions in the shock wave and on the body surface, respectively.

Calculations were made for segments of R = 0-4 m over the cited range of V_∞. In most cases, temperature T_∞ ahead of the shock wave was assumed to be 250°, and in all calculations P_∞ was assumed to be 10^{-4} atm. As with flow around a sphere, the radiation effect on p and V was found to be practically nonexistent and extremely weak with respect to the distribution of the velocity component v. Also analogous to the flow around a sphere, the flow difference with and without radiation was greatest at the body surface. The temperature distribution parameter was the one most affected by shock layer radiation (Fig. 2). The higher the flight speed,

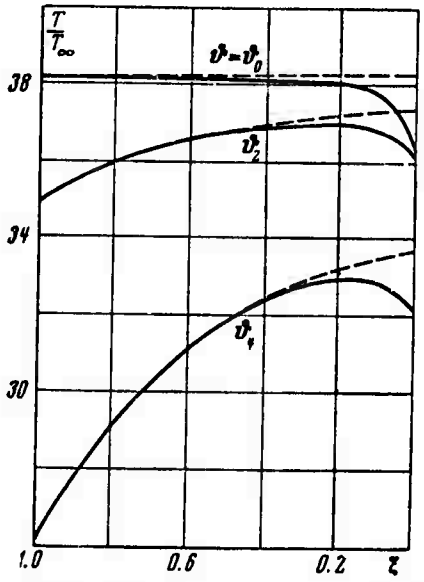

Fig. 2. Relative temperature distribution at V_∞ = 9.85 km/sec, R = 1 m with (solid lines) and without (dashed lines) allowance for radiation flow along the lines ϑ_2 = 0.747, ϑ_4 = 1.141.

the more noticeable was the radiation effect on T distribution. Radiation cooling was also intensified by an increase in R (Fig. 3) .The plots in Fig. 2 versus those in Fig. 3 illustrate the effect of the flow velocity around the segment. A decrease in T of the shock layer results in a decrease in

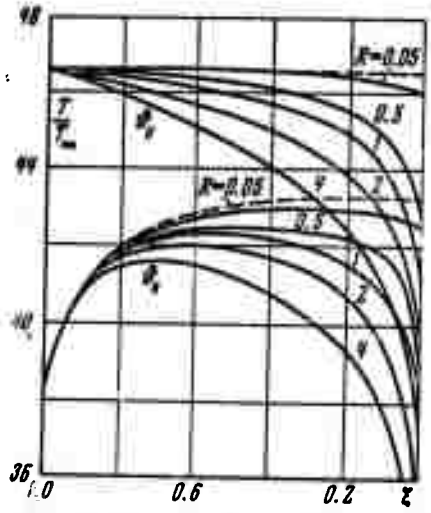

Fig. 3. Relative temperature distribution at V_∞ = 12 km/sec and R = 0.05-4.

layer thickness. It was shown that the radiation energy flux to the stagnation point increases with an increase in R, primarily due to spectral line radiation, in agreement with spectroscopic theory. The universal dependence of the ratio of radiation flux to a body and at the stagnation point is also valid for a spherical segment. An earlier conclusion that the nose of a streamlined body is one area where radiation heating exceeds convective heating applies also to a spherical segment.

The effect of radiation near the rounding point on gas dynamic parameters distribution in a shock layer was also analyzed on the basis of the energy conservation equation. This equation indicates that as $Q \to 0$, the total enthalpy H along different flow lines is even affected by small radiation fluxes (Fig. 4). Fig. 4 illustrates the phenomenon of radiative freezing which occurs when a particle is carried out of the region affected by radiation to a colder region before the particle energy is significantly affected. This phenomenon determines changes in distribution of gas dynamic parameters near the symmetry axis and, in particular, causes a sharp drop of H. In regions far from the symmetry axis, particles propagating along the flow lines do not lose energy because of the high velocity and low Q of radiation

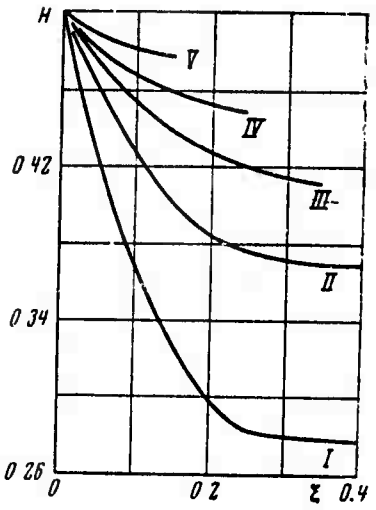

Fig. 4. Distribution of total enthalpy H along different flow lines. ξ is the distance traveled by a particle from the shock wave.

flux. The radiation near the rounding point therefore does not significantly affect distribution of aerodynamic parameters of the shock layer. Calculations showed that allowance for the geometry of the radiative volume is not required in the vicinity of the rounding point.

Kokin, G. A. and Ye. V. Lysenko. Pitot tube pressure in supersonic rarefied gas flow. MZhiG, no. 1, 1972, 195-199.

Readings of four Pitot tubes in a low density wind tunnel at M_∞ = 2.5, 2.6, 3.2, and 5.4 are compared to Pirani and McLeod pressure gauge data. The experiments were designed to evaluate a correction to Pitot tube readings in a supersonic rarefied gas flow. The d/D parameter of the experimental Pitot tubes (Fig. 1) was 0.1-0.2 and 0.5-0.9 for 1, 2 and 3 tube types, and the ℓ/d parameter was 1 and 50-100 for the 1 and 2, 3 types. The mean free path λ_∞ of molecules in a free stream flow was 0.5, 1.2-0.9, 3.3-2.4, and 0.5-0.4 mm, respectively, at the cited M_∞ values. The Knudsen number ($Kn_\infty = \lambda_\infty / D$) dependence on the relative Pitot tube readings at the cited M_∞ is also plotted in Fig. 1, where p_{o*} is the measured Pitot tube pressure and p_{o2} is the Pitot pressure behind the compression shock.

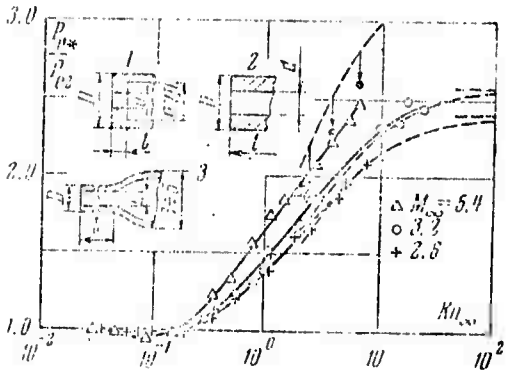

Fig. 1. Geometry of Pitot tubes and experimental plots of P_{o*}/P_{o2} versus Kn_∞. Dotted lines - theoretical plots for $r/R = 0.5$ or ≈ 0.863. Arrows indicate theoretical values corrected for thermal conductivity of the tube.

To evaluate the correction to the Pitot tube readings, the correction to the Pitot tube readings, the asymptotic pressure ratio p_{oF}/p_{o2} in free molecular flow around the tube was formulated using known relations, including that of Rayleigh. The derived formula served to calculate and plot p_{oF}/p_{o2} ratios for thermally insulated tubes of different ℓ/d parameters and for $M_\infty = 1$-9. The relation

$$\frac{p_{o*}}{p_{o2}} = \frac{p_{oF}}{p_{o2}}\left(1+\frac{s_\infty}{2\sqrt{2}\,Kn_\infty}\left\{\left[h_1\left(\frac{T_\infty}{T_0}\right)^{1/2}+\frac{h_2}{s_\infty}\right]F(s_\infty)+\right.\right.$$
$$\left.\left.+\frac{h_1 G(s_\infty)}{2s_\infty}\left(\frac{T_\infty}{T_0}\right)^{1/2}\right\}E\left(\frac{r}{R}\right)\right)^{-1}$$
$$h_1=\frac{3\pi-2}{6\sqrt{\pi}},\qquad h_2=\frac{2\pi-3}{3\pi},\qquad E\left(\frac{r}{R}\right)=\frac{r}{R}+\left[1-\left(\frac{r}{R}\right)^2\right]^{1/2} \qquad (1)$$
$$F(s)=1/2\sqrt{\pi}(1+\operatorname{erf} s)-s\exp(-s^2)$$
$$G(s)=(s^2+1)\exp(-s^2)$$

was derived for a thermally insulated, long cylindrical tube in a nearly free molecular streamline flow, where $S_\infty = M_\infty/V_\infty$, the ratio between the stream mass velocity and the most probable thermal velocity of molecules; and r and R are the inner and outer radii of the tube. This relation was derived in approximation of a single collision between the incident molecules and those emitted by the tube. The p_{o*}/p_{o2} values for $M_\infty = 2.6$ and 3.2 calculated from (1) are in good agreement with corresponding experimental

values (Fig. 1). An additional correction factor C for thermal conductivity was introduced into (1) to obtain theoretical p_{o*}/p_{o2} values at $M_\infty = 5.4$ in agreement with the experimental data. The experimental and theoretical data were used to plot a universal Kn dependence of the parameter $\xi = (p_{o*}-p_{o2})(p_{oF}-p_{o2})^{-1}$, independent of M_∞. The plot can then be used to determine M_∞ from measured Pitot tube pressure.

Zakharchenko, V. F., M. V. Tsvetkova, and Ye. E. Borovskiy. Supersonic flow around a porous cone. PM, no. 2, 1972, 132-134.

Supersonic air flow around a circular pointed cone with a permeable surface was investigated in connection with the control of incident heat flux and drag on streamlined bodies. Shadow photographs were obtained of the unperturbed flow around a 0.197 rad half angle cone at 0-0.24 values of the injection parameter $(\rho V)_1$, where ρ_1 and V_1 are the density and velocity of the injected gas. The Mach number M_∞ of the incident unperturbed flow was 2.9, the Reynolds number Re_∞/m was 2.6×10^6, and the ratio $T_{0\infty}/T_{01}$ of stagnation temperatures of the external and injected gas was 1. Photographs were used to determine the angle Θ_s between the compression shock front and the direction of the unperturbed flow. It was assumed that the free stream boundary is also conic at uniform gas injection through the conic surface and that the pressure along the boundary is uniform. The boundary can then be assimilated to an impervious surface of an imaginary cone as well as its position, i.e. the angle $\Delta\Theta$ between the boundary and the cone surface. Pressure p along the boundary can therefore be calculated as in a problem of supersonic flow around a cone. Calculations indicate that both Θ_s and $\Delta\Theta$ increase continuously with increases in injection $(\rho V)_1$, the rate of increase depending on the $(\rho V)_1$ value. The pressure coefficient $\bar{p}_s$ on the boundary was calculated using available data on supersonic flow around cones. Plots of the relative pressure coefficient $\bar{p}_1 - \bar{p}/\bar{p}$ along the cone surface at different $(\rho V)_1$ values (Fig. 1) show a qualitative pattern of variations of the pressure coefficient $\bar{p}_1$ in the presence of air injection in comparison with the flow $(\bar{p})$ around an impervious cone, i.e. in the absence of air injection. The experimental $\bar{p}_1 - \bar{p}/\bar{p}$ value is shown (Fig. 2) to depend significantly on the coordinate x/L and $(\rho V)_1$.

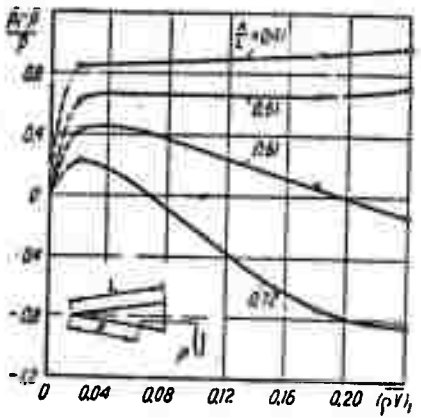

Fig. 1. Relative pressure coefficient versus injection parameter.

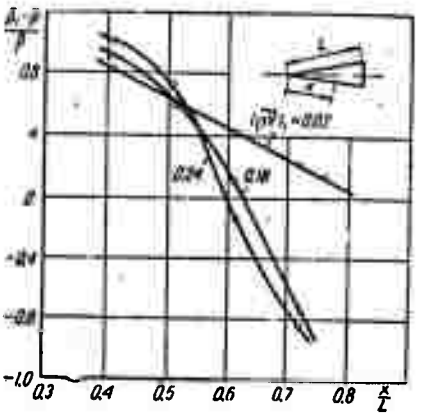

Fig. 2. Relative pressure coefficient versus coordinate x/L at fixed points of the cone generatrix.

The data reveal a significant dependence of incident flow parameters on the injection pressure and make it possible to calculate the drag on a permeable surface cone. Total drag calculations should include an allowance for injection drag which can amount to 10% of the total drag at a low injection pressure.

Bykov, B. P., and S. I. Kozlov. Ion and electron kinetics in a disturbed ionosphere at altitudes of 100~200 km. Geomagnetizm i aeronomiya, no. 2, 1972, 340-342.

Results are described of an investigation on kinetics of ions and electrons at altitudes $100 < h < 200$ km in a disturbed atmosphere. The disturbing action is assumed to significantly increase the degree of ionization α of air, so that N_2^+, O_2^+ and O^+ are formed approximately in direct relation to the N_2, O_2 and O contents at these altitudes. Investigation is limited to values $\alpha \ll 1$, so it is considered that the atmosphere is not warmed up due to a sharp rise of α, i.e. electrons, neutrons and ions of gas have the high level of temperature distribution existing in normal ionosphere.

Form. no.	Reaction	Velocity const × cm^3 per sec
1	$O^+ + N_2 \rightarrow NO^+ + N$	$\alpha_1 = 2 \cdot 10^{-12}$
2	$O^+ + O_2 \rightarrow O_2^+ + O$	$\alpha_2 = 4 \cdot 10^{-11}$
3	$N_2^+ + O \rightarrow O^+ + N_2$	$\alpha_3 < 1 \cdot 10^{-11}$
4	$N_2^+ + O \rightarrow NO^+ + N$	$\alpha_4 = 2,5 \cdot 10^{-10}$
5	$N_2^+ + O_2 \rightarrow O_2^+ + N_2$	$\alpha_5 = 1 \cdot 10^{-10}$
6	$O_2^+ + N_2 \rightarrow NO^+ + NO$	$\alpha_6 < 1 \cdot 10^{-15}$
7	$O_2^+ + e \rightarrow O + O$	$\alpha^*(O_2^+) = 2,2 \cdot 10^{-7} (T_e/300)^{-1}$
8	$N_2^+ + e \rightarrow N + N$	$\alpha^*(N_2^+) = 3 \cdot 10^{-7} (T_e/300)^{-0.5}$
9	$NO^+ + e \rightarrow N + O$	$\alpha^*(NO^+) = 4,4 \cdot 10^{-7} (T_e/300)^{-1}$, $200^\circ K \leqslant T_e \leqslant 500^\circ K$
		$\alpha^*(NO^+) = 0,9 \cdot 10^{-7} (T_e/1000)^{-0.5}$, $T_e > 500^\circ K$

Table 1.

The general scheme of elementary processes used in this work and their velocity constants are given in Table 1. On the basis of these reactions kinetic differential equations are obtained which were solved by computer. Calculations are done for a wide range of altitudes and values of N_{eo}, at day and night conditions. Results of calculations for daylight conditions at $\alpha_3 = 10^{-11}$ and $\alpha_6 = 10^{-15}$ cm^3/sec are plotted. The main characteristic features of ion and electron kinetics in a disturbed ionosphere are seen to be as follows: 1) The role of N_2^+ ions is significant only at the initial moment after disturbance, not exceeding in most cases ~1 sec;

2) At lower altitudes, as in a normal atmosphere, recombination takes place mainly according to a square law. However, with an increase of N_{eo} after the disappearance of N_2^+ over a certain time, velocity variation may follow a linear law. The duration of this time significantly increases at higher altitudes; 3) The time behavior of $[NO^+]$ differs little from predictions. Even at upper altitude regions, the role of this ion is small, except when $N_{eo} < 10^6$ cm^{-3}; 4) To a first approximation, at all altitudes the main molecular ion is O_2^+; 5) The principal difference in behavior of ions and electrons in night conditions from day consists in the fact that the dissociative recombination level increases, so that the role of N_2^+ and NO^+ ions substantially decreases; and 6) The decay time of electron concentration from N_{eo} to normal values of an undisturbed ionosphere has only a slight dependence on the value of N_{eo}.

These conclusions also hold up under varying values of the unknown velocity constants α_3 and α_6. All calculations were done assuming $\alpha_1 - \alpha_6$ to be independent of temperature.

Alimov, V. A., L. M. Yerukhimov, and T. S. Pyrkova. Theory of the F_{spread} phenomenon in the ionosphere. Geomagnetizm i aeronomiya, no. 5, 1971, 790-797.

An analysis is given of possible factors which cause stretching of the return r-f pulse from an ionospheric probe, or the F_{spread} effect. The authors use the diffraction theory of pulsed signal spread in a nonuniform ionosphere, together with data on nonuniformity distribution vs. altitude in the F-layer, and diffusivity data on returned signals. Both ground-based and satellite transmitters are considered, and the variation in spread effect at different latitudes is considered. Using an averaged model of the F-layer structure, the authors obtain expressions for electron density variation $\Delta N/N$ in the equatorial, middle and high latitudes. Following this the characteristic of returned pulsewidth τ is obtained for several possible $\Delta N/N$ models, assuming either an exponential or parabolic variation within a layer, as tabulated in Table 1. Graphical comparisons are given of theoretical and calculated behavior of the depth of the diffusivity zone $\Delta z \equiv c\tau$ as a function of signal frequency. Fig. 1 gives this relation for the extremes of equatorial and polar latitudes, based on ionogram data from the Alouette satellite. These

Model of non-uniform layer	Exponential layer	Parabolic layer
$\overline{(\Delta N)^2}(z) = \text{const}$	$\tau \sim \omega^{-2}$	$\tau \sim \omega$
$\overline{(\Delta N/N)^2}(z) = \text{const}$	$\tau \approx \text{const}$	$\tau \sim \omega^2$
$\overline{(\Delta N)^2}(z) = B/A - z$	—	$\tau \approx \text{const}$
$\overline{(\Delta N/N)^2}(z) = A_1 e^{-\alpha z}$	$\tau \sim \omega$	—
$\overline{(\Delta N/N)^2}(z) = C_1 + B_1 e^{\alpha z}$	$\tau \sim \sqrt{C_1 + B_1/\omega^2}$	—

Table 1.

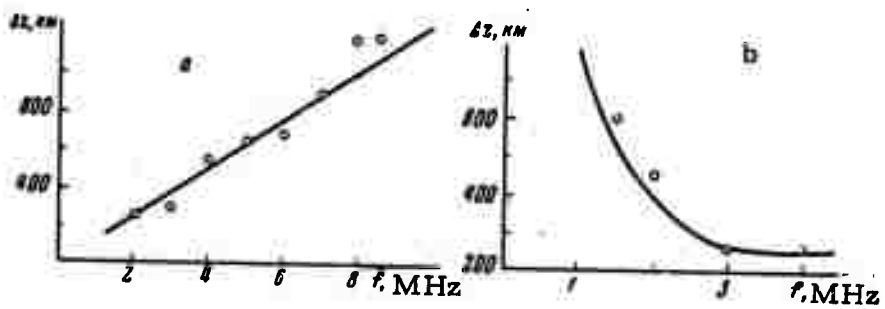

Fig. 1. Δ z(f) for satellite signals.
a - equatorial, b - polar latitudes

results show a distinct variance from analogous data using a ground-based probe system, as seen in Fig. 2, indicating the discrete nature of inhomo-

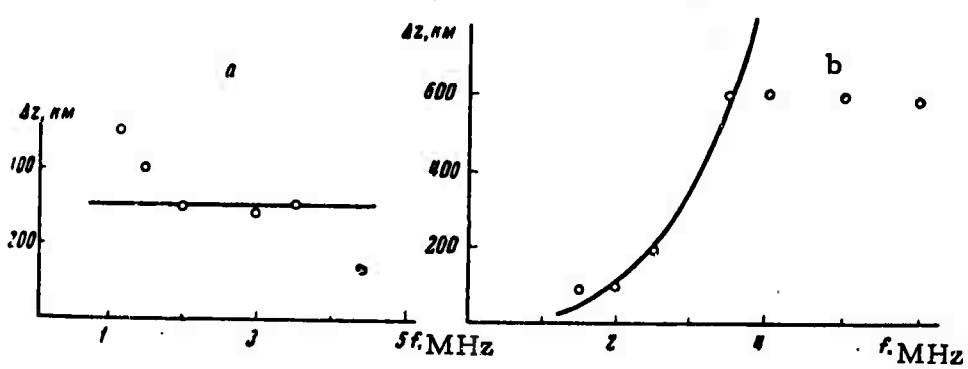

Fig. 2. Δ z(f) for ground-based signals.
a - equatorial, b - polar latitudes

geneities in differing portions of the F-layer. The findings appear to establish that the F_{spread} mechanism is generally caused by scattering of the signal pulse on local electron density variations in areas on the order of 1--5 km across. The variation in spread behavior is then governed by the noncorrelation in spectral response of the pulse, as it is reflected from different levels of the F-layer.

Vashchenko, V. I., Yu. N. Matyushin, A. K. Parfenov, Yu. A. Lebedev, and A. Ya. Apin. Heat liberation in a low-velocity detonation regime. FGiV, no. 1, 1971, 121-126.

The heat of explosion and the composition of the products of powdered tetryl explosive conversion were determined experimentally for two discrete detonation regimes. Low-velocity (D = 2.1 km/sec) detonation was emphasized to verify an earlier proposed mechanism. Cylindrical tetryl charges (ρ = 0.95 g/cm^3, d = 20 mm, ℓ = 100 mm) in 0-25 mm thick water envelopes were detonated in a calorimeter by TNT/NaCl (50/50) or RDX primers initiating low-velocity detonations, or an RDX primer initiating a normal velocity (D = 4.5 km/sec) detonation. The measured heats of explosive conversion Q outlined in Fig. 1 show the differences between the two detonation regimes. The gaseous products of the low-velocity detonation contained a significant amount of nitrogen oxide. The solid residue of unreacted tetryl was

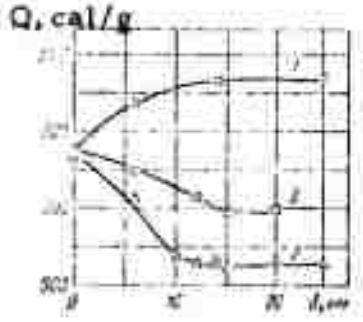

Fig. 1. Heat of explosion of tetryl vs. thickness of water envelope. 1 - normal detonation velocity; 2 - low-velocity detonation without allowance for unreacted tetryl; 3 - low-velocity detonation with allowance for unreacted tetryl.

20% of the initial charge in a 12-20 mm thick envelope. These experimental data confirmed the earlier proposed point mechanism for low-velocity explosive combustion, in which explosive particles ignite at separate points on the surface and burn up in parallel layers. Detonation velocity D, calculated by the method of successive approximations, was 3.7 km/sec which is higher than

the experimental D(2.1 km/sec). This discrepancy is apparently due to the much higher relative amount of the unreacted tetryl residue (~70%) in the reaction zone, which determines D. The measured explosion pulse of a low-velocity detonation was lower by a factor of 1.7 than the pulse of a normal detonation due to a significantly lower detonation wave pressure. A low-velocity detonation regime is extremely unfavorable in industrial applications of solid explosives, because of the presence of toxic gases, the increased danger of ignition of CH_4-O_2 mixtures, and the decreased effectiveness of the explosion.

Merzhanov, A. G., and E. A. Shtessel'. Thermal explosion in liquid reactive systems in the presence of heat convection. FGiV, no. 1, 1971, 68-76.

Thermal explosion experiments were carried out using 1:2 hexamethylene di-isocyanate (HDI) - alcohol mixtures in flat and cylindrical containers, under conditions favoring heat transfer by natural convection. The main purpose was to correlate the thermal explosion limit δ_* with the Rayleigh criterion of natural convection where g is gravity, φ is the coefficient of volume

$$\mathrm{Ra} = \frac{g \varphi R T_*^2}{\nu a E} r^3 \qquad (1)$$

expansion, T_* is the critical spontaneous ignition temperature, r is the characteristic dimension, ν is the kinematic viscosity, a is the conductivity temperature, and E is the activation energy of chemical reaction. The correlation to be determined was formulated as

$$\delta_* = \delta_0 \cdot f(\mathrm{Ra}) \qquad (2)$$

and the problem was reduced to finding f(Ra). The kinetic parameters in (1) and in the expression for δ_* and ν of the reactive mixtures were determined experimentally. Thermophysical parameters for calculations of Ra and δ_* were taken from the literature. T_* was determined by the abscissa of the inflection point of the experimental plot of ΔT_{max} versus T_0 of the heat carrier. The Frank-Kamenetskiy parameter δ_0, without allowance for convection, was calculated using a known formula. The tabulated T_* experimental data exceeded by ~30°C the T_* theoretical data owing to the effect of natural convection. The experimental plot of f(Ra) and its interpolation formula were used to evaluate the coefficients of internal α_{eff} and external α heat transfer, and the

temperature distribution within the reaction zone in the presence of free convection. The effect of convection on δ_* dependence versus Ra was strongest at high α and disappeared at low α, corresponding to Biot numbers ranging from 2.4 to 6. The theoretical analysis of thermal explosion in liquids reacting without gas evolution in the presence of convection revealed a satisfactory agreement between theoretical and experimental f(Ra) data.

Kukhtevich, V. I., I. V. Goryachev, and L. A. Trykov. Zashchita ot pronikayushchey radiatsii yadernogo vzryva (Protection against the penetrating radiation of a nuclear explosion). Moscow, Atomizdat, 1970, 190 p.

An engineering design method is presented for the protection of ground structures against the penetrating radiation of a nuclear explosions. The book is based on Soviet and Western open source materials published in 1958-1969; Soviet sources make up about 50% of the 123 references.

Physical aspects of nuclear explosion are treated only briefly, since they are covered well enough in several recent Soviet and Western monographs. Emphasis is placed on neutrons and gamma-rays produced at the atmosphere - ground boundary and their penetration through a typical protective shield. Numerous published data on characteristics of ionizing radiation are assembled for use in the design of protection against nuclear radiation.

Formulas and numerical data are given for calculation of the dose rate of primary gamma radiation propagating from a point source and from a spherical radioactive cloud through an infinite atmospheric medium. The effect of a shock wave created by an explosion on the propagation of primary gamma-rays is evaluated in the cases of aerial and ground explosions. Formulas are also given for the dose rates of primary and secondary gamma -radiation with allowance for the shock wave effect, as well as the time, explosive force, distance from the explosion center, and ascent velocity of the radioactive cloud. Numerical values for an integral dose of gamma radiation at a given distance from the explosion center are described by formulas for low and high explosive forces, and plots of gamma-ray accumulation rate versus time are shown. Theoretical data are included on: spatial distribution of slow neutrons released by a nuclear explosion and formed in air by moderation and diffusion of delayed neutrons; integral neutron albedo from the ground surface and coefficients of the angular distribution function of scattered

neutrons; and characteristics of neutrons reflected from the ground by a nuclear explosion in the atmosphere. Calculated data are also presented on integral gamma-radiation albedo in a nuclear explosion.

Other tables give theoretical and experimental data on transmission of nonscattered neutrons and total neutron dose through an iron shield of varying thicknesses and at different angles of incidence; transmission of a total dose of neutrons through water, polyethylene, and iron shields; transmission of nonscattered neutrons from a nuclear reactor through an iron, concrete, or polyethylene shield; and angular distribution of the dose rate of scattered neutrons beyond an iron or polyethylene shield. Experimental and theoretical data are plotted and tabulated on angular distribution (differential albedo) and integral albedo of neutrons back-scattered from water, ground, and iron at different neutron beam angles of incidence.

Theoretical mass coefficients of attenuation of nonscattered gamma-radiation by different materials are tabulated and discussed. Theoretical transmission coefficients of gamma-radiation scattered by iron shields of varying thicknesses and at different angles and characteristic angles of scattering for specific energies and materials are tabulated. Formulas used to calculate the tabulated data are given. Empirical formulas are cited for calculating integral energy albedo of gamma quanta back-scattered from protective shields. The approximate formula for bremsstrahlung energy of beta-electrons is given and data on the relative contribution of spectral components of bremsstrahlung were tabulated. Secondary gamma-radiation yield beyond the shield is analyzed, and the numerical values of the constants for calculation of the yield are tabulated for water, iron, and concrete. Calculated yield functions for different shield thicknesses are plotted.

Two methods of designing the protection of ground structures are outlined: (1) an exact method involving the use of computers and, (2) a simplified method using approximate formulas. Both methods require a knowledge of the barrier and geometry factors of radiation attenuation. The formulas for calculation of these factors are given, and the sequence of mathematical operations associated with the two methods is described. The precise method consists of six consecutive steps.

The effects are evaluated of the multiple scattering of radiation on the inner walls of a structure.

Appendices contain 8 tables of barrier factors of transmission of neutrons and gamma-radiation through various materials, and two tables for yields of trapped gamma-radiation for various materials.

Korobeynikov, V. P., V. A. Levin, and V. V. Markov. Explosion of a combustible gaseous mixture. IN: Nauch. trudy In-t mekh. Mosk. un-ta no. 11, 1971, 83-89. (RZhMekh, 1/72, #1B211)

A theoretical study was made of the explosion of a stationary inviscid and thermally nonconductive gas mixture, and of its combustion with allowance for ignition delay and a subsequent reversible reaction proceeding simultaneously in both directions. The initial gas flow is described by strong point-explosion formulas. A strongly supercompressed detonation wave decomposes into compression shock and ignition fronts. Front separation increases in time depending on the symmetry pattern, explosion energy, energy of activation, and the adiabatic exponent. In the second phase, energy liberated by a chemical reaction is taken into account in the numerical calculation of the flow. It is shown that detonation combustion is not restored in this case.

Rodionov, V. N., and A. P. Sukhotin. Parameters of elastic waves generated by a spherical explosion in metals of different strength. FGiV, no. 1, 1971, 142-146.

An experimental study was made of the effect of yield point σ in uniaxial elongation of A-00 aluminum (1), D-16 annealed (2), and D-16 hardened duralumin (3) on the parameters of an elastic compression wave generated by a 0.2 g spherical charge of TEN. A diagram of the experiment is shown in Fig. 1. The metal samples had similar mechanical characteristics,

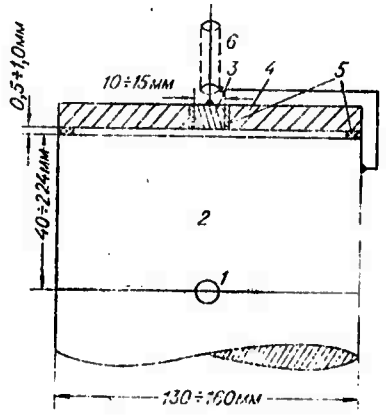

Fig. 1. Experimental setup: 1 - explosive charge; 2 - metal block; 3 - pickup plate; 4 - guard ring; 5 - insulators; 6 - cable.

with the exception of differences in strength. The measured σ was 450, 1600, and 3000 kg/cm for samples (1), (2) and (3). Velocity rise time τ_1, positive phase duration τ_2, and maximum mass velocity U_m were measured on oscilloscope traces of free metal surface displacement. The experimental plots τ_1 (r), τ_2 (r), (Fig. 2), and $\lg U_m(\lg r)$ indicate that elastic waves are generated by the explosion, and the observed differences in temporal wave parameters are the effect of strength only. This effect

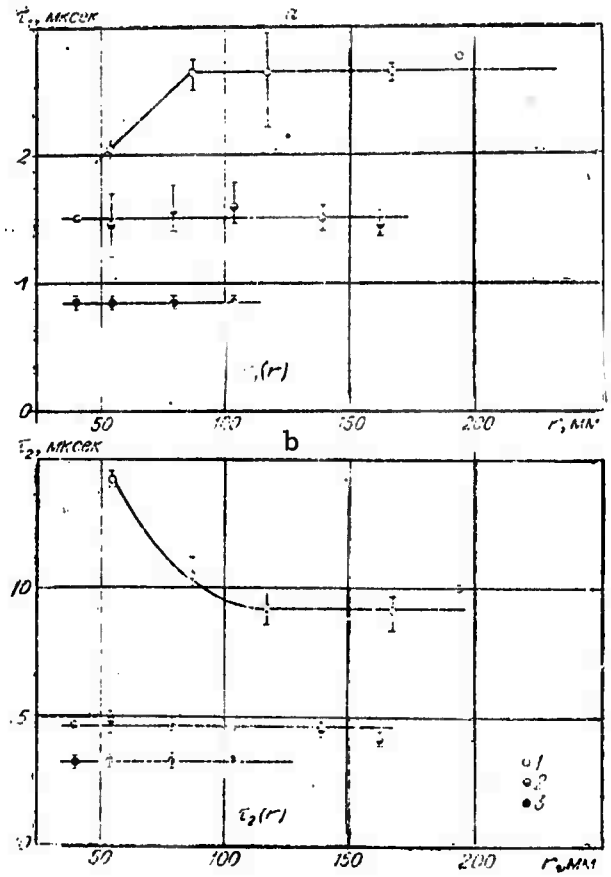

Fig. 2. Velocity rise time (a) and positive phase duration (b) versus distance r from the explosion center.

was also evident in variations between the measured volume of the explosion cavities of the three metal samples (1.3, 0.75, and 0.42 cu cm, respectively). The linearity of the calculated plots of the relative maximum mass velocity versus distance from the explosion center confirms that the extent of plastic

deformation is determined by the static σ of the metal. The motion pattern and state of the metal in the elastic region was reconstructed from the experimental data and the equation of plasticity. The effect of σ on the motion of the boundary line R_* at which the difference of principal stress is equal to σ of the metal is shown in Fig. 3. An increase

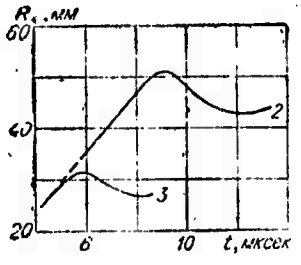

Fig. 3. The effect of σ of the 2 and 3 metals on boundary line R_*

in σ affects both the amplitude and temporal parameters of R_* motion.

Krupnikov, K. K., V. F. Kuropatenko, A. T. Sapozhnikov, B. N. Simanov, and V. A. Simonenko. Calculation of explosions in a medium with polymorphic phase transition. DAN SSSR, v. 202, no. 2, 1972, 300-301.

An explosion in a quartz-like medium was calculated on a computer using a RAND(raschet adiabaticheskikh nestatsionarnykh dvizheniy) program for nonstationary adiabatic motion. The program takes into account the polymorphic phase transition of quartz into "stishovit". A two-liquid model was adopted for the medium with a gas bubble in its center; high pressure expansion of the bubble simulated a point explosion. In the region of continuous flow, pressure P and internal energy E of each phase were calculated from the equations

$$dE + P\,dV = 0, \tag{1}$$

$$P = P_x(\rho) + \Gamma\rho(E - E_x) \tag{2}$$

where $P_x = \frac{\rho_0 c_0^2}{n}(\delta^n - 1)$, $E_x = \frac{c_0^2}{n}\left[\frac{\delta^{n-1} - n}{n-1} + \frac{1}{\delta}\right] + E_0$, $\delta = \rho/\rho_0 = 0.605$.

$n_1 = 4$, $n_2 = 2.7$, $\Gamma_1 = \Gamma_2 = 0.55$, $E_0 = \text{const}$. P, V, and E were correlated by a P = P(T) equilibrium curve and the equation of state of the mixture,

$$E - E_* = [T\,dP(T)/dT - P(T)](V - V_*)$$

where V_* and E_* are, respectively, specific volume and internal energy of one of the phases along the equilibrium curve. In many cases, expansion shock and bifurcated compression waves appear at the phase mixture boundary. Allowance was made in the RAND program for these waves. The calculated shock wave parameters were plotted against a dimensionless variable $\bar{r} = r/r_g$, where $r_g = \left[Q/(\rho_0 C_0^2)\right]^{1/3}$ (Fig. 1). The plots show that P and U

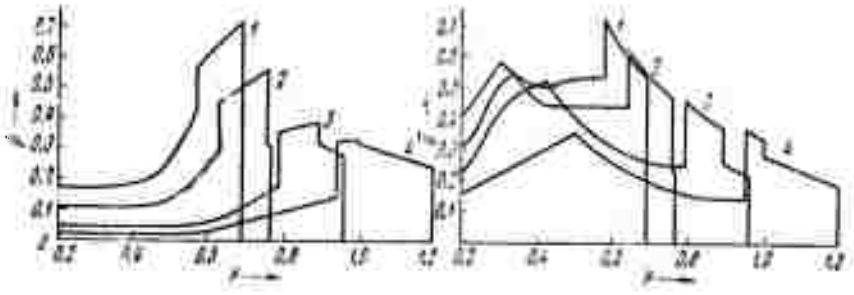

Fig. 1. Dimensionless pressure P and velocity $\bar{U}$ versus time: 1 - before bifurcation of the first shock wave; 2, 3, and 4 - after bifurcation.

behind the first shock wavefront increase significantly before dropping stepwise at the front of the expansion shock wave.

Ocheretin, V. N. Study of shock wave formation from exploding wires in water. EOM, no. 5, 1971, 39-41.

A description is given of an experiment on the formation of shock waves in water from an exploding wire. The experimental sketch is given in Fig. 1. Tests were conducted with steel and copper wires of 0.15 mm dia and 90 mm length, each with an initial voltage of 50 kv and a discharge capacity of 1 μf. Photographs were taken at the rate of 600,000 frames per second; two photographs are given illustrating steel and copper wire explosions. It was noted that the channel formed from the explosion of a

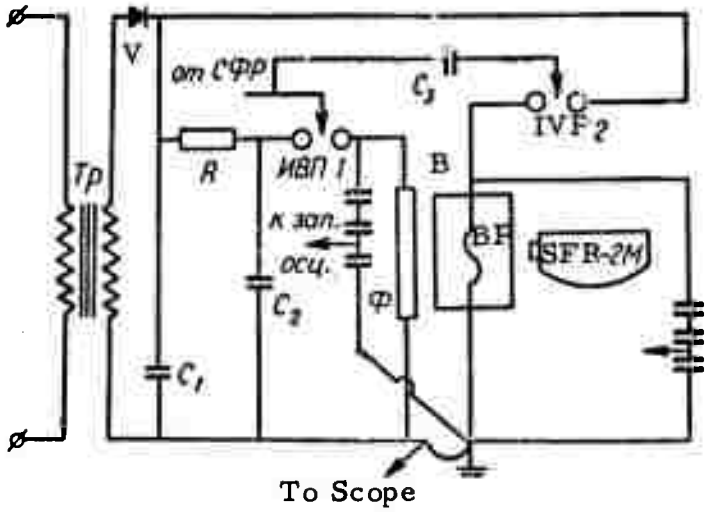

Fig. 1. Experimental diagram. TR - high voltage step-up transformer; V - rectifier; IVP1, IVP2 - spark gaps; B - test vessel; ϕ - aluminum foil; BP - exploding wire.

steel wire had a uniform structure, while that formed by copper wire was nonuniform. Energy levels in the channels were measured at 150 kj/cm^3 and 115 kj/cm^3 for steel and copper wire respectively. From the test results, the author recommends use of steel wires, rather than copper or brass, for its superior hydrodynamic parameters.

Aristov, V. V., K. S. Karplyuk, and V. P. Pavlenko. Three-wave interaction coupling effect on development of explosive instability. UFZh, no. 2, 1972, 307-314.

A theoretical analysis is given of the nonlinear interaction of positive and negative energy waves, for the case of mutual coupling action among the waves. The study derives from the established fact that interaction of three waves with a negative energy wave results in a so-called explosive instability, where the amplitudes of all waves increase without bound during some limited interval. Specifically, for the four wave case defined by wave vector k_i and frequency ω_{ki}, the problem assumes the resonance conditions

$$\mathbf{k} - \mathbf{k}_2 = \mathbf{k}_1, \quad \mathbf{k} + \mathbf{k}_2 = \mathbf{k}_3,$$

$$\omega_k - \omega_{k_2} = \omega_{k_1}, \quad \omega_k + \omega_{k_2} = \omega_{k_3}.$$

Two limiting cases are examined: the first in which the phases of the interacting waves are taken to be correlated over the interaction interval, and the second in which a chaotic phase relationship exists. In the latter case it is shown that for the four-wave case with one negative energy wave, all interacting with a weakly-turbulent plasma, explosive instability will always occur.

Vaynshteyn, B. I., V. I. Zenin, and I. L. Babichenko. On the effect of dynamic compression of explosive charges on detonability. IN: Detonatsiya vzryvchatykh veshchestv i bezopasnost' vzryvnykh rabot. Moskva, Izd-vo Nedra, 1967, 77-82.

A study is reported on the effect of explosive charge compaction on its detonability. Factors treated include crushing of explosive constituents and uneven compaction within the charge volume. It is found that crushing of components of type PZhV-20 ammonite, particularly trotyl, by dynamic

compression, causes no significant loss in detonability, nor does the uneven density resulting from the compression. It is assumed that the reduction in detonability of dynamically compressed explosives results from uneven density of the explosive in the direction of the diameter of the charge, associated with significant distortion of the shape of the detonation wave.

Dremin, A. N., S. A. Koldunov, and K. K. Shvedov. Shock wave-initiated detonation of low-density explosive charges. FGiV, no. 1, 1971, 103-111.

Detonation experiments using low-density (0.78-1g/cm^3) charges of TNT and tetryl are described. Particle size was 0.1-1 mm at 8-25 kbar initial shock wave pressure. All experimental wave velocity profiles during detonation transition exhibited a steady decay, in contrast to compacted and cast explosive charges. Energy liberation is consequently most intensive immediately behind the shock front. The depth profiles of the shock front parameters and the extent of the transition region depend on the initial shock pressure, as well as particle size and density.

Lidorenko, N. S. and A. V. Sidyakin. On the possibility of thermal explosion in fine metal powders. DAN, v. 202, no. 3, 1972, 566-569.

The phenomenon of sudden high temperature jump during the heating of fine metal powders and its subsequent almost instantaneous caking is explained using the characteristics of caking kinetics. The interdependence of the rate of caking and the temperature increase can lead to conditions analogous to thosenecessary for a heat explosion. Frenkel's (ZhETF, 16, 29, (1946)) model is used, where the process of powder caking is represented as the viscous flow of powder particles under the effect of surface tension forces. An advantage of this model, besides simplicity, is in its explanation of the process of the transformation of the surface energy of powder particles into heat. An equation describing caking kinetics was

obtained by Frenkel by equating the surface tension forces to the viscous friction acting on each particle. This model is applicable only for the extremely fine powder, with particle sizes of the order of 100 Å and low caking temperatures, when the viscous flow effect is predominant. Starting with the heat conductivity equation and equations derived for the Frenkel viscous flow model, the following well-known heat explosion equation is obtained:

$$\frac{\partial T}{\partial t} = \frac{\Theta}{\tau_0} e^{-E/T} + \chi \Delta T \qquad (1)$$

where T = powder temperature; $\Theta = (Z/4)(3\sigma/e\rho_0 a)$; Z = powder coordination number; σ = specific surface energy; c = heat capacity; a = particle radius; $\tau_0 = (2\eta_0 a/3\sigma)$; η_0 = characteristic constant; E = characteristic constant, ($E \gg T$); χ = heat conductivity of powder. The solutions to (1) agree with the experimental data depicted in Figure 1.

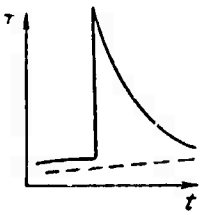

Fig. 1. Characteristic caking temperature T as a function of time. Solid line - $T > T_c$, Dotted line - $T < T_c$.

Independent of the model used to describe the caking phenomenon, the heat explosion equation gives a good estimate of the surface energy of the substance. This relationship has been experimentally confirmed. If the powder is placed in a container having a characteristic radius r, its behavior is determined by the so-called explosion parameter δ. (D. A. Frank-Kamenetskiy, Diffusion and heat transfer in chemical kinetics, M., 1967, ch. 7)

$$\delta = \frac{E\Theta}{T_0^2} \frac{r^2}{\chi} \frac{1}{\tau_0} \exp(-E/T_0) \qquad (2)$$

where T_0 = temperature of the container walls and r = characteristic radius of the container. For the values of $\delta < \delta_c$ (δ critical depends on the type of the container), a certain stationary temperature distribution prevails in the powder. For $\delta \geq \delta_c$, the stationary temperature distribution is no longer possible and a thermal explosion takes place. The rate of caking is deduced from the above equation, as well as T_c as a function of the system's size. The authors suggest that experimental verification of this equation would be satisfactory for other models, and point out that if it were so verified the value of self-diffusion activation energy would be definable.

Popov, V. N. and V. I. Chernyshov. Equation of state of a helium-nitrogen mixture. IAN Energ, no. 3, 1971, 162-165.

A procedure for statistical mechanical treatment of experimental compressibility data is described, to determine virial coefficients for He, N_2, and He-N_2 mixtures in the 273 - 773°K range of temperatures and at pressures to 400 bar. The virial coefficients B, C, D, E are given in polynomial form as functions of T. The coefficients of the polynomials are tabulated. The virial equations of state for He, N_2, and He-N_2 mixtures were developed from the described treatment of the experimental data. The equation of state for a He-N_2 mixture where the index m refers to the mixture,

$$z_m = 1 + B_m\rho + C_m\rho^2 + D_m\rho^3 + E_m\rho^4. \qquad (1)$$

describes the experimental results within $\pm$ 0.20%. Compressibility factors and density ρ values calculated from (1) were in satisfactory agreement with earlier experimental values over the experimental temperature and pressure ranges. This fact indicates that the caloric data calculated from (1) are sufficiently accurate and reliable for design of technological processes and solution of structural design problems.

B. Recent Selections

i. Shock Wave Effects

Adadurov, G. A., O. N. Breusov, A. N. Dremin, V. N. Drobyshev, and A. I. Rogacheva. Effect of dynamic pressure on subgroup IV oxides. FGiV, no. 2, 1971, 272-275. (RZhMekh, 4/72, #4V1195)

Adadurov, G. A., V. V. Gustov, and P. A. Yampol'skiy. Device for confinement of materials subjected to shock compression at varying pressures. FGiV, no. 2, 1971, 284-289. (RZhMekh, 4/72, #4V1525)

Aleksandrov, V. Ye., and L. I. Baron. Installation for studying the effect of an initial shock pulse during dynamic destruction. Zavodskaya laboratoriya, no. 11, 1971, 1394-1395. (RZhMekh, 4/72, #4V1189)

Barmin, A. A., and A. G. Kulikovskiy. Ionization and recombination fronts in a magnetic field. IN: Sbornik. Gidromekhanika, v. 5, 1970, Moskva, 1971, 5-31. (RZhF, 3/72, #3G54)

Batsanov, S. S., Ye. V. Dulepov, E. M. Moroz, L. V. Lukina, and V. V. Roman'kov. Effect of explosions on materials. Shock compression of rare earth metal fluorides. FGiV, no. 2, 1971, 266-269. (RZhMekh, 4/72, #4V1194)

Berezin, Yu. A., and G. I. Dudnikova. Thermal conductivity effect on the structure and critical parameters of shock waves in plasma. ZhPMTF, no. 2, 1972, 8-14.

Boyko, M. M., V. A. Letyagin, and V. S. Solov'yev. Experimental investigation of shock wave attenuation in steel. ZhPMTF, no. 2, 1972, 101-104.

Dubovik, A. V., V. K. Bobolev, and N. S. Malega. Effect of gas occlusion configuration in nitroglycerin charges on shock resistance. FGiV, no. 3, 1971, 412-418.

Gelunova, Z. M. Recrystallization of metals and alloys during shock wave treatment. IN: Sbornik. Vysokoskorostnaya deformatsiya. Moskva. Izd-vo Nauka, 1971, 80-84. (RZhF, 4/72, #4Ye523)

Golubinskiy, A. I., and V. A. Kazakov. Traveling shock wave flow around a moving plate. MZhiG, no. 2, 1972, 173-176.

Koriyev, V. M., and V. N. Solodovnikov. Axisymmetric form of stability loss of elastic cylindrical shells under shock. ZhPMTF, no. 2, 1972, 95-100.

Lepik, Yu. Propagation and reflection of large amplitude plane plastic waves in a thick plate. Uchenyye zapiski Tartuskogo universiteta, no. 277, 1971, 234-257. (RZhMekh, 4/72, #4V612)

Lyubimova, M. A. Density distribution in a rarefied wave generated by explosion of a diaphragm in a shock tube. ZhPMTF, no. 2, 1972, 130-131.

Nigmatulin, R. I., and N. N. Kholin. Physico-chemical processes during shock wave propagation in metals. MTT, no. 2, 1972, 189.

Otpushchennikov, Ye. N., S. Ya. Lovkov, and I. Kh. Kostin. Experimental investigation of stress concentration around a circular opening under the effect of a plane compression wave. Kontsentratsiya napryazheniy, no. 3, 1971, 106-112. (LZhSt, 15/72, #47780)

Soldatov, G. P. Nonlinear wave motion on a liquid surface. MZhiG, no. 2, 1972, 62-66.

Torelov, V. A., and L. A. Kil'dyushova. Experimental investigation of air ionization parameters in front of a strong shock wave. MZhiG, no. 6, 1971, 17-22.

Trofimov, V. S., and A. N. Dremin. Structure of a nonideal detonation front in solid explosives. FGiV, no. 3, 1971, 427-428.

Vysokoskorostnaya deformatsiya. Voprosy povedeniya metallicheskikh materialov pri impul'snom nagruzhenii. (High-speed deformation. Behavior of metallic materials under pulse loads.) Moskva, Izd-vo Nauka, 1971, 128 p. (RZhF, 4/72, #4Ye695K)

Wlodarczyk, E. Closed solution to a problem on plane shock wave propagation in a plastic polytropic medium with elastic unloading. Biul. WAT J. Dabrowskiego, no. 10, 1971, 31-41. (RZhMekh, 4/72, #4V610)

Yaremenko, D. N., I. D. Kedrin, V. M. Verchuk, Yu. S. Mikheyev, V. S. Ivanko, A. A. Rizhko, O. M. Dubovik, Yu. B. Ivanov, V. A. Tychinin, A. A. Vorotnikov, and A. I. Zhosan. Studies on deformation and destruction of a solid by a shock load. IN: Sbornik. Gidrodinamika, tverdoye telo. Dnepropetrovsk, 1971, 3-25. (RZhMekh, 4/72, #4V700)

Zhmayeva, Ye. A., and A. I. Kharitonov. Formation of a bow shock around blunt bodies in shock tubes. MZhiG, no. 6, 1971, 131-136. (RZhMekh, 4/72, #4B224)

ii. Hypersonic Flow

Antonov, A. M., and A. Y. Pashins'kiy. Asymmetric triangular plate with blunt leading edges in hypersonic flow. DAN UkrSSR, no. 12, 1971, 1083-1086. (RZhMekh, 4/72,

Borovoy, V. Ya., and V. N. Kharchenko. Experimental investigation of flow and heat transfer in the discontinuity zone of an axisymmetric body with a conic shield. MZhiG, no. 2, 1972, 35-40.

Chirikhin, A. V. Effect of nonequilibrium of free stream flow on shock wave detachment. Uchenyye zapiski TsAGI, no. 5, 1971, 122-125. (RZhMekh, 4/72, #4B220)

Chushkin, P. I. Supersonic flow around conical bodies. IN: Trudy Sektsii po chislovym metodam v gazovoy dinamike 2-go Mezhdunarodnogo kollokviuma po gazodinamike vzryva i reagiruyushchikh sistem. Moskva, v. 2, 1969, 87-106. (RZhMekh, 4/72, #4B216)

Druker, I. G., and L. Ya. Treyer. Flow calculation in the vicinity of the critical point during liquid coolant feed. ZhPMTF, no. 2, 1972, 44-48.

Gadion, V. N., V. G. Ivanov, G. I. Mishin, S. N. Palkin, and L. I. Skurin. Electronic and gas dynamic parameters of hypersonic wakes behind models moving in argon. ZhTF, no. 5, 1972, 1049-1055.

Gaponov, S. A., and A. A. Maslov. Numerical solution to problem of full stabilization of a supersonic boundary layer. ZhPMTF, no. 2, 1972, 39-43.

Ivanov, V. V., and A. V. Krasil'nikov. Pressure distribution on a delta wing with blunt edges at low angles of attack. MZhiG, no. 2, 1972, 166-169.

Mikhaylov, V. N., and V. S. Tamilov. Supersonic flow over an edge formed by intersecting plates. MZhiG, no. 2, 1972, 162-166.

Minostsev, V. B. Supersonic three-dimensional flow around segmented bodies. IN: Trudy Sektsii po chislovym metodam v gazovoy dinamike 2-go Mezhdunarodnogo kollokviuma po gazodinamike vzryva i reagiruyushchikh sistem. Moskva, v. 2, 1971, 68-86. (RZhMekh, 4/72, #4B222)

Morozov, M. G. Supersonic turbulent boundary layer characteristics. I-FZh, v. 22, no. 5, 1972, 885-889.

Musanov, S. V. Viscous gas flow with channel shear. Uchenyye zapiski TsAGI, no. 5, 1971, 26-34. (RZhMekh, 4/72, #4B196)

Polyanskiy, O. Yu. Effect of nonequilibrium processes on gas dynamic parameters in hypersonic devices and at the critical point of a blunt body. Uchenyye zapiski TsAGI, no. 5, 1971, 17-25. (RZhMekh, 4/72, #4B218)

Saltanov, G. A., and R. A. Tkalenko. Supersonic two-phase flow around a wedge. MZhiG, no. 2, 1972, 83-88.

Sigalov, G. F. Supersonic flow around slender bodies at Mach numbers near to unity. DAN UkrSSR, no. 11, 1971, 1023-1027. (RZhMekh, 4/72, #4B212)

Struminskiy, V. V., A. M. Kharitonov, and V. V. Chernykh. Laminar-to-turbulent boundary layer transition at supersonic speeds. MZhiG, no. 2, 1972, 30-34.

Stulov, V. N. Strong blowoff on a blunt body surface in supersonic flow. MZhiG, no. 2, 1972, 89-97.

iii. Soil Mechanics

Aliyev, A. M. Longitudinal wave properties at the base of the earth crust. DAN AzSSR, v. 27, no. 10, 1971, 55-57.

Gorbacheva, N. P. Effect of explosive detonation rate and charge construction on seismic explosion wave parameters in loess. FGiV, no. 2, 1971, 290-295. (RZhMekh, 4/72, #4V752)

Interpretatsiya i obnaruzheniye seysmicheskikh voln v neodnorodnykh sredakh. (Interpretation and detection of seismic waves in inhomogeneous media.) Moskva. Izd-vo Nauka, 1971, 180 p.

Kolesnikov, Yu. A., and L. N. Malinovskaya. Pulsed seismic waves. DAN SSSR, v. 204, no. 1, 1972, 80-83.

Kulikov, V. I., and A. F. Shatsukevich. Dissipation of detonation products from a confined cavity during an explosion in fill ground. FGiV, no. 3, 1971, 441-446.

Strel'chuk, N. A., G. L. Khesin, I. Kh. Kostin, Ye. V. Yureneva, V. B. Zateyev, and N. A. Freyshist. Solution of wave dynamics problems by a photoelasticity method. IN: Sbornik. VII Vsesoyuznaya konferentsiya po polyarizatsionno--opticheskomu metodu issledovaniya napryazh. Tallin, v. 3, 1971, 101-110. (RZhMekh, 4/72, #4V140)

Vovk, A. A., and A. V. Mikhalyuk. Wave process characteristics in a ground mass during explosions by air-casing charges. ZhPMTF, no. 2, 1972, 105-110.

Vovk, A. A., G. I. Chernyy, and A. V. Mikhalyuk. Effect of explosive properties on the effectiveness of explosions in soils. FGiV, no. 3, 1971, 446-450.

Yagodkin, G. I., M. P. Mokhnachev, and M. F. Kuntysh. Prochnost i deformiruyemost' gornykh porod v protsesse ikh nagruzheniya. (Strength and deformability of rocks under loading.) Moskva. Izd-vo Nauka, 1971, 148 p. (RZhMekh, 4/72, #4V837K)

Zakharov, M. N., and I. N. Ivashchenko. Theory of plastic flow in soils. MTT, no. 2, 1972, 185-188.

iv. Exploding Wire

Dolmatov, K. I. Current break during electric explosion of a wire. IAN Uzb, Ser. fiz-mat. nauk, no. 1, 1972, 97-98.

Kaliski, S. Cumulation of plasma and magnetic field during explosion of a heavy conductive shell. Biul. WAT J. Dabrowskiego, no. 11, 1971, 9-16. (RZhF, 4/72, #4G16)

Kaliski, S. Plane electromagnetic field cumulation under relativistic initial velocities of a conductive shell. Biul. WAT J. Dabrowskiego, no. 11, 1971, 17-23. (RZhF, 4/72, #4G7)

v. Equations of State

Dulov, V. G. Equations for three-dimensional stationary gas flow using special dynamic variables. IN: Trudy. Sektsii po chislovym metodam v gazovoy dinamike 2-go Mezhdunarodnogo kollokviuma po gazodinamike vzryva i reagiruyu hchikh sistem. Moskva, v. 2, 1971, 107-115. (RZhMekh, 4/72, #4B217)

Kolysko, L. E., L. V. Mozhginskaya, and E. Ya. Gorodinskaya. Measuring device for p-V-T-N data at low pressures. ZhFKh, no. 4, 1972, 1046-1048.

Malyshev, V. V. Equation of state for uranium hexafluoride over a wide range of state parameters. Atomnaya energiya, no. 4, 1972, 313.

Migdal, A. A. Equation of state near a critical point. ZhETF, v. 62, no. 4, 1972, 1559-1573.

Pal'tsev, L. A. Local equilibrium states for moderately dense gases. IN: Sbornik. Chislovyye metody mekhaniki sploshnoy sredy. Novosibirsk, v. 2, no. 3, 1971, 85-89. (RZhF, 3/72, #3Ye18)

Pridatchenko, Yu. V., and Yu. I. Shmakov. Rheological equations of state for weak polymer solutions with rigid ellipsoid macromolecules. ZhPMTF, no. 2, 1972, 125-129.

Rabotnov, Yu. N., and Yu. V. Suvorova. Deformation law for metals under uniaxial loading. MTT, no. 2, 1972, 189.

Savel'yev, G. Ya., and N. V. Shutov. Improved method for calculating virial coefficients. FGiV, no. 3, 1971, 451-453.

Vasserman, A. A., and A. Ya. Kreyzerova. Computerized method for synthesis of an equation of state for a liquid based on experimental P, V, and T data. ZhPMTF, no. 2, 1972, 119-124.

Zhdanov, V. A., and V. F. Konusov. Theory of an equation of state for solids. IN: Sbornik. Itogi issledovaniy po fizike 1917-1967. Tomsk, 1971, 87-102. (RZhF, 3/72, #3Ye458)

vi. Atmospheric Physics

Benediktov, Ye. A., G. V. Bukin, Yu. V. Kushnerevskiy, S. N. Matyugin, N. P. Mozerov, Yu. K. Perekhvatov, and M. D. Fligel'. Reception of Kosmos-381 satellite signals from a magnetic coupling region. Kosmicheskoye issledovaniye, no. 2, 1972, 302-303.

Ferdinandov, Ye. S. Ultrashort wave propagation in a heterogeneous isotropic plasma. Godishn. Vissh. Mash-elektrotekhn. in-t, no. 3, 1968, 39-46. (RZhF, 4/72, #4G222)

Khakimov, F. Kh. Potential mechanism for the existence of earth radiation belts. DAN TadzhSSR, v. 14, no. 9, 1971, 19-22. (RZhF, 4/72, #4G178)

Litvinova, T. P. Space-time function for correlation of wave amplitude fluctuation in a locally "frozen" turbulent atmosphere. IN: Trudy uchebnykh institutov svyazi. Ministerstvo svyazi, no. 54, 1971, 3-9. (RZhF, 3/72, #3Zh137)

Popov, G. V. Qualitative modeling of geophysical phenomena in the laboratory. IN: Sbornik. Fizika plazmy. Moskva. Izd-vo Atomizdat, no. 3, 1971, 61-69. (RZhF, 3/72, #3G27)

Shem'i-zade, A. E. Seasonal extremes in concentration of nuclear fission products in the atmosphere. Atomnaya energiya, no. 4, 1972, 350-352.

vii. Miscellaneous Explosion Effects

Anikina, L. D., D. K. Arkhipenko, N. S. Vartanova, T. N. Grigor'yeva, and V. I. Mali. Structural changes in mica from explosion effects. FGiV, no. 3, 1971, 436-440.

Bakhrakh, S. M., R. F. Trunin, A. V. Balabanov, N. P. Kovalev, V. A. Kotov, and Yu. K. Orekin. Initial stage of an explosion with ejecta. IAN Fizika Zemli, no. 12, 1971, 32-38.

Barzykin, V. V., E. A. Shtessel', F. I. Dubovitskiy, and A. G. Merzhanov. Heat transfer mechanism for thermal explosion of liquid explosives. FGiV, no. 2, 1971, 304-306.

Dubnov, L. V., V. A. Sukhikh, and I. I. Tomashevich. Nature of local microsources of decomposition in condensed explosives under mechanical effects. FGiV, no. 1, 1971, 147-149. (RZhMekh, 4/72, #4B754)

Korobeynikov, V. P. Third international colloquium on gas dynamics of explosions and reactive systems. MZhiG, no. 2, 1972, 192.

Merzhanov, A. G., and E. A. Shtessel'. Thermal explosions in liquid reactive systems with heat convection. FGiV, no. 1, 1971, 68-76. (RZhMekh, 4/72, #4B715)

Remizova, N. I. Elastic wave propagation in a three-dimensional medium under the effect of a concentrated impulse. IN: Sbornik. Teoreticheskaya i prikladnaya mekhanika, no. 2, 1971, 3-6. (RZhMekh, 4/72, #4V114)

Rodionov, V. N., and A. P. Sukhotin. Elastic wave parameters during spherical explosions in metals of various strengths. FGiV, no. 1, 1971, 142-146. (RZhMekh, 4/72, #4V133)

Vashchenko, V. I., Yu. N. Matyushin, V. I. Pepekin, and A. Ya. Apin. Explosion energy of water-saturated hexogene. FGiV, no. 3, 1971, 429-432.

Zakharenko, I. D., and T. M. Sobolenko. Thermal effects in the coupling zone during explosive welding. FGiV, no. 3, 1971, 433-436.

Zinchenko, A. D., V. N. Smirnov, and A. A. Chvileva. Measurement of electrical conductivity of explosion products in detonation of TG 40/60 cast compounds. FGiV, no. 3, 1971, 422-426.

3. Geosciences

A. Abstracts

Bulin, N. K. New data on the crustal structure of the Baltic shield. IN: AN SSSR. Doklady, v. 198, no. 3, 1971, 657-660.

The deep structure of the Earth's crust in the Baltic shield has been studied by deep seismic sounding (DSS) as well as by seismological and gravimetric methods. DSS data were obtained along four profiles in the northern part of the shield, while seismological data were obtained along the 350-km-long Vyborg - Sortavala - Spaskaya Guba profile, as well as at four permanent seismograph stations (see Figure 1). The article describes the results of seismological research and gives an estimate of the crustal thickness for the entire Baltic shield.

(Continued with figure on next page)

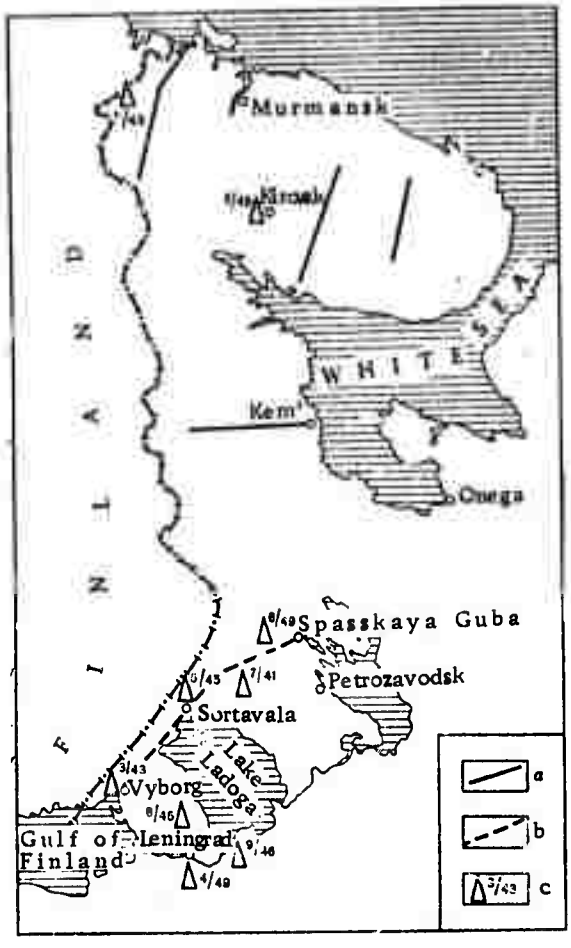

Fig. 1. Location of Profiles and Seismographic Stations in the Eastern Part of the Baltic Shield.

a - DSS profiles (1958-1965); b - seismographical profile (1965-1967); c - permanent or mobile seismographic stations; (1 - 4 - stations of the USSR Academy of Sciences, 5 - 9 mobile stations (number in denominator is the average crustal thickness, based on earthquake converted waves, in km).

The section along the Vyborg - Spaskaya Guba profile (shown in Fig. 2) was determined from both converted PS and compressional waves generated by distant earthquakes and engineering explosions.

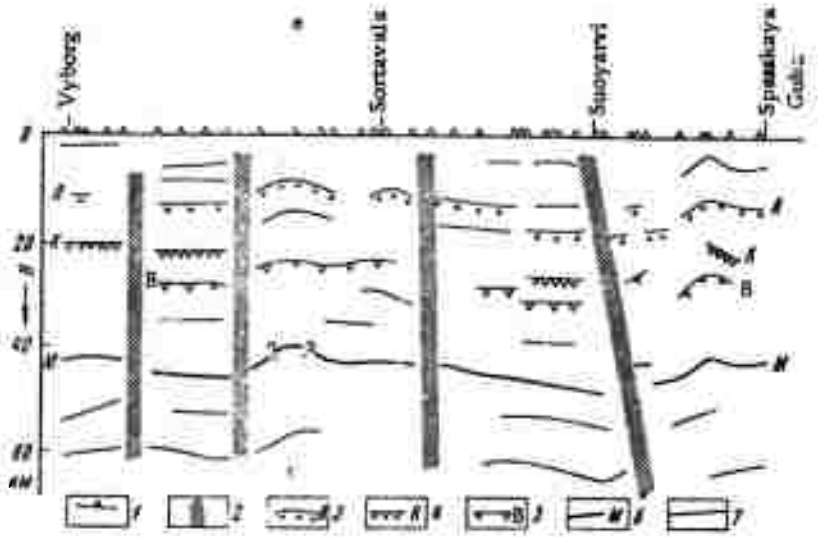

Fig. 2. Section of the Southern Part of the Baltic Shield (simplified), Constructed using Converted PS Waves of Earthquakes and Explosions (1965-1967). 1 - recording points reduced to the profile line; 2 - zones of abrupt changes of the characteristics of the section and conversion interface relief, possibly related to deep-seated faults; 3 - 7 - averaged position of the seismic horizons (conversion interfaces): 3 - A horizon in "granite" layer, 4 - Conrad discontinuity, 5 - horizon in "basaltic" layer, 6 - Mohorovicic discontinuity; 7 - other (unidentified) conversion interfaces in the crust and upper mantle.

As can be seen in Figure 2, the crust and upper mantle are distinctly divided into blocks down to the depths of 60 km. A refracting interface with a refractor velocity v_r = 6.8 km/sec at a depth of about 10 km and a refracting-reflecting interface with v_r = 8.5 km/sec at a depth of 47-51 km have been identified by compressional waves. The latter has been interpreted as the Mohorovicic discontinuity. The main seismic discontinuities identified through earthquake converted waves are the M horizon in the 39-50 range and the A horizon in the 8.5 - 18 km range (corresponds to the refracting interface with v_r = 6.8 km/sec).

The average parameters of the crustal layers are: 1) crustal thickness is 44 $\pm$ 5 km, 2) depth to the A horizon is 13 $\pm$ 5 km, while the thickness of the layer bounded by the A and M horizons is 30.5 $\pm$ 1.5 km, 3) the ratio of the thicknesses of the upper (above the A horizon) and lower parts of the crust is 0.43. Thus, the depth to the Mohorovicic discontinuity in the southern part of the shield exceeds the previously accepted depth by 5-15 km or more (based on gravity data).

The average crustal parameters obtained previously by DSS along a 100-km-long segment of the Pechenga - Lovno profile are reviewed. From this review, it was determined that: 1) the depth to the Mohorovicic discontinuity is 42 $\pm$ 3 km; 2) the depth to the horizon with v_r = 6.8 km/sec is 13 km and the thickness of the "layer" with velocity v_p = 6.8 - 7.5 km/sec (lower part of a "granulite - basite" layer, after Litvinenko, 1968) is 29 km; and 3) the ratio of the thicknesses of the upper (above the horizon with v_r = 6.8 km/sec) and lower parts of the crust is 0.45.

On the basis of seismological studies in the southern part of the shield, very reliable results from DSS, and data obtained in Finland, the crustal thickness of the Baltic shield has been estimated to be 38 - 50 km, with an average value of 42 - 44 km. This estimate of the crustal thickness of the Baltic shield is in agreement with DSS data on the Ukraine and Voronezh crystalline massifs (Kosminskaya, I. P., et al. Geofiz. byull. Mezhvedomstv. geofiz. komit. no. 20, 1969). Based on the present data derived for the Baltic shield, it is recommended that previously derived data (Deminitskaya, R. M., Kora i mantiya Zemli, 1967), be reinterpreted, since they yield a 10-15 km lesser thickness value for the Baltic shield as compared with the Ukrainian shield and Voronezh massif.

Andreyev, A. A. Some general problems of the crustal structure of Sakhalin, based on deep seismic sounding and gravity data. Geologiya i geofizika, no. 2, 1971, 61-68.

A combined interpretation of deep-seismic sounding (DSS) and gravity data, measured on the island of Sakhalin, was conducted to obtain additional information on the deep structure of the crust in the region. In this article, sections along profiles VI - VI and III - III (see Fig. 1) are discussed, with emphasis on the geological interpretation of velocity (or density) discontinuities within the sedimentary cover.

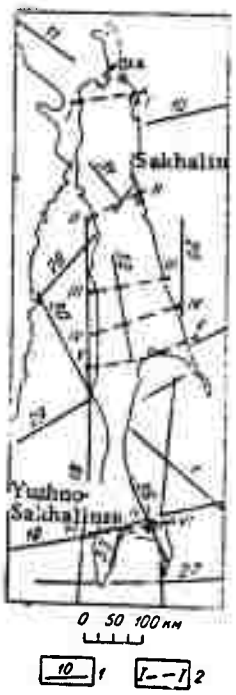

Fig. 1. Location of Profiles.
1 - DSS profiles and their numbers.
2 - geological-geophysical sections.

The section along profile VI - VI was derived from DSS data from profile 19 and gravimetric data, as shown in Figure 2. The velocity discontinuities were interpolated so that their morphology satisfied the observed Δg field.

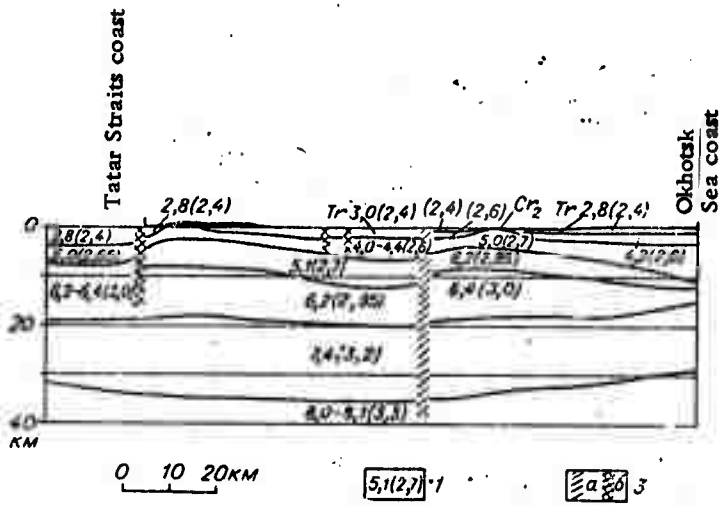

Fig. 2. Section VI - VI.

1 - velocities (densities) 3 - faults:
a) from geophysical data and
b) from geological-geophysical data.

Seismic discontinuities with v_r = 4.8 and v_r = 5.0 - 5.1 km/sec, observed in the West Sakhalin mountains, Susunay depression, and Korsakov plateau regions, are interpreted as the surface of the Upper Cretaceous and Mesozoic - Paleozoic formations, respectively. However, in the Tartar Straits region, which is characterized by a density distribution different from adjacent regions, two seismic discontinuities with v_r = 5.0 and 6.2 - 6.4 km/sec were assumed to correspond to the above interfaces. Seismic discontinuities with v_r = 7.4 and v_r = 8.0 - 8.1 km/sec observed over the entire profile were interpreted as the top of basaltic layer and the bottom of the crust, respectively. The crust is divided into blocks in the upper portion (above the basaltic layer), with the blocks being characterized by different velocity and density distributions. Gravity effect computed for the above interfaces showed that no single interface constitutes the predominant part of the calculated Δg anaomalies.

The section along profile III - III was constructed using seismic (DSS profiles 18, 20, 30 and a RWCM profile) and gravity data (profile III - III). Two versions of the sections which differ only in the structure of the sedimentary cover are shown in Figures 3a and 3b.

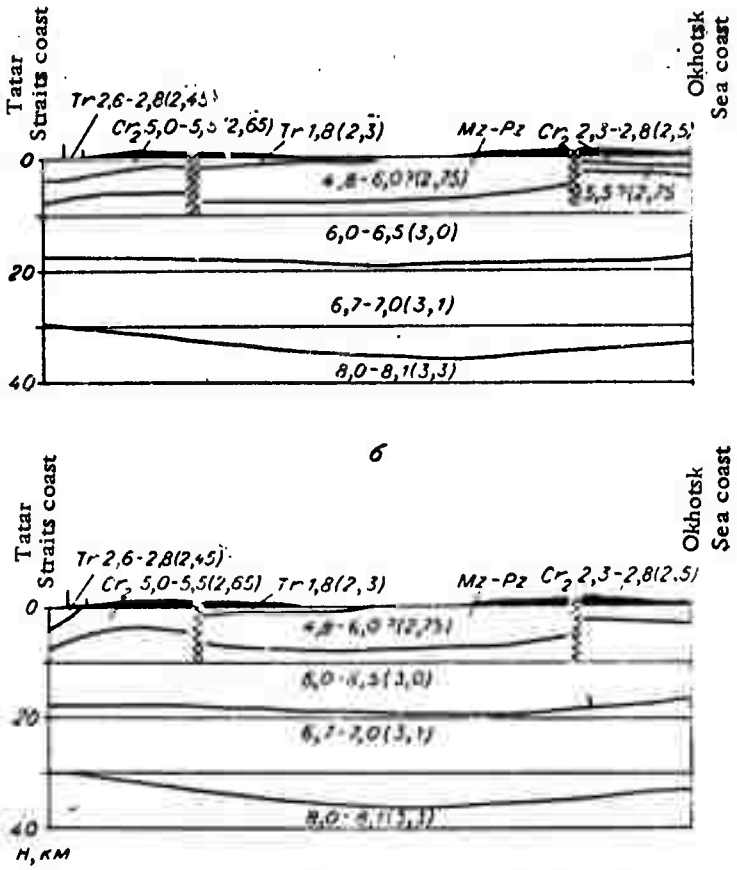

Fig. 3. Two Versions of the Section Along Profile III - III.

The crust is divided into three blocks corresponding to 1) the West Sakhalin anticlinorium, 2) the Poronay depression and western part of the East Sakhalin anticlinorium, and 3) the eastern part of the East Sakhalin anticlinorium. Velocity discontinuities with v_r = 8.0, 6.7 - 7.0, and 6.0 - 6.5 km/sec are interpreted as the Mohorovicic discontinuity, the top of basaltic layer, and an interface underlying some volume of Mesozoic-Palezoic rock, respectively. It is concluded that the results obtained confirm the existence of faults extending to a depth of 8 - 10 km, and that the crustal thickness beneath the axial part of the island of Sakhalin amounts to 33 - 35 km.

Antonenko, A. N., and G. K. Dubrovin. Structural characteristics of the upper mantle of Mugodzhary. IN: AN KazSSR. Institut geologicheskikh nauk. Trudy, no. 30, 1971, 22-28.

A comprehensive analysis of geophysical data obtained in the central Ural and Mugodzhary regions is made, and certain assumptions are derived on the structure of the upper mantle beneath the Mugodzhary folded system. The results of seismological, magnetotelluric, geothermal, and gravimetric studies are briefly reviewed. The following manifestations led to the hypothesis of the existence of a structural block in the upper mantle of the Mugodzhary folded system: a) a conversion interface at a depth of 150-155 km; b) azimuthal anomalies of $\pm 4^{o}$ (observed) and $\pm 11^{o}$ (actual) for distant earthquakes; and c) the presence of a high-conductivity layer with its surface at a depth of 160-200 km.

The upper boundary of the block is assumed to coincide with the Mohorovicic discontinuity and its lower, with a conversion interface at 150-155 km; its thickness is 100 km with its width corresponding to the Mugodzhary system. Its existence is confirmed by gravimetric and geothermal data (low temperature gradient), as well as seismological data (foci of local earthquakes in the upper mantle). The block is characterized by high seismic-wave velocity, excessive density, relative coolness, high specific resistivity, and significant viscosity. It is surrounded by a low-velocity layer with its depth of occurrence at 80-100 km. In the adjacent Tyumen - Kustanay downwarp, the eastern part of the Russian platform, and the northern Ciscaspian depression regions, the proximity of this layer to the diurnal surface causes regional negative Δg anomalies and high geothermal gradients.

Suvorov, V. D., S. V. Krylov, A. L. Rudnitskiy, and A. L. Krylova. Deep seismic studies of the Earth's crust on the south of the West Siberian Platform. Geologiya i geofizika, no. 5, 1971, 110-117.

A study of the deep crustal structure of the West Siberian platform has been conducted using point deep-seismic sounding along the 600 km long Ishim - Barabinsk profile. The techniques of generating and recording

of seismic waves, as well as the dynamic and kinematic characteristics of the recorded wave fields, are discussed. As a result of the study, data have been obtained on crustal layering, the block structure of the consolidated crust, and the relief of the Mohorovicic discontinuity. The velocity section along the Ishim - Barabinsk profile is shown in Figures 1a and 1b.

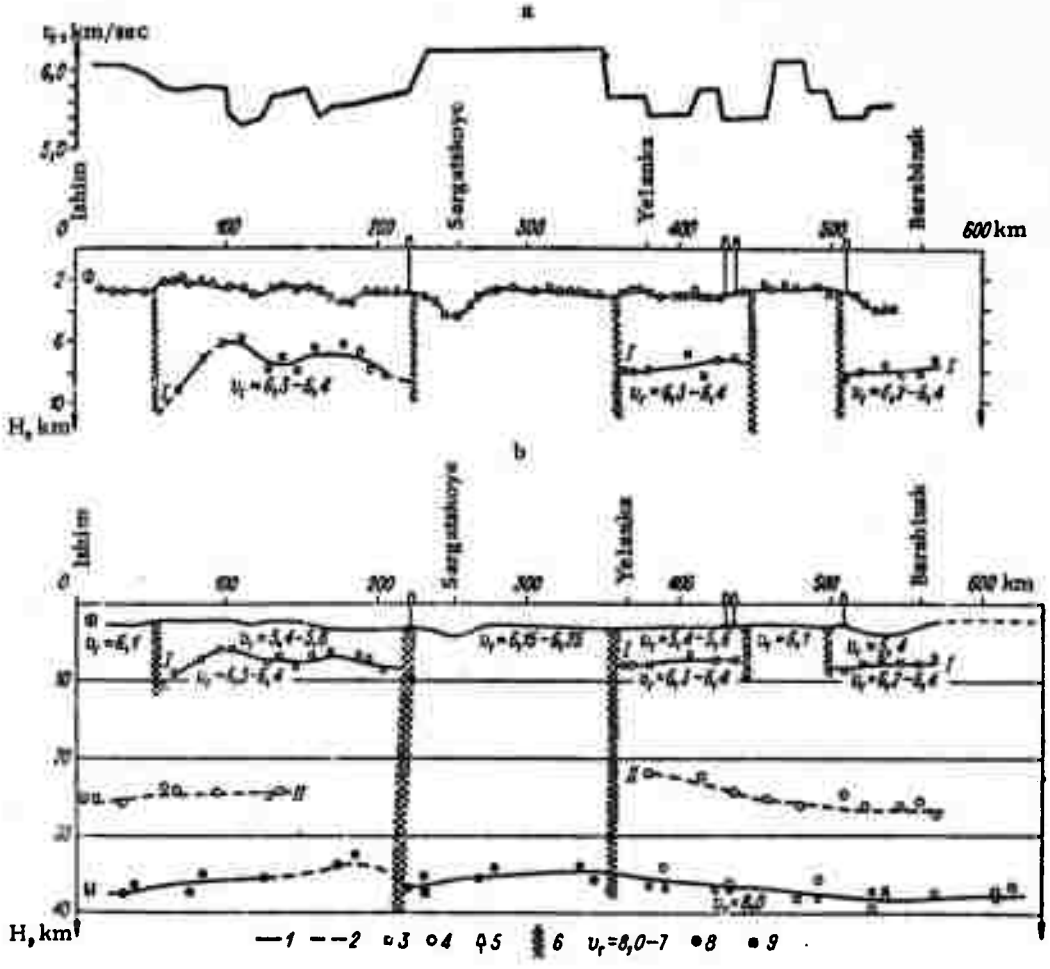

Fig. 1. Velocity Section of Ishim - Barabinsk Profile.

a - Velocity section of the upper part of the crust and graph showing refractor velocity at the surface of the basement. b - Velocity section of the crust: 1 - seismic interfaces, Φ - surface of Prejurassic basement, I - II - intercrustal interfaces, M - Mohorovicic discontinuity; 2 - interfaces from less reliable data; 3 & 4 - depths from refracted and reflected waves; 5 - boreholes; 6 - probable zones of deep-seated faults; 7 - refractor velocity, km/sec; 8 & 9 - II type record of waves from the Mohorovicic discontinuity.

The basement surface is a sharp discontinuity with v_r = 5.3 - 6.2 km/sec at a depth of 2 - 4.5 km. It separates the Mesozoic-Cenozoic sedimentary cover (layer velocity 2.6 km/sec) and the consolidated crust. The bottom of the crust is at a depth of 35 - 38 km, with a refractor velocity of 8.0 km/sec (determined only for the eastern segment of the profile). The mean layer velocity of the consolidated crust is 6.4 km/sec. In the upper part of the consolidated crust, two interfaces have been identified: intermittent refracting surface I at a depth of 6 - 10 km (v_r = 6.2 - 6.4 km/sec) and reflection surface II at a depth of 22 - 26 km, which was not observed with sufficient confidence along the entire profile.

Three large blocks with differing deep structures and velocity distribution have been identified and designated as follows:

1. The western block is separated by a zone of deep-seated faulting on the east. Its crustal thickness amounts to 34 - 38 km. The basement surface is characterized by a significant variation of refractor velocity, i.e., 5.4 - 6.1 km/sec. Refracting surface I is at a depth of 6 - 10 km, with v_r = 6.3 - 6.4 km/sec. Reflecting surface II at 24 - 26 km is not identified with sufficient confidence.

2. The central block which is characterized by a more homogeneous consolidated crust and basement surface, with a stable refractor velocity of 6.25 km/sec. The depth to the Mohorovicic discontinuity is 35 - 36 km, and it is a very sharply defined seismic discontinuity, as in the western block.

3. The eastern block is separated by the Omsk zone of deep-seated faults on the west. The upper part of the consolidated crust is characterized by very sharp heterogeneity. The basement surface plunges from 2.5 to 4.0 km in the Barabinsk region. Refracting surface I is at a depth of 7 - 8 km, with v_r = 6.2 - 6.7 km/sec. Reflecting surface II plunges smoothly toward the east from 22 to 26 km. The Mohoricic discontinuity in this block is not as sharply defined a discontuity as in the other two blocks.

Puchkov, S. V., and D. Garagozov. Calculation of the effects of ground-water level on ground-motion intensity during earthquakes. IN: AN TurkSSR. Izvestiya. Seriya fiziko-tekhnicheskikh, khimicheskikh i geologicheskikh nauk, no. 4, 1971, 55-63.

The effect of the ground water level in unconsolidated sandy-clayey soil on the intensity of ground motion during earthquakes is considered. A method for calculating motion velocity in compressional and shear waves in the ground-water level is developed as are formulas for evaluating the increase in earthquake intensity due to the change of the ground-water level. It is determined that motion velocity in seismic waves varies with the depth of the ground-water level according to a hyperbolic law with an exponent of 1/6. The increment of intensity of an earthquake due to a change of the depth of ground water level from z_2 to z_1 can be expressed as $\Delta B = 1.1 \log \frac{z_2}{z_1}$, where $z_2 > z_1$.

An experimental hyperbolic curve representing the dependence of the increment of the earthquake intensity on the ground water level has been obtained for the Ashkhabad district. It was found that ground water at depths exceeding 10-12 m does not affect ground-motion intensity at the surface. However, ground water at shallower depths has a considerable effect on the intensity of ground motion.

Bezrodnyy, Ye. M. Seismic shear-wave reflections from the Conrad discontinuity, based on seismological data. IN: Uzbekskiy geologicheskiy zhurnal, 1971, 1, 20-23.

An analysis of kinematic and dynamic characteristics of shear waves from the Tashkent earthquake aftershocks was made for the purpose of demonstrating the possibility of recording near-normal (subcritical) reflections of SH waves from crustal interfaces. On the basis of the analysis of observational data and the velocity distributions for the region, four pronounced phases of shear waves were identified. These were interpreted as: $\bar{S}'$ and $\bar{S}''$ - waves singly and doubly reflected between the free surface and the Paleozoic basement; and S'_k - waves

reflected from a crustal interface at a depth of 12-15 km. Taking into account the kinematic characteristics of S'_k waves and previously obtained data on the Conrad discontinuity ($H \approx 10$ km), the conclusion was drawn that there exist possibilities for recording near-normal reflections from the Conrad discontinuity. The "shadow" zone observed for S'_k waves was explained as due to a zone of crushed rock within the focus of the Tashkent earthquake.

Kurbanov, M., and V. I. Lykov. The relationship of recent tectonic movements and the seismicity of southern Turkmeniya to characteristics of crustal structure. IN: AN TurkSSR. Izvestiya. Seriya fiziko-tekhnicheskikh, khimicheskikh i geologicheskikh nauk, no. 1, 1972, 32-37.

A comprehensive analysis of seismological, geodetic, and geological data was conducted to determine the relationship between recent tectonic movements and the seismicity of southern Turkmeniya to its tectonic structure. Releveling showed continuing formation of structure of the first kind in the Ciskopetdag downwarp region, where negative structures are characterized by the negative sign of recent motion. The faults identified as being transverse to the trend of the downwarp coincide with zones of changes of sign of recent motions. The zones of highest velocity gradient of recent motions coincide with the zones of deep-seated faults occuring in recent times. The hypocenters of earthquakes are concentrated along these faults, from the uppermost part of the crust down to the upper mantle. The intersection of two systems of regional faults characterized by opposite horizontal motions leads to the formation of zones of compression and tension. A circular seismically active zone of the transcrustal type divides the South Caspian intrageosynclinal megadepression (with a suboceanic crust) from regions with continental crust. Recent vertical movements of the Earth's surface in southern Turkmeniya are the result of tectonic development of a vast region of southwestern Asia.

Zunnunov, F. Kh. Interpretation of reflected waves in deep seismic sounding. IN: AN UzSSR. Doklady, no. 10, 1970, 50-52.

The problem of selecting the effective velocity for the interpretation of time distance curves of reflected waves in DSS is discussed.

The effective velocity in the layer above the Mohorovicic discontinuity was evaluated from the time distance curves of normal and wide-angle reflections using the method of velocity model selection based on the equality of distances between actual and apparent shot points. Time distance curves were computer converted into lines $\frac{t_{oi}(x)}{2}$ using velocities of 6000, 6200, 6400, and 6600 m/sec. It was found that the best result was obtained with a velocity of 6200 m/sec. The time distance curve converted with that velocity was then used for plotting the seismic section.

Yepifanov, A. A. The crustal thickness in eastern and central Ciscaucasia. IN: AN GruzSSR. Soobshcheniya, v. 65, no. 2, 1972, 313-315.

The mapping of the Mohorovicic discontinuity beneath the eastern and central Ciscausasian region has been accomplished based on multi-parameter correlation of seismic and gravimetric data. Multiparameter correlative equations $H_M = f\ \Delta g_{res,h}$ (where H_M - depth of the Moho discontinuity, $\Delta g_{res,h}$ - residual gravity anomaly) obtained for two DSS profiles were extrapolated throughout the entire region. The crustal thickness over a large part of eastern and central Ciscaucasia does not vary significantly, and the minimum thickness of 40 km occurs in a belt confined to the Manych downwarp system. It increases slightly toward the north reaching 42-43 km, while it increases considerably toward the south. The maximum thickness of 62-63 km corresponds to the central zone of the Greater Caucasus. Another depression in the Mohorovicic discontinuity is confined to the eastern zone of the Greater Caucasus where the crustal thickness is 53 km.

Bulin, N. K., Ye. A. Fronyayeva, V. I. Bubnova, V. N. Tolmanov, and Ye. I. Erglis. The deep structure of the southwestern Altay region from seismological data. Sovetskaya geologiya, no. 4, 1969, 97-109.

An analysis was made of PS, P and S waves recorded by mobile, permanent, and temporary seismographic stations from (a) distant, nearby, and local earthquakes and (b) engineering explosions. The purpose of the analysis was to study the deep structure of the crust and upper mantle in the southwestern Altay region. In the May-October 1966 period, observations were conducted with mobile seismographic stations at 51 points along the Charsk - Leninogorsk (I - I) and Kokpetky - Zyryanovsk - Stolboukha (II - II) profiles, as well as at several regional seismographic stations (see Fig. 1).

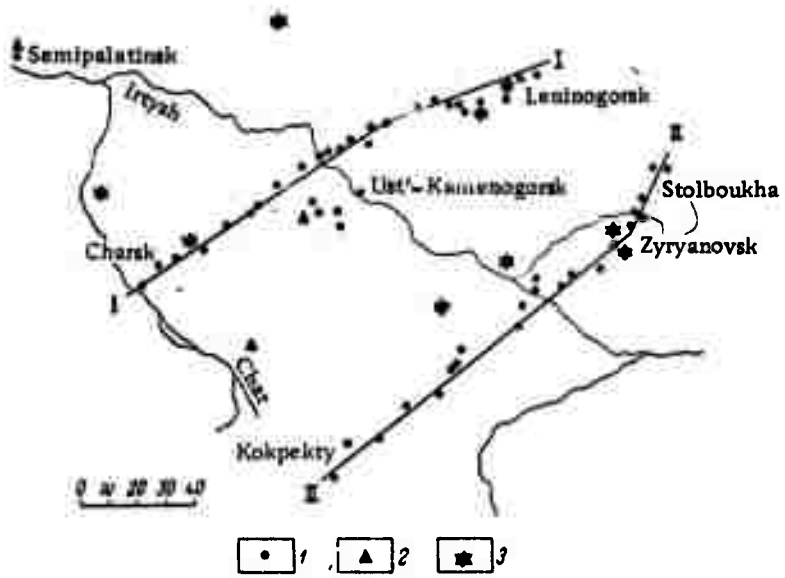

Fig. 1. Chart Showing Seismographic Stations, Shot Points, and Profiles.

1 - Points of observation by mobile seismographic stations;
2 - permanent and temporary seismographic stations; and
3 - shot points of engineering explosions.

Sections (see Fig. 2a and 2b) along the profiles were derived from seismological data, taking into account existing data on gravity and magnetic anomalies and the density and magnetization of rock in southwestern Altay and adjacent regions.

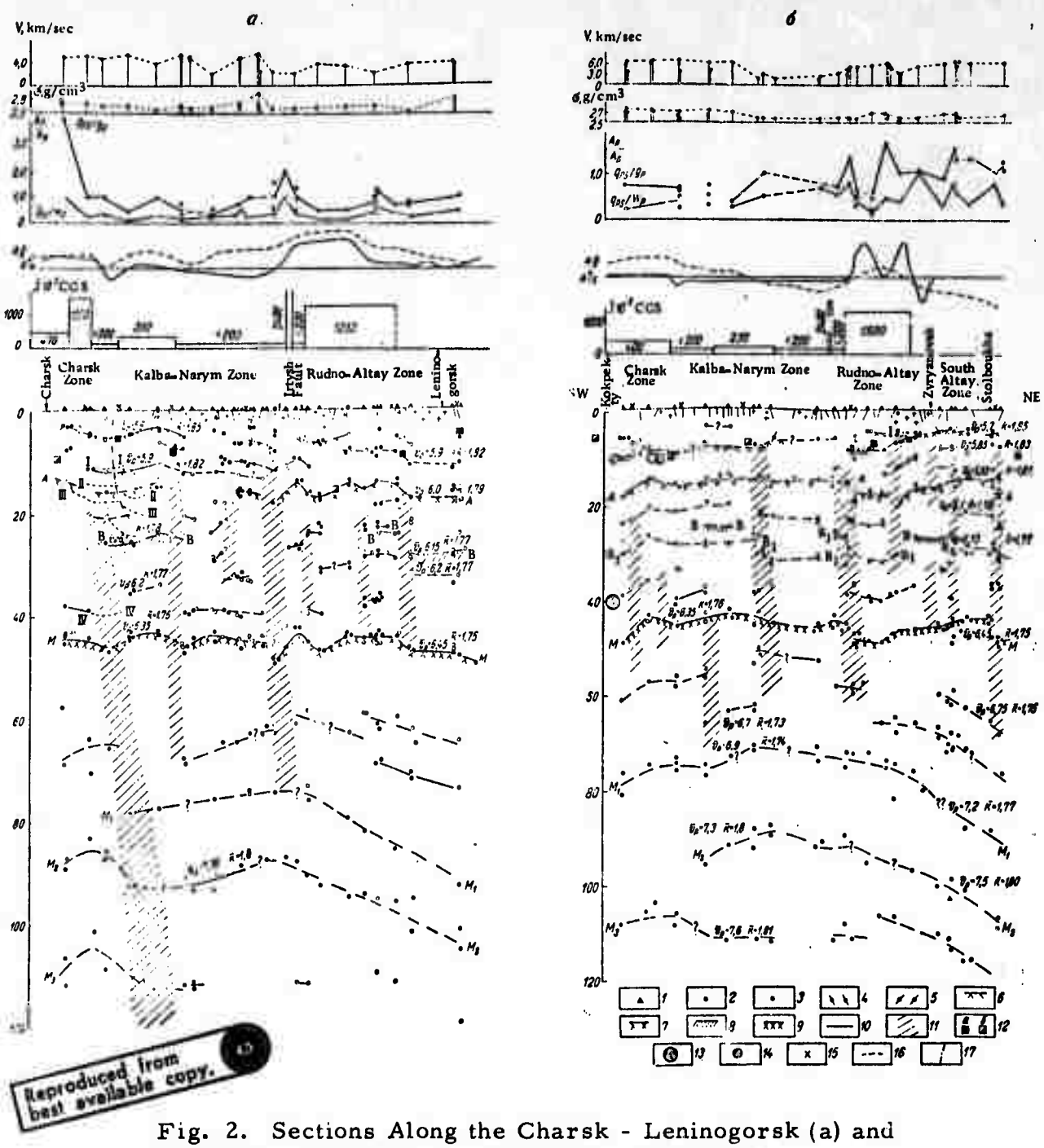

Fig. 2. Sections Along the Charsk - Leninogorsk (a) and Kokpekty - Zyryanovsk - Stolboukha (b) Profiles.

1 - Observation points; 2 - depth of conversion interface, based on reliable observation data on PS waves from distant earthquakes; 3 - the same, based on less reliable data; 4 - the same, based on nearby earthquakes; 5 - the same, based on engineering explosions; 6 - Predevonian basement surface; 7 - reference horizon A;

8 - horizon B (Conrad surface); 9 - Mohorovicic discontinuity 10 - strong conversion interfaces in the upper mantle; 11 - deep-seated fault zone; 12 - lower edges of magnetized bodies (a) less than 30 km from the profile and (b) 30 — 60 km from the profile; 13 - earthquake hypocenters K = 10; 14 - K = 7 - 9; 15 - faults, based on geological data; 16 - reflecting horizons, based on seismic prospecting data; 17 - faults, based on seismic prospecting data. Curves above sections represent: maximum V_P distribution; maximum density (σ) distribution; distribution of the relative amplitudes of the horizontal components of compressional (q_P) and converted (q_{PS}) and waves for the Mohorovicic discontinuity (W_P is the vertical compression wave component); distribution of magnetic (ΔTa) and gravity (Δg) anomalies; and mean rock magnetization (J).

The following conversion interfaces are identified:

1. A conversion interface at a depth of 3.2 - 9.0 km (corresponding v_r = 5.7 - 6.1 km/sec), interpreted as the surface of the Predevonian basement or as the surface of the consolidated crust. Its depth gradually increases in a southeasterly direction.

2. Horizon A at a depth of 13 - 19 km, interpreted as an interface within the "granitic-metamorphic" layer.

3. Horizon B at a depth of 23 - 29 km (v_r = 6.7 - 6.8 km/sec), interpreted as the surface of the "basaltic" layer or Conrad discontinuity.

4. Horizon M at a depth of 42 - 50 km (v_r = 8.1 - 8.3 km/sec), interpreted to be the Mohorovicic discontinuity.

5. Horizons M_1, M_2, and M_3 at depths of 72 - 93, 83 - 108, and 103 - 114 km, respectively. These horizons plunge in a northeasterly direction.

The Mohorovicic discontinuity was mapped, with two zones of minimum depths (43 - 45 km) observed which are confined to the Charsk - Kalba -Narym and Rudno-Altay structural zones. Maximum depths (48 - 50 km) were observed in a narrow band which corresponds to the Irtysh folded zone.

The majority of the vertical seismic discontinuities identified were confidently interpreted as deep-seated fault zones. All of these, except for the Charsk zone, are characterized by an almost vertical dip. The Charsk and Kalba-Narym faults extend to a depth of 130 km, while others are considerably less deep.

The relief of the Mohorovicic discontinuity and crustal thickness compare favorably with results derived from gravity and seismic data; however, a significant number of previous determinations of crustal thickness are 5 - 10 km less than those derived in the present article.

Kondorskaya, N. V., and A. R. Rakhimov. Results on the computer determination of the focal position of the 1948 Ashkhabad earthquake, using observations of the WWNSS. IN: AN TurkSSR. Izvestiya. Seriya fiziko-tekhnicheskikh, khimicheskikh i geologicheskikh nauk, no. 3, 1971, 53-62.

Computer calculations of the coordinates of the 1948 Ashkhabad earthquake focus have been carried out using the observational data of the world-wide network of 134 seismograph stations, within a focal distance range of 7 - 130°. Epicentral coordinates were calculated at fixed focal depths (h = 0, 10, 15, 33) from various sets of data: seismograms recorded at 134 stations with Δ=7 - 130° and seismograms recorded by 70-80, 48-50, 30-32, 20-22 and 10-12 distant stations with Δ >20°. The results obtained are shown in the form of tables and polar diagrams. The accuracy of determination of epicentral coordinates is discussed and found to be sufficiently high with a 0°.1 semi major axis of "error" ellipse. It was shown that epicentral coordinates do not vary with fixed focal depth, when only a network of distant stations with Δ >20° is used for the calculation, and that the network of 48-50 stations uniformly distributed around the epicenter at a distance Δ >20° provided limited accuracy. A focal depth of about 25 km was determined with rather low accuracy, since the nearest observation station was at Δ = 7°. The coordinates of the epicenter were compared with the results obtained by macroseismic study of the earthquake. The epicenter of the Ashkhabad earthquake, as determined from instrumental data, was found to be shifted by 20 km toward the northeast with respect to the epicenter determined from macroseismic data.

Kurbanov, M., K. Dzhamanov, and T. Tokareva. Tilt observations in the Ashkhabad area. IN: AN TurkSSR. Izvestiya. Seriya fiziko-tekhnicheskikh, khimicheskikh i geologicheskikh nauk, no. 5, 1971, 124-127.

Data from tilt measurements in the seismically active area of Ashkhabad and the parameters of earth tides computed from these data are examined. Observations during December 1968 - September 1970 were conducted at the Ashkhabad station by two sets of tiltmeters along the N-S and E-W directions, and the positioning and installation of the instruments is described. A tilt of the earth's surface of 4 arc seconds (northward) along the N-S leg and 1.25 arc seconds (eastward) along the E-W leg were observed over the above period. The average values of tidal parameters were computed by two methods, with values of $\gamma_{M2} = 0.784$ and $\gamma_{M2} = 0.781$ obtained by the Matveyev and Pertsev methods, respectively. The results differ significantly from results previously obtained for the same area, as well as from the results for adjacent central Asian regions.

B. Recent Selections

Akhmedov, G. A., et al. Status of and future tasks in geophysical research projects on the problem of Mesozoic oil in Azerbaydzhan. IN: AN Azer SSSR. Izvestiya. Seriya nauk o Zemle, no. 4, 1972, 8-16.

Aliyev, A. M. Study of the properties of compressional waves near the base of the crust. IN: AN Azer SSR. Doklady, v. 37, no. 10, 1971, 55-57.

Anikina, L. D., et al. Changes in the structure of micas due to explosion effects. Fizika goreniya i vzryva, no. 3, 1971, 436-440.

Belyayevskiy, N. A Deep crustal structure of the USSR. Priroda, no. 4, 1972, 32-43.

Constantinescu, L. General outline of precursor events for strong earthquakes. Studii si cercetari de geologie, geofizica si geografie. Seria geofizica, v. 10, no. 1, 1972, 16-22.

Enescu, D., et al. Structure of the Earth's crust and upper mantle in the Carpathian curvature. Studii si cercetari de geologie, geofizica si geografie. Seria geofizica, v. 10, no. 1, 1972, 23-41.

Kalinin, V. A. A universal equation of state for solids. IN: AN SSSR. Izvestiya. Fizika Zemli, no. 4, 1972, 16-23.

Khitarov, N. I., et al. Melting and crystallization of quartz tholeite under high pressure, and the evaluation of tholeite magmas under abyssal conditions. Geokhimiya, no. 4, 1972, 428-436.

Krylov, S. V., et al. Deep seismic research in Zabaykal'ye Geologiya i geofizika, no. 12, 1971, 108-112.

Kulikov, V. I., and A. F. Shatsukevich. Leakage of detonation products from a confined cavity during an explosion in embanked soil. Fizika goreniya i vzryva, no. 3, 1971, 441-446.

Mamedov, S. G. Use of the correlations between the depths of occurrence of boundaries of basic crustal discontinuities and Bouguer anomalies in Azerbaydzhan. Azerbaydzhanskoye neftyanoye khozyaystvo, no. 3, 1972, 8-10.

Misharina, L. A., and N. V. Solonenko. Stresses in the foci of weak earthquakes in Pribaykal'ye. IN: AN SSSR. Izvestiya. Fizika Zemli, no. 4, 1972, 24-36.

Purcaru, G., and D. Zorilescu. Modeling the occurrence of Vrancea intermediate earthquakes and their informational characteristics. Studii si cercetari de geologie, geofizica si geografie. Seria geofizica, v. 10, no. 1, 1972, 87-102.

Radu, C., and D. Jianu. Study of the 21 December 1969 earthquake. Studii si cercetari de geologie, geofizica si geografie. Seria geofizica, v. 10, no. 1, 1972, 43-54.

Shcherbakova, B. E. Nature of waves recorded with "Zemlya" equipment in areas of eastern Siberia. Sovetskaya geologiya, no. 4, 1972, 88-101.

Shutkin, A. Ye. Elastic-wave velocity in the permafrost rock of the Vilyuyskaya syneclise. Geologiya i geofizika, no. 12, 1971, 112-116.

Vashchenko, V. I., et al. Explosive energy of water-saturated hexogene. Fizika goreniya i vzryva, no. 3, 1971, 429-432.

Volarovich, M. P. Electric conductivity and elastic properties of eclogite under high temperatures and pressures. IN AN SSSR. Izvestiya. Fizika Zemli, no. 4, 1972, 53-65.

Voronkov, O, K., and T. V. Itunina. Effect of water-filled pores and cracks on elastic-wave velicity in rock samples and in a massif. Geologiya i geofizika, no. 11, 1971, 97-109.

Yepinat'yeva, A. M., et al. Experimental study of velocity anisotropy in sedimentary layers. IN: AN SSSR. Izvestiya. Fizika Zemli, no. 4, 1972, 37-52.

Zakharenko, I. D., and T. M. Sobolenko. Heat effects in the weld zone during explosive welding. Fizika goreniya i vzryva, no. 3, 1971, 433-436.

Zgirovskiy, N. Z., and V. A. Vyatkin. Determination of mean velocity from the travel-time curves of asymmetric converted head waves. Geologiya i geofizika, no. 11, 1971, 125-128.

4. Particle Beams

A. Abstracts

Abramovich, V. U., and V. I. Shevchenko. Nonlinear theory of dissipative instability of a relativistic beam in plasma. UFZh, no. 2, 1972, 329-332.

A brief treatment is given of conditions for dissipative instability, occurring upon interaction of a relativistic particle beam with a dense plasma. The analysis assumes a high collision frequency, and is performed using a quasilinear approximation for beam relaxation. A one-dimensional case is first considered with the plasma assumed to be in a strong magnetic field, for which the differential equations of relaxation are given. A three-dimensional model is then treated, but without the presence of the external magnetic field. It is shown that the beam energy required to generate oscillatory instability is of the same order of magnitude for both the assumed models. In any case a criterion for dissipative instability is that $\Delta v < \delta/k$, where Δv is thermal velocity spread in the beam, δ is increment of beam instability, and k = wave number of the unstable harmonic. It follows from this that a sufficient spread of electron velocities in the beam would prevent the cited instability from occurring.

Ayvazov, V. Ya., and B. O. Bertush. Forming films of stoichiometric composition during electron-irradiated evaporation of Al_2O_3 in vacuum. NM, no. 2, 1972, 259-262.

A study is reported on factors affecting the composition and physical properties of the condensate during electron-irradiated evaporation of corundum in vacuum, and also on the determination of optimum conditions for formation of Al_2O_3 films of stoichiometric composition. Dielectric constant ϵ, loss tangent δ, film thickness γ, and coefficient of optical absorption α were experimentally measured; and their characteristic curves as a function of the parameter Ng/Nm are drawn (Fig. 1), where Ng = flow of active (liberated) gas and Nm = molecular flow of the evaporating substance.

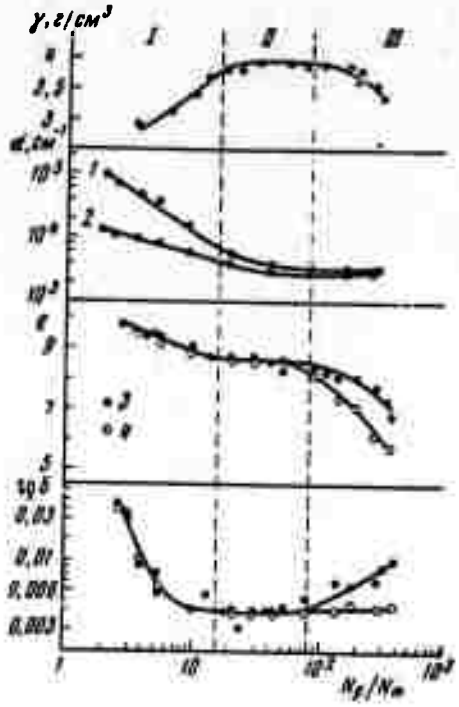

Fig. 1. Relationship between γ, α, ϵ, tg δ and Ng/Nm. 1 - $\lambda = 0.2\mu$; 2 - $\lambda = 0.4\mu$; 3 - in air; 4 - in vacuum.

Optimum conditions for formation of Al_2O_3 film close to stoichiometric composition is found in the range $15 < Ng/Nm < 80$, where $\epsilon = 8.6$ and $\gamma = 3.9$ g/cm^2. From the test results, the following conclusions are drawn: 1) Heating of Al_2O_3 by a focused electron beam in vacuum gives rise to a significant dissociation of the evaporating substance; 2) Condensate properties are governed by the rate of precipitation, temperature of the substrate and the degree of vacuum; and 3) The composition and dielectric properties of the film are determined by the relation Ng/Nm.

Kovalev, V. P., V. P. Kharin, V. V. Gordeyev and V. I. Isayev. Isotropic neutron source based on the LUE-25 linear electron accelerator. Atomnaya energiya, v. 32, no. 2, 1972, 173-175.

Results are described of an experiment to obtain an isotropic neutron source by proper selection of target shape and material in a LUE-25 linear electron accelerator. Angular distributions and discharge of photoneutrons from a lead target bombarded by 23 Mev electrons were studied. Threshold reactions $P^{31}(n,p)Si^{31}$, $Al^{27}(n,p)Mg^{27}$ and $Al^{27}(n,\alpha)Na^{24}$ having effective thresholds of 2.7, 4.5 and 8.1 Mev respectively, were used for detection of neutrons. A peculiarity of the LUE neutron source is the presence of a high bremsstrahlung background noise. Angular distribution of bremsstrahlung from the target was also studied and the noise level was measured. A nearly isotropic angular distribution (within limits of 15%) was observed when using a spherical lead target of 60 mm diameter with a 20 mm deep well. The photoneutron discharge for such a configuration was registered at 4×10^{10} neutron/μa x sec. The minimum value of the bremsstrahlung for the above target was measured at an angle of 145° to the electron beam direction, and was equal to 1.7 r/μa x min. The peak value was at zero angle and at 90°, at which the noise level was 3.3 r/μa x min. Fig. 1

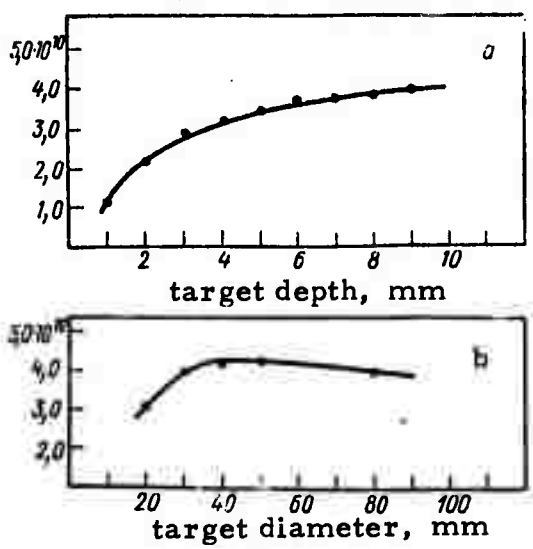

Fig. 1.

shows the neutron yield as functions of target geometry.

Kolesnikov, P. M., N. S. Kolesnikova and I. B. Gabris. Acceleration of plasma in a coaxial device with optimum inductive energy storage. I-FZh, v. 21, no. 6, 1971, 1117.

A theoretical study is given on the operation of a coaxial plasma accelerator from an inductive energy storage with a ferromagnetic core. The case of minimum energy loss in the inductive storage is studied, when the current source follows the relation I = A (Sh at + b Ch at), where I = current of the charging cycle; a, b = constants and t = time. Equations for transient processes in the feed circuit and in plasma acceleration are solved by taking into consideration the mass-transfer processes expressed in dimensionless variables. Results of the quantitative investigation show that inductive energy storage with an optimum law of current variation in the charging circuit significantly changes the character of transient processes in the storage accelerator system and improves characteristics of the accelerated plasma. Optimum selection of parameters can lead to an increase by several times in plasma velocity, compared to a similar accelerator operating under a non-optimum law of current variation.

Morozov, A. I. Plasma accelerators. Conference in Moscow. VAN, no. 7, 1971, 95-97.

A summary is given of some 200 papers presented at the First All-Union Conference on Plasma Accelerators, held February 8 - 12, 1971 in Moscow under sponsorship of the Scientific Council on Plasma Physics, AS USSR, and the Ministry of Higher and Secondary Specialized Education. All plasma-dynamic devices discussed are included under the general heading of the plasma accelerator(PA). After the opening speech by L. A. Artsimovich, A. I. Morozov discussed general physical problems of the PA which he defined as a system for ion acceleration without disturbing quasineutrality. The two basic physical problems of development and adjustment of the PA arise in connection with the near-wall effects and plasma instabilities. An up-to-date state-of-the-art of PA research and development was summarized in review papers presented by A. A. Porotnikov, A. A. Kalmykov, L. V. Leskov, M. I. Pergament, A. V. Zharimov, Yu. V. Yesipchuk, and A. A. Plyutto. The review makes it evident that a further development of the PA, specifically to a high-energy (10-100 keV) particle accelerator badly needed for fusion and astrophysical R and D, would take several years of collective

effort. A review by S. D. Grishin and the papers of I. N. Golovin, G. L. Grozdovskiy, I. M. Podgornyy, L. S. Polak, and N. N. Rykalin dealt with the present and potential applications of PA in nuclear fusion research, aerodynamics, experimental astrophysics, plasma chemistry, and metallurgy, respectively. Discussion of the papers led to the conclusion that current research on applications of high-energy (≥ 10 eV) plasma is not yet fully developed. The author concludes that development of the PA would considerably advance the solution of the nuclear fusion problem.

Ternov, I. M., V. G. Bagrov, Yu. I. Klimenko, O. S. Pavlova, and V. R. Khalilov. Stimulated emission from relativistic electrons moving in a low intensity plane wave. VMU, no. 6, 1971, 691-695.

An approximation of weak waves analysis is presented on the problem of stimulated emission from relativistic electrons moving in a monochromatic plane electromagnetic wave. Equations are obtained for the probability and the intensity of radiation, and spin effects are analyzed. Wavefunctions describing electron motion in an elliptically polarized plane monochromatic electromagnetic wave are given as exact solutions to Dirac equations. The radiation emitted by a moving electron is caused by the perturbation effect of an incident(quantized) electromagnetic wave. The assumption $1 \gg \gamma_1 \gg \gamma_2$, which can be experimentally realized with powerful laser beams and for which a single photon emission (or absorption) process is the most probable, is used. General expressions for the probability of stimulated single photon radiation (absorption) emitted by an electron in a unit time interval are discussed. The given equations are cited as being useful for numerical computations of the stimulated emission under appropriate experimental conditions. The total probability of stimulated emission from an unpolarized electron is computed as well as the total emission intensity. For the purposes of qualitative analysis, the above expressions are simplified using additional restrictions on radiative transitions. The probability of transitions with spin reorientation and their dependence on the initial (or final) spin orientation are considered. The spin reversal probability determines the degree of electron beam polarization. Maximal polarization effect is obtained when the electron spin vector is parallel to the direction of incident electromagnetic wave propagation. Analysis of a simplified expression for the probability of transition with spin reversal shows that maximum polarization

and probability are obtained with a circularly polarized incident wave. Conditions are given for the complete polarization of electrons. It is estimated that considerable polarization is possible for electrons with energies up to 50 mev; for higher electron energies the lifetime of the initial electron state and the transition probability decrease rapidly. In principle it is therefore possible to obtain polarized electrons using powerful laser beams.

Doroshenko, A. N., and I. M. Rayevskiy. Short-circuiting of pulse solenoid by semiconductor diodes. PTE, no. 1, 1972, 118.

Results are described of the application of power diodes in series for shunting of a 7.8 ka pulsed current solenoid at a storage battery energy of 100 kilojoules. Four power diodes were connected in series, as shown in Fig. 1, each operating at an inverse voltage of 900 v and an operating

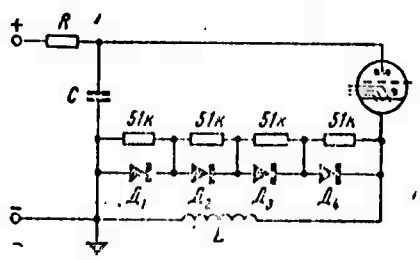

Fig. 1. Experimental diagram.

current of 500 a. The solenoid, with an inductance L = 0.7 mh, was fed from a condenser battery with a capacitance C = 15 μf through an ignitron. The diodes were connected in the reverse direction with respect to the source, and therefore do not affect circuit operation until the capacitor voltage drops to zero. As soon as a positive potential appears on the anode of the diode, the Q of the discharge circuit drops sharply, and the solenoid current shorts through the diodes. This circuit thus allows the short circuited solenoid to pull a current up to 7.8 ka at a voltage on the condenser battery of 3 kv. Comparative oscillograms of current and voltage pulses with and without the diodes are included, showing the stretching effect of the diodes on the current pulse.

Bakal, S. Z. Effect of air pressure on the erosion action of anode and cathode flares. EOM, no. 5, 1971, 20-21.

One of the ways to decrease the erosion of electrodes during a drop in air pressure is to lower the erosion action of a flare. In this work, the relationship between the erosion effect of flare and the air pressure was investigated. Figure 1 gives the experimental diagram. The cylindrical

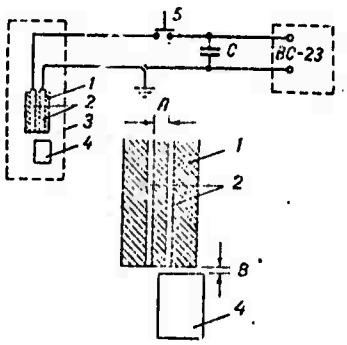

Fig. 1. Experimental sketch. 1 - ceramic tube; 2 - cylindrical electrodes; 3 - vacuum chamber; 4 - test specimen; 5 - high voltage circuit breaker. A - discharge gap; B - distance between flare-shaped electrode and specimen.

electrodes are made of steel with a 1.5 mm diameter. Erosion was determined on a cylindrical steel and copper specimen of 6 mm diameter and 10-12 mm height. Experiments were conducted at pressures of 760, 100, 10 and 10^{-1} torr. At each value of pressure, six series of five-pulse combinations were applied, and erosion was measured after the fifth pulse. After every discharge series, the steel electrodes were moved by 0.3-0.5 mm, and flush ground using the plane face of a ceramic tube. Results of the

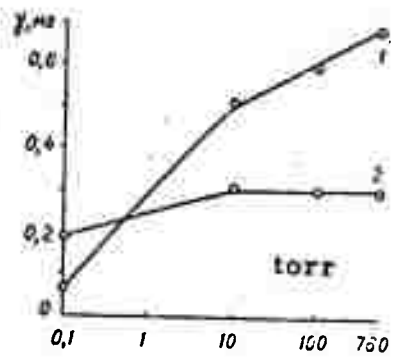

Fig. 2. Relationship of erosion action of (1) anode; and (2) cathode to air pressure.

experiments are given in Fig. 2. The erosion effect of an anode flare at atmospheric pressure is seen to be 1.5 - 2 times greater than that of a cathode flare. When the air pressure was lowered from 760 to 10^{-1} torr, the erosion effect of the anode and cathode flares decreased by 10 and 2 times, respectively.

Zakatov, L. P., A. S. Kingsen, A. G. Plakhov, and V. D. Ryutov. Spectral investigation of electromagnetic self-radiation in a plasma-beam system. ZhETF, v. 61, no. 3, 1971, 1009-1015.

The object of this work was to measure the frequency spectrum of e-m radiation from plasma interacting with a powerful electron beam.

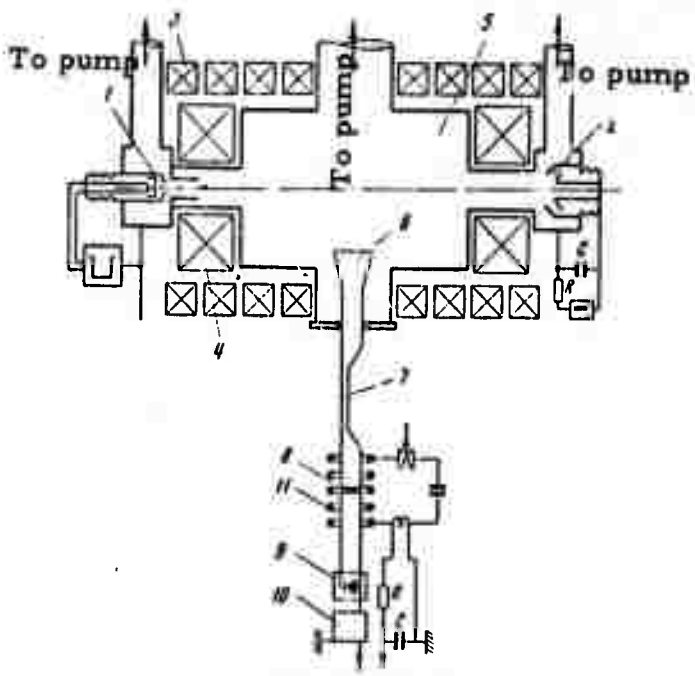

Fig. 1. Experimental device.
1 - electron gun; 2 - plasma injector; 3 - main magnetic field coil; 4 - screw type coil; 5 - vacuum chamber; 6 - horn antenna; 7 - waveguide; 8 - InSb crystal; 9 - detector head; 10 - preamplifier; 11 - solenoid for linear magnetic field in crystal.

A sketch of the experimental arrangement and the ultrahigh frequency spectrum analyzer is shown in Figure 1. The magnetic field intensity was 1 koe at the center of the chamber, and 5.25 koe at the end. The electron beam and hydrogen plasma were injected in the trap along the axes of the system so as to collide. Plasma concentration was 10^{12} - 10^{13} cm^{-3} and electron temperature T_e was 5 ev. Beam parameters were: energy $\epsilon \approx 30$kev, current 10a, pulse duration $\tau = 250\,\mu s$, and particle concentration $n_b \sim 2 \times 10^9$ cm^{-3}. A new type of spectrum analyzer is introduced here which is based on the existence of slow-damping electromagnetic waves in solid plasmas. Oscillograms obtained using the analyzer are shown in Fig. 2, and analytical results are illustrated in Fig. 3. It is seen that the intensity

Fig. 2. Spectrum analyzer oscillograms at various plasma concentration. a - $n \sim 7 \times 10^{12}$ cm^{-3}; b - $n \sim 4 \times 10^{12}$ cm^{-3}; c - $n \sim 1 \times 10^{12}$ cm^{-3}; d - linear magnetic field H .

peak lies close to the plasma frequency $\omega_p \ell$, and the radiation power of a 1 cm^3 plasma equals $P\,\omega_p \ell \approx 2 \times 10^{-2}$ watt/cm^3 (Fig. 3a): and $P2\,\omega_p \ell \approx 5 \times 10^{-3}$ watt/cm^3 at a concentration of $n \approx 4 \times 10^{12}$ cm^{-3} (Fig. 3b). The energy density of the Langmuir noise in the plasma, estimated on the basis of radiation with a frequency of $2\,\omega_p \ell$, is $W \approx 1.4$ ergs/$cm^3 \sim 2 \times 10^{12}$ ev/cm^3

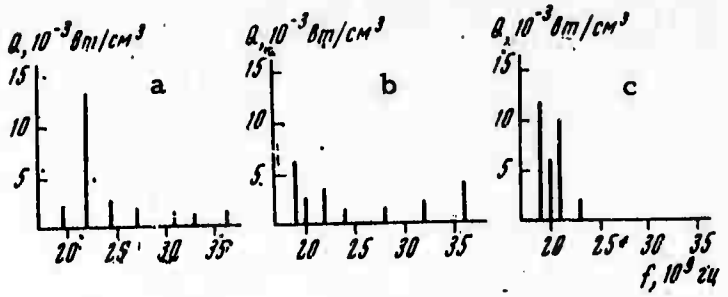

Fig. 3. Radiation power of 1 cm^3 plasma at a given frequency interval (f_k, f_{k+1}) for different plasma concentrations. a - $n \sim 7 \times 10^{12}$ cm^{-3}; b - $n \sim 4 \times 10^{12}$ cm^{-3}; c - $n \sim 1 \times 10^{12}$ cm^{-3}.

at $n \approx 4 \times 10^{12}$ cm^{-3}. The presence of radiation with a frequency $\omega_p \ell$ indicates that low frequency oscillations are also produced in plasma along with Langmuir radiation.

Lopatin, V. V., and V. Ya. Ushakov. Equipment for investigating optical and electrical characteristics of nanosecond breakdown in condensed media. PTE, no. 1, 1972, 144-146.

A description is given of a device consisting of a nanosecond pulse generator of amplitudes to 400 kv with regulated duration, a recording circuit of pulsed predischarge current of an amplitude $\geq$ 5 ma, an electron-optical gate and an optical amplifier (Fig. 1). The glycerin condenser, with a capacitance of 2 μf, is charged through a choke coil by an Arkad'yev-Marks generator. During the operation of the arc commutator in N_2 at a pressure of 15 atm a voltage wave is propagated with a rise time of 3 nsec. The experimental discharge chamber is located in a section of the L_1 line and is adjusted in accordance with the impedance. A constant discharge up to 96 nsec may be obtained; pulse length is controlled by the shearing discharger, in which discharge takes place on the teflon surface.

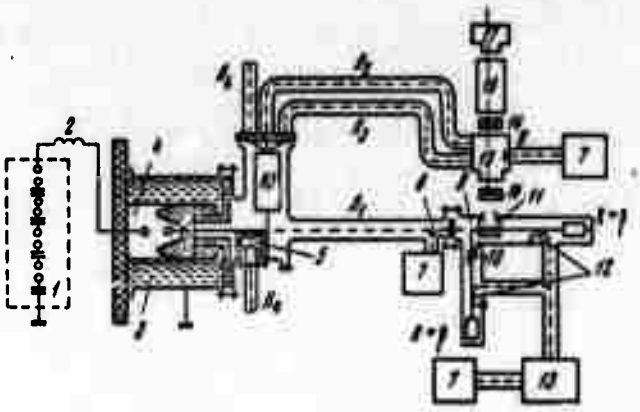

Fig. 1. Experimental device for observing nanosecond pulses. 1 - microsecond pulse generator; 2 - charge choke coil; 3 - glycerin condenser; 4 - arc commutator in compressed N_2; 5 - shearing discharger; 6, 8 - capacitive voltage divider; 7 - oscillograph, I2-7; 9 - T-junction; 10 - compensating capacitor; 11 - experimental discharge chamber; 12 - current transformer; 13 - amplifier, UZ-5A; 14 - lens; 15 - electron-optical gate; 16 - light amplifier; 17 - camera.

Experiments were performed with two types of dischargers - a nonregulated dual electrode and a trigatron type. In the first case, the electrodes were placed in the teflon cylinder, filled with an insulating liquid and the discharge was generated. The time spread of discharger operation does not exceed 50% and decreases with decreasing pulse duration. An intensifier arc in the trielectrode discharger was formed in the 1 mm ring gap, between a grounded copper cylinder placed in the teflon cylinder and a disc type ignition electrode, fed by L_4. The gap between main electrodes is regulated during varying voltages to maintain a steady over-voltage coefficient. The time spread of discharger operation at pulse duration τ_i = 40 nsec was $\pm$ 8 nsec, and at τ_i = 12 nsec = $\pm$ 1.0nsec. One-fourth of the cylinder volume was filled with air in both types of dischargers, to improve the shear stability and protect the teflon surface from the discharge. The liquid dischargers, despite their simplicity in construction, are only slightly inferior to the more complex discharger described by G. S. Korshunov and others (ZhTF, no. 8, 1969, 1430).

Compensation for capacitive current during recording of the predischarge current was done using a bridge circuit with Rogovskiy transformers. Transformer parameters were selected experimentally using a

model comprising a G5-12 generator, a UZ-5A amplifier and a I2-7 oscillograph. A current of 5 Ma was recorded by the amplifier.

Optical recording of a predischarge phenomena was obtained according to the method given by Yu. Ye. Nesterikhin, and R. I. Soloukhin (Methods of high-speed measurements in gasdynamics, Nauka, 1967). For optical image projection, a Yupiter-3 type short focusing objective lens was used.

Nagaybekov, R. B. Ionization processes and ion supercharge in the cathode spot of a vacuum arc discharge. ZhTF, no. 11, 1971, 2350-2352.

Calculations have shown that for the existence of a fast-moving arc discharge the ion current density should be very high, on the order of 10^5 - 10^6 a/cm^2. This density is possible only in the case of intensive evaporation of the cathode and a high effectiveness of ionization by electron collision. A mathematical expression is therefore derived for the ionization probability of atoms in the cathode spot and curves are drawn in relation to their concentration for current levels of 10^5 – 10^6 a/cm^2 for a copper cathode (Fig. 1). It is seen that the ionization probability is close to unity up

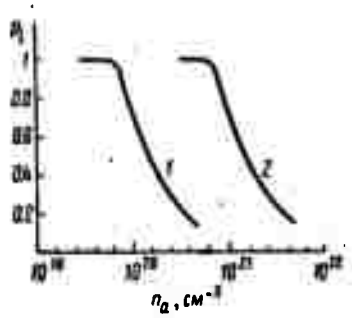

Fig. 1. Relationship of ionization probability of atoms in a cathode (copper) spot to concentration. 1 - 10^5 a/cm^2; 2 - 10^6 a/cm^2.

to an atom density $n_a \approx 7.5 \times 10^{19}$ cm^{-3}, and starts dropping at $n_a > 7.5 \times 10^{19}$ cm^{-3}. Results of the calculation of atom flow, evaporation rate, cathode spot temperature and atom concentration for a copper cathode at various E and distances λ_i from the cathode are given in Table 1. Due to the result of

E, в/см	ν_e, $см^{-2} \cdot сек.^{-1}$	G, $г/см^2 \cdot сек.$	T, °K	n_g, $см^{-3}$
10^4	$7.5 \cdot 10^{22}$	8	2850	$7.75 \cdot 10^{17}$
10^5	$7.5 \cdot 10^{23}$	80	3400	$7.1 \cdot 10^{18}$
10^6	$7.5 \cdot 10^{24}$	800	4350	$6.25 \cdot 10^{19}$

Table 1.

overcharging of ions at distances of 5×10^{-7} - 10^{-6} cm from the cathode, a layer of ions is seen to exist, creating a field of 5×10^7 v/cm.

Bagirov, M. A., V. P. Malin, and Yu. N. Gazaryan. Breakdown of polymer dielectrics under the action of electric discharges resulting from thermo-oxidation destruction of their macromolecules. IAN Az, no. 3, 1971, 9-14.

Based on previous results of Cooper and Prober (Polymer Sci, 44, no. 144, 1960), the possibilities were studied of erosion due to the thermal destruction of polymeric bonds at contact points of a specific arc discharge channel with a polymeric surface. Mathematical expressions are developed and calculations are made for the temperature field of an arc channel of an electric discharge in a gaseous gap between dielectrics, one of which is a polymer. Results are plotted in graphs, and the following conclusions are made: 1) At contact points of the polymer surface with the arc, the temperature is insufficient for thermal decomposition of polymer bonds in an oxygen-free medium, but is sufficient for thermo-oxidizing decomposition; 2) The polymer film erosion rate increases with a rise in the temperature of the atmospheric medium, in which ionization aging takes place.

Namitokov, K. K., D. P. Solopikhin and I. Ya. Surovtsev. Radiographic study of structural changes in electrodes from the effect of discrete electrical pulse discharges. FiKhOM, no. 6, 1971, 11-16.

Structural changes (mainly in the crystallization process) were studied inside and near a unit hole on electrodes made of: a) annealed and deformed nickel, and b) a mechanically compressed mixture of copper and nickel powders. The electrodes were subjected to the effect of a single high current pulsed discharge. A nickel specimen was heated in vacuum to 900°C for two hours and deformed by uniaxial compression so that its thickness decreased by 64%. With this specimen as cathode and an undeformed nickel element as anode, a single discharge was generated in air from a battery with C = 800 μf, voltage U = 240v and resistance R = 0.1 ohm. An x-ray was obtained of the affected area after the discharge. For the second specimen, copper powder, pre-reduced by hydrogen at 800°C for one hour, was mixed with nickel and pressed at 5 T/cm^2. X-ray records obtained for both of these specimens show the diverse effect of the temperature gradient on the structural change of electrode materials. A special x-ray camera developed for the experiment is described and illustrated.

Bek-Bulatov, I. Kh., and R. B. Nagaybekov. On the state of the cathode spot region during arc discharges in vacuum. ZhTF, no. 11, 1971, 2383-2384.

Characteristics of cathode spots as functions of high temperature and voltage gradients are examined. On the basis of the thermal balance relaxation time of atoms and the time between two successive collisions, it is shown that the basic cathode characteristics (work function of electrons, heat of evaporation, temperature, etc) are also applicable to a cathode spot, taking into account the high temperature effect and the field voltage ($\sim 10^7$ v/cm). The temperature T and its rate of increase in a cathode spot were determined for copper. At $t = 10^{-6} \sim 10^{-5}$ sec and $Q = 10^7$ watt/cm^2, results were: $T = 4000 \sim 4400^\circ$K and $\frac{dT}{dt} = 10^8 \sim 10^9$ deg/sec. The findings disagree with those of L. B. Leb on cathode surface properties (Fundamental processes of electric discharges in gas. Gostekhizdat, 1950). Conditions for which Leb's conclusions possibly hold true would require an ion current density of 10^8 - 10^9 a/cm^2. This does not appear to be a reasonable figure, since to maintain such an ion current density would require an ion concentration at the spot close to that of a solid ($\sim 10^{22}$ - 10^{23} cm^{-3}).

Konobeyevskiy, S. T., Zh. S. Takibayev, A. G. Abdullin and V. F. Grishchenko. Investigation of parameter changes in a diamond lattice irradiated at various temperatures by high-speed electrons. DAN SSSR, v. 202, no. 3, 1972, 560-561.

Natural diamond powder was irradiated in a U-10 linear heavy current accelerator with a water-cooled attachment at temperatures of 80°C and 236°C. The specimen was examined using a URS-60 x-ray device with a RKU-114 camera before and after irradiation by 2.3 Mev electrons. Results show that the cyclic change of a diamond lattice is a function of electron radiation dosage, which is approximately expressible as $\frac{\Delta a}{a} : I = 0.11.10^{21}$ el/cm^2, as shown in Fig. 1. This is about 70 times less than the effect of neutron irradiation ($10/10^{21}$ n/cm^2). The coefficient is valid for irradiation at T = 236°C with radiation doses of 4.66×10^{20}; 7.02×10^{20} and 1.05×10^{21} el/cm^2, reflecting a nearly linear growth rate by dosage. A similar linear relationship was also found for irradiation at 80°C (Fig. 1) which shows that a change in irradiation temperature does not change the stability of resulting defects.

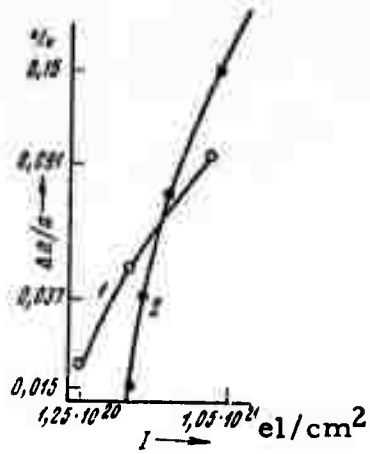

Fig. 1. Change of parameters of diamond lattice a from electron radiation dose I. 1 - at 80°C, 2 - at 236°C.

It was also noted that the lattice defects induced by electron bombardment were permanent, evidently of a graphite type of center, which remained even after anneal at 1000°C.

Lavrovskiy, V. A., Ye. G. Shustin, and I. F. Kharchenko. Experimental observation of oscillations in electron distribution functions during beam-plasma interaction. ZhETF P, v. 15, no. 2, 1972, 84-87.

A plasma-beam discharge was obtained in hydrogen in a linear magnetic field of 0.2 ml with an initial beam energy of 1 kev at currents of 20-40 ma. A sawtooth pulse was applied as a beam retarding voltage. Pulse amplitude was 1.5 kv at a rise rate of 6.10^9 v/sec. The measuring scheme worked in a single stage triggering mode during stationary beam injection, with a measuring circuitry bandwidth upper limit of not less than 200 MHz. High frequency oscillations were noted in a range of 1000 MHz while LF oscillations were observed at up to 600 KHz. At sufficiently low pressures ($p = 5 \times 10^{-6}$ torr), the delay curve is in the form of a stepped pulse and its differentiation yields a bell-shaped electron distribution function with an initial dispersion of 40 ev. By increasing the pressure to $p = (1 \sim 3)10^{-3}$ torr, the form of the curve changes and excitation of both HF and LF oscillations

occurs. A nonmonotonic change in slope of the delay curve with a change in retarding voltage (Fig. 1) is a significant factor, attesting to the multipeak distribution function of electrons. Specific electron groups have an energy dispersion in the range of 20-100 ev, and some of these groups occur simultaneously. With a further increase in pressure, the multipeak distribution curve characteristic is maintained, but a general spreading of the curve in the direction of lower velocities is noticed, along with the appearance of particles with velocities higher than Vo. At a higher recording time constant of (T = 10 msec), oscillation-free smoothing of the distribution function takes place with the formation of a plateau in the excitation regimes of the most intensive H F oscillations.

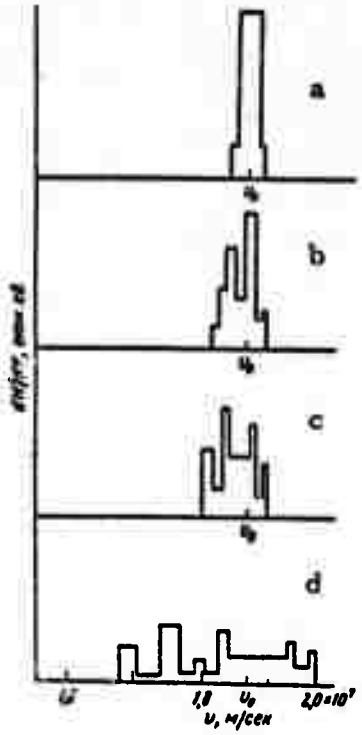

Fig. 1. Electron velocity distribution vs. pressure. Pressures are: a - 5×10^{-6} torr; b - 1.3×10^{-3} torr; c - 2×10^{-3} torr; and d - 2.7×10^{-3} torr.

Vorob'yev, A. A., O. B. Yevdokimov, and N. P. Tubalov. Effect of charge reversal in a dielectric charged by an electron beam. FTT, no. 12, 1971, 3691-3692.

Tests are described which demonstrate that the volumetric charge of an electron-bombarded dielectric may reverse after sufficient elapsed time. Plexiglas disks of 4.5 mm thickness were covered by 5-micron aluminum foil and irradiated by electrons with 0.8-1.2 Mev energy at a current density of 0.5 μa/cm^2 for 15-20 sec. To determine space charge, the effect of an electric field on the passage of beta-particles through the dielectric was utilized. The charged specimen was periodically irradiated by beta-particles from a strontium-iridium source and the number of particles before and after radiation was measured. The relationship of the change with time of beta-particles as a function of electric field is shown in Fig. 1. At energies of 0.8 and 1.2 Mev, the quantity $\Delta N/N_0$ is seen to change sign, where N_0 and N are the total particle counts before and after radiation. This corresponds to sign change of effective space charge in the

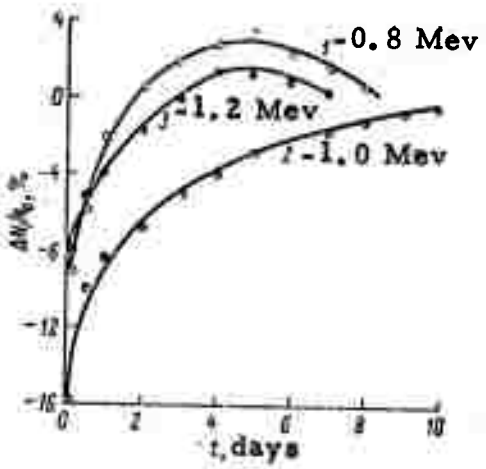

Fig. 1. Relative change of beta-particle count with time. Charge energies shown on curves.

dielectric. This effect is attributed to the electret state of plexiglas since the effect is not observed in polystyrene, which, in effect, does not display an electret state.

Musin, A. K., and M. A. Tyulina. Deionization of plasma dispersing in vacuum. ZhTF, no. 12, 1971, 2539-2544.

Deionization of an expanding plasma cloud during arcing between refractory electrodes in vacuum was investigated. Experiments were conducted with tungsten electrodes in an arc-quenching chamber as shown in Fig. 1. Arc quenching was simulated by a thyratron. The theoretical

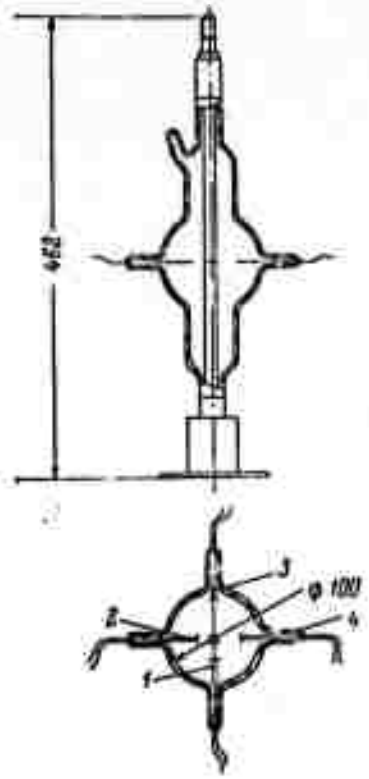

Fig. 1. Experimental vacuum-arc quenching chamber with probes. Distance from the chamber axis in mm: 1 - 23; 2 - 15; 3 - 40; 4 - 26.

distribution of charged particles and experimental results are compared. A change in charged particle concentration with time was determined from the rate of probe current drop. At an arc channel of radius $r \sim 10^{-1}$ cm and plasma dispersion rate of $v_d \sim 10^6$ cm/sec, the theoretically calculated concentration drop on a probe placed 2 cm from the arc axis begins $\sim 2.10^{-6}$ sec

after arc quenching, whereas the characteristic time of the change of concentration at a given point is $\sim 10^{-7}$ sec. These values show good agreement with experimental values.

Ivanov, N. V., G. P. Maksimov, A. I. Markin, and V. P. Smirnov. Inductive titanium hydride film injector. ZhTF, no. 12, 1971, 2631-2633.

An inductive titanium hydride film injector is described, in which a plasma bunch is formed by an inductive discharge on the surface of a ceramic disk with an applied layer of titanium. The disk diameter was 11.4 cm. The coil had a diameter of 13 cm and a width equal to 10 cm. Voltages to 50 kv were applied through a discharger with a capacitance of 0.1 or 0.7 μf. The value of the electric field on the disk periphery reached 650 v/cm. Intensity of the constant magnetic field varied from 250 to 1000 oe. Plasma bunch motion and parameters were studied in a 180 cm magnetic circuit. The injector contributed to the attainment of a lateral cross-section homogeneous plasma bunch of 10 cm diameter with a concentration of $10^{12} \sim 10^{14}$ cm^{-3}, and a total of ionized particles up to 10^{18}. Results of the experimental study of plasma parameters in relation to discharge characteristics are shown in Figs. 1 and 2.

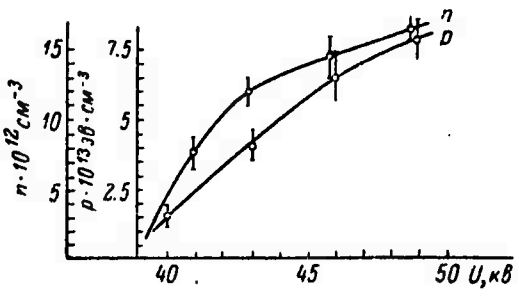

Fig. 1. Concentration and lateral electron pressure of plasma vs. discharge voltage. C = 0.1 μf, Ho = 500 oe.

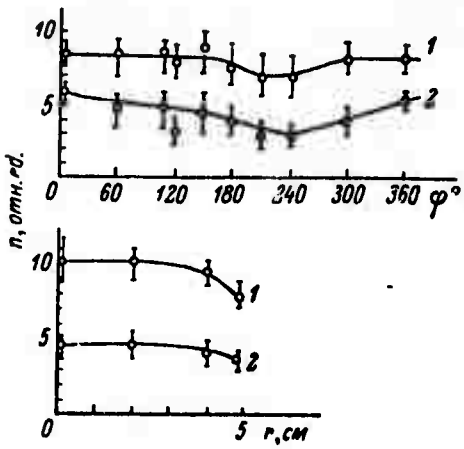

Fig. 2. Azimuthal and radial distribution of plasma concentration. 1 - 10; 2 - 40 μsec.

Golovanivskiy, K. S., and A. D. Guseynova. Study of a plasma beam, generated by a Penning type discharger with a strong radial electric field. ZhTF, no. 9, 1971, 1876-1880.

It is experimentally shown that a plasma, generated by a Penning type source, can possess an anisotropic electron temperature. The appearance of anisotropy is connected with electron acceleration in a direction perpendicular to a magnetic field under the influence of a strong electric field of excited discharge. The Penning type plasma source is shown in Fig. 1; Fig. 2 outlines the overall experimental setup. The source discharge chamber is a copper cylinder of 140 mm length and 44 mm diameter. A stainless steel anode of 38 mm length and 37 mm diameter is placed in the middle of the chamber. The anticathode is a stainless steel disc of 42 mm diameter and 3 mm thickness, with a 10 mm diameter aperture at its center. The cathode is a tungsten wire of 0.5 mm diameter, which is heated by a current of about 10 a. The cathode and anticathode are held at zero potential while a positive potential of up to 500 v is applied to the anode.

Discharge current was varied over the 200 ~ 400 ma range. The discharge

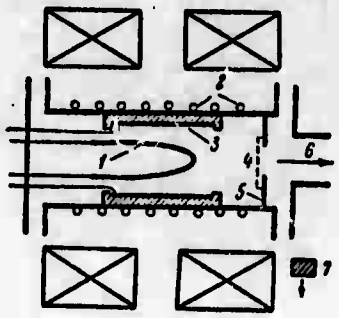

Fig. 1. Plasma source.
1 - cathode; 2 - water coil;
3 - anode; 4 - screen; 5 - anti-
cathode; 6 - plasma beam; 7 - glass.

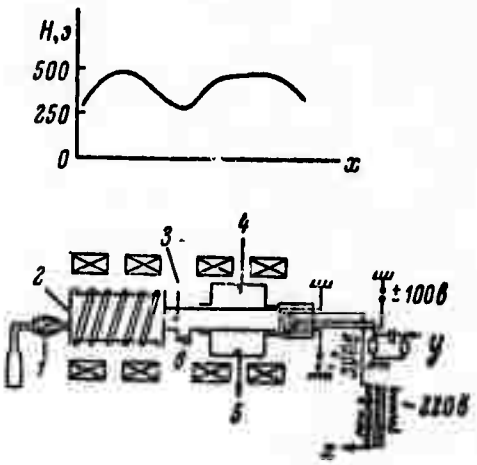

Fig. 2. Experimental setup.
1 - valve; 2 - plasma source;
3 - probe; 4 - frequency-modulated
signal (λ = 12 mm); 5 - recording of
resonance curve; 6 - pumping.

chamber was cooled by water. The magnetic field in the vicinity of the source was varied between 100 to 600 oe; argon pressure in the source was kept at 2.10^{-3} torr. A relationship of the energy of fast and slow electrons as a function of source anode voltage U_a was obtained (Fig. 3). Results of measurements of lateral and linear electron temperatures $T_{e\perp}$ and $T_{e\parallel}$

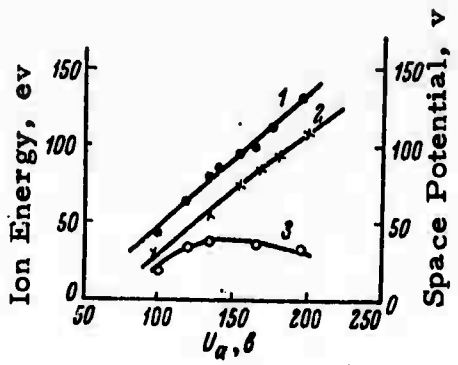

Fig. 3. Relationship of ion energy and space potential versus source anode voltage. 1 - fast ions; 2 - slow ions; 3 - space potential.

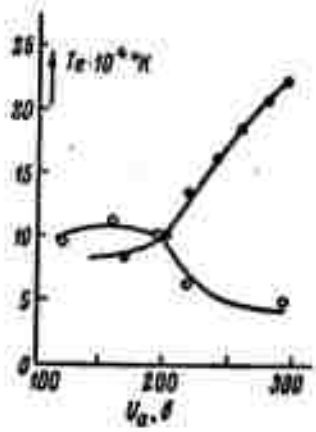

Fig. 4. Relationship of lateral and linear electron temperature to anode voltage.

in relation to U_a are plotted in Fig. 4. The maximum anisotropy factor $\tau = T_{e\perp} / T_{e\parallel}$ was 5. It is concluded: 1) A Penning source with a strong radial electric field can generate a plasma beam with a concentration to 10^{10} cm^{-3} without additional ion extraction from the discharge; 2) Beam ions are divided into two groups according to energy: fast ions, with a non-compensated space charge, which accelerate with a cathode potential drop and an energy level equal to 50 - 70% of the anode voltage; and slow ions,

with energies of 20 - 40 ev, which fall on the beam due to the ambipolar propagation of gas-discharge plasma along the magnetic field.

Gavrilenko, T. B., and G. O. Karapetyan. Resistance of activated glasses to a current of accelerated electrons. ZhPS, v. 15, no. 6, 1971, 1110-1112.

Tests on cathode resistance to electron bombardment are described. The article deals with several cathodoluminescent glasses, and treats the composition and excitation state factors determining the resistance characteristic. Experiments were conducted with borax, silicate and borosilicate glass, activated by trivalent terbium and cerium. Characteristic curves for aluminized specimens of various glass under similar radiation conditions (V = 20 kv, j = 5. 10^{-7} a/cm^2) are given in Fig. 1.

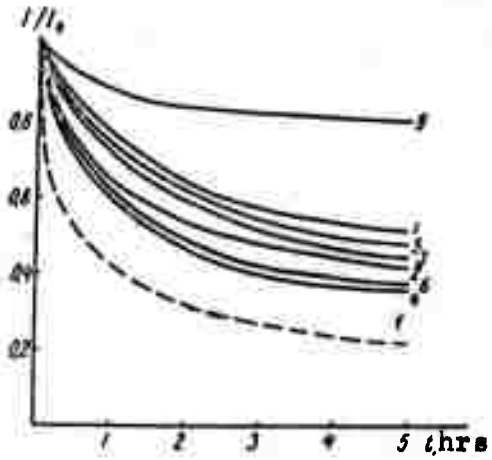

Fig. 1. Relative decrease of brightness of the cathode-luminescence glow of glass specimen during 5 hours of continuous excitation (V = 20 kv, j = 5.10^{-7} a/cm^2). Dashed curve is for 18-2 glass at V = 20 kv, j = 1μa/cm^2. Curve numbers correspond to glass numbers in Table 1.

The molecular composition of the glasses is listed in Table 1, in which activator concentration is given in wt % oxide above 100. It was noted that the oxide content of the glass is the determining factor in resistance

to accelerated electron current. An optimum concentration of boric oxide exists in a series of borosilicate glasses, which if increased sharply

Ser. No.	Glass No.	Li_2O	Al_2O_3	SiO_2	MgO	CaO	BaO	B_2O_3	Ce_2O_3	Tb_2O_3	Parameters $c \cdot 10^{17}$, cm^2
1	25-5	1	10	50	25	25	—	—	0,5	—	1,45
2	1-7	—	20	—	40	—	—	40	0,5	—	3,57
3	18-2	—	—	50	25	25	—	—	0,5	—	2,65
4	20-1	10	10	60	—	20	—	—	10,0	—	4,63
5	25-T	20	15	50	—	—	15	—	—	0,5	1,95
6	45-T	15	15	50	—	—	20	—	—	10,0	4,60
7	15-9	10	10	57	20	—	—	3	0,5	—	2,30
8	15-10	10	10	55	20	—	—	5	0 5	—	0,092
9	15-11	10	10	53	20	—	—	7	0,5	—	0,086
10	15-12	10	10	50	20	—	—	10	0,5	—	0,148

Table 1. Composition of glass (Mol %) and disintegration parameter c, given by: $I = I_0/(1 + CN)$, where I - initial intensity, I_0 - intensity of aged screen, N - total no. of electrons falling on the specimen during radiation.

lowers the stability of the specimen (Fig. 2). Measurements revealed that glass containing about 6-7 mol % of boric oxide was the most stable. Oxides

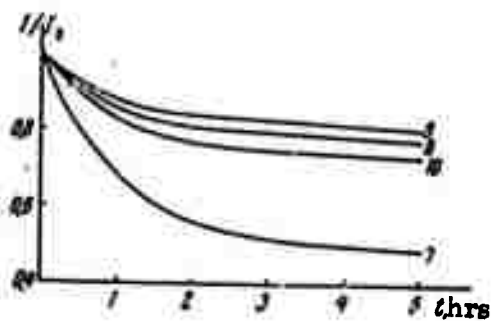

Fig. 2. Relative decrease of brightness of borosilicate glass with 0.5% Ce_2O_3 and varying boric oxide content. Curve numbers are the same as in Table 1.

of alkali-earth elements in glass, and their atomic weights, do not affect resistance to electron irradiation, but additions in alkaline oxide content do lower the resistance. The effect of temperature on the darkening of the operating layer of glass was also investigated. Dark spots appearing in glass specimens after electron bombardment vanished when the specimens were heated to 450°C.

Kalyatskiy, I. I., G. S. Korshunov, and G. A. Kiselev. Variation in spark gap resistance in water from the action of a high pulsed voltage. EOM, no. 6, 1971, 32-37.

Relationships are experimentally determined for high voltage resistance in a spark gap in water, in terms of the specific resistance of the water, the electric field configuration and the spark gap width δ. Fig. 1

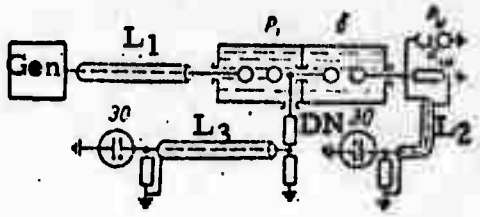

Fig. 1. Experimental diagram. L_1, L_2, L_3 - cable; Gen - generator (Arkad'yev-Marks), P_1 - peaking discharger in transformer oil; P_u - air gap. δ - spark gap in water

is a diagram of the principal experimental circuit and Fig. 2 illustrates the most complex element of the experimental arrangement, the coaxial discharge chamber. The experimental results are plotted (3 curves and 1 oscillogram are given), from which the authors make the following

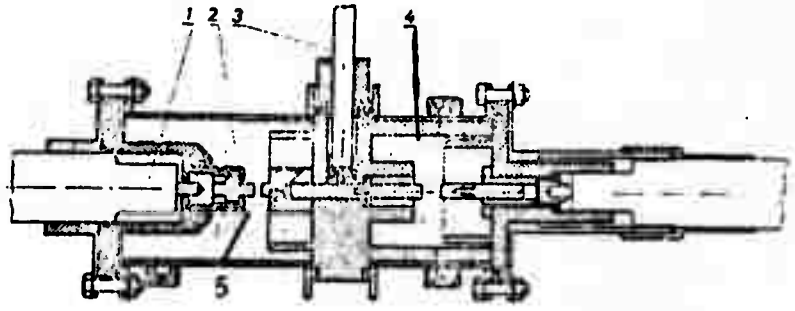

Fig. 2. Experimental discharge chamber. 1 - cable KPV-1-300; 2 - peaking discharger; 3 - outputs to voltage divider; 4 - spark gap in water; 5 - transformer oil.

conclusions:

1) The findings have application in the calculation and construction of high voltage electrode systems operating in water, and in the development of high voltage pulse-shaping circuits, loaded by spark gaps in water.

2) A hemisphere-hemisphere electrode system possesses the highest resistance during the application of w high voltage pulse in using a uniform electric field. This has significance in the construction of a peaking nanosecond type discharger operating in water.

3) A sharp decrease of high voltage resistance was noted in a non-uniform electric field (pointed-base electrode system). This should be considered when designing an electrode system for operation in water.

4) To reduce load pulse deformation and to obtain a high resistance spark gap in water, high voltage rectangular pulses with nanosecond fronts are recommended for various electrophysical methods of treatment and destruction of solids.

Artyukh, V. G., L. G. Lisenko, and S. A. Smirnov. Circuit for rapid switching of heavy currents in an inductive storage. PTE, no. 1, 1972, 119-120.

A circuit is described which allows commutation of currents at a given moment of time (Fig. 1). Capacitor batteries 1 and 2 are precharged by a charging device, not shown in the figure. On triggering the discharger P_1 in the discharge circuit (battery 1, discharger P_1, inductive storage L and wire P_k in series), a sinusoidal commutation current flows through the circuit. Loads L_H and R_H are shunted by P_k, so that practically no current flows through. On triggering discharger P_2 in its discharge circuit (battery 2, discharger P_2, wires P_k and P_g in series), a regulating current of a value higher than the commutation current starts to flow. The discharger P_2 is triggered at the moment of the first maximum of switched current. Due to the regulating current, the wires P_k and P_g explode and the switched current flows through loads L_H, R_H and R_{sh}.

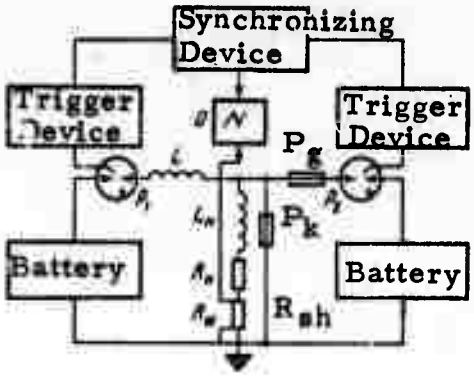

Fig. 1. Experimental scheme.
P_1, P_2 - regulating discharger;
L - inductive storage, 130 μh; P_g - additional exploding wire; P_k - commutation wire; R_H - resistive load 0.1 ohm; L_H - inductive load, 2 μh; R_{sh} - shunt; Battery 1 - 3360 μf, 5 kv; Battery 2 - 140 μf, 5 kv.

To increase the pressure in the gap formed after the explosion of wires, the wires are placed in discharge chambers of the type shown in Fig. 2. A description of the dischargers and trigger devices used in this experiment are given in a paper by I. I. Aksenov et al (PTE, no. 3, 1970, 166).

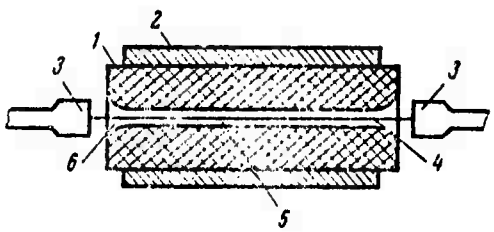

Fig. 2. Discharge chamber for wires.
1 - insulator; 2 - steel tube; 3 - outlets; 4 - wire; 5 - discharge channel; 6 - channel widening.

The maximum value of switched current obtained in the experiment was approximately 25 ka for wires of 14 mm diameter. The time spread of the initial moment of switching was mainly determined by a momentary instability of the synchronizing device, and did not exceed a few tenths of a microsecond. Tests showed that the device permits simple, reliable switching of currents up to 10^4--10^5 a, using laboratory type inductive storage.

Krivitskiy, Ye. V., V. V. Shamko and V. L. Apostoli. Analysis of energetic parameters of an underwater spark discharge path. EOM, no. 5, 1971, 48-50.

Approximate mathematical expressions are derived for parameters of an underwater arc discharge channel. The expressions define time behavior of current power and resistance in terms of the remaining circuit parameters. From these relations an expression is derived for maximum power N_{max} in an underwater path of a given length. This expression has been experimentally verified and results tabulated (Table 1).

Path No.	$C \cdot 10^6$, f	$U_0 \cdot 10^{-4}$, v	$L \cdot 10^6$, h	$l \cdot 10^{-2}$ m	$N_{max} \cdot 10^{-8}$, W	
					Calc.	Expt.
1	9,0	4,7	1,16	10	11,8	10,7
2	9,0	4,7	1,16	4	6,5	6,35
3	9,0	4,7	12,0	9	2,65	2,78
4	2,83	4,65	7,5	12	2,9	2,83
5	2,83	4,65	7,5	6	2,0	1,65
6*	1,0	7,0	4,3	5	2,8	3,75
7*	1,0	6,2	3,8	8	3,85	3,5
8	1,0	4,0	3,2	6	1,98	1,78
9	1,0	4,0	3,2	4	1,51	1,47
10*	1,0	3,8	3,2	6	1,9	1,6
11	1,0	4,4	18,9	4	0,41	0,3
12	0,1	4,7	4,04	6	0,76	0,53
13	0,1	4,8	4,04	4	0,64	0,55
14	0,1	4,7	4,04	2	0,4	0,33

Table 1. Maximum power transmitted in paths of length l.

* Data of V. V. Arsent'yev (PMTF, no. 5, 1965) and G. S. Bondarenko (IVUZ Elektromekhanika, no. 5, 1968).

Table 1 shows that the difference between the experimental and calculated results does not exceed 25%, which is acceptable for practical applications. It is thus shown that, given only the initial parameters of the discharge circuit and the distance l between electrodes, it is possible to calculate magnitude and time to maximum power, eliminating the need for experimental work. No other channel parameters are given in the cited study.

B. Recent Selections

Abramovich, V. U., and V. I. Shevchenko. Nonlinear theory of dissipative instability of a relativistic beam in plasma. ZhETF, v. 62, no. 4, 1972, 1386-1391.

Abroyan, M. A., G. A. Nalivayko and S. G. Tsepakin. Pulsed source of negative hydrogen ions. ZhTF, no. 4, 1972, 876-879.

Anitov, N. M., V. M. Baranova and A. A. Polyakova. Relationship of cut-off arc current in hydrogen to duration of the current pulse. IN: Elektronnaya tekhnika, Nauchno-tekhnicheskiy sbornik, Gazorazryadnyye pribory, no. 3(23), 1971, 45-48. (RZhF, 3/72, #3G188)

Arutyunov, V. V., and V. F. Baranov. Approximation of the cross section of bremsstrahlung generated in light absorbents by electrons with 0.05-5 Mev energy. IN: Sbornik. Voprosy dozimetrii i zashchity ot izlucheniy. Moskva, Atomizdat, no. 12, 1971, 171-172. (RZhF, 4/72, #4V453)

Arutyunov, V. V., V. F. Baranov, R. Ya. Zaytsev, K. A. Trukhanov and V. V. Tsetlin. Effect of electric field on characteristics of fast electron beams in a dielectric. IN: Sbornik. Voprosy dozimetrii i zashchity ot izlucheniy. Moskva, Atomizdat, no. 12, 1971, 57-61. (RZhF, 4/72, #4V450)

Auzinya, L. K., V. E. Liyepinya, M. V. Zake, V. K. Mel'nikov, V. K. Mel'nikov, I. A. Ungurs and U. A. Tsiyelens. Method for complex experimental investigations of thermophysical processes in a chemically active coaxial plasma jet with Ti particles. IAN Latv. (Fiz.), no. 2, 1972, 60-68.

Avramenko, M. I., and V. S. Kuznetsov. Phase focusing of intense ion bunches of nanosecond duration. Electrofizicheskaya apparatura, no. 9, 1971, 63-68.

Babykin, M. V., Ye. K. Zavoyskiy, A. A. Ivanov, and L. I. Rudakov. Estimation of possibilities for using powerful relativistic electron beams for thermonuclear synthesis. IN: Plasma physics and control. Nuclear fus. res. 1971. Proc. int. conf. Madison, 1971, v. 1. Vienna, 1971, 635-643. (RZhF, 3/72, #3G390)

Belomoyeva, R. V., V. M. Levin, I. A. Prudnikov, R. V. Sinitsyn and Yu. F. Chichikalov. Present state and trends in development of linear electron accelerators for radiation therapy. Atomnaya energiya, v. 32, no. 5, 1972, 405-406.

Belyayev, A. P., and P. I. Ryl'tsev. Fokusirovka puchka v elektronoprovode modeli kollektivnogo uskoritelya. (Beam focusing in an electron conductor of a collective accelerator model.) Dubna, 1971, 16 p. (RZhF, 4/72, #4A530)

Berezin, A. B., L. V. Dubovoy, B. V. Lyublin, and D. G. Yakovlev. Spectroscopic study of parameters of a turbulent plasma. ZhTF, no. 5, 1972, 946-952.

Bogdankevich, L. S., A. A. Rukhadze, and V. P. Tarakanov. Limiting currents in electron beams with a relativistic energy spread. ZhTF, no. 4, 1972, 900-901.

Bogdanov, Ye. P., L. K. Orlov, and Yu. A. Romanov. Instability of space-separated plasma beams. III. IVUZ Radiofiz, no. 4, 1972, 521-527.

Bonch-Osmolovskiy, A. G. On the dynamics of collision of charged particle bunches in connection with the impact mechanism of acceleration. Atomnaya energiya, v. 31, no. 2, 1971, 127-131.

Bondarenko, B. V., and V. A. Kuznetsov. Investigation of mechanical stability of film-type chromium field emitters. ZhTF, no. 5, 1972, 1093-1095.

Borisov, D. G., A. I. Gryzlov, I. A. Prudnikov, and E. Kh. Emirov. Linear accelerator of charged particles. Author's certificate USSR, # 276268, published April 16, 1971. (RZhF, 4/72, #4A477P)

Boytsov, Yu. P., S. A. Valuyskiy, M. V. Konstantinova, and V. I. Prokhorov. Application of an electron microscope for controlling field emitters and probes. PTE, no. 2, 1971, 245-246.

Breyzman, B. N., D. D. Ryutov, and P. Z. Chebotayev. Nonlinear effects during the interaction of an ultrarelativistic electron beam with plasma. ZhETF, v. 62, no. 4, 1972, 1409-1423.

Buts, V. A. Waves in electron beams moving with variable speed. ZhTF, no. 4, 1972, 709-715.

Collective methods of particle acceleration in plasma and in high-current electron beams. VAN, no. 4, 1972, 12-19.

Fursey, G. N., I. D. Ventova, L. Ye. Valuyeva and V. M. Zhukov. Investigating conditions for forming effective high-current field-emission cathodes from refractory metals (W). ZhTF, no. 5, 1972, 1056-1060.

Fursey, G. N., and N. V. Yegorov. A stable semiconductor field-emission cathode. ZhTF, no. 5, 1972, 1090-1092.

Garber, R. I., V. I. Afanas'yev, B. I. Levandovskiy, and Kh. I. Pruger. Investigation of bondings of tantalum films to the surface of needle-shaped tungsten microcrystals. FMiM, no. 4, 1972, 890-893.

Gorgoraki, V. I. Plasma in a shielded space. DAN SSSR, v. 204, no. 1, 1972, 63-65.

Grebenyuk, A. F. Design of electron guns forming disc-like beams. IN: Radiotekhnika. Respublikanskiy mezhvedomstvenniy tematicheskiy nauchno-tekhnicheskiy sbornik, no. 17, 1971, 14-19. (RZhF, 3/72, #3Zh446)

Gross, L. P., V. N. Gusarov, and A. V. Shal'nov. Spectral density of radiation from electron bunches during interaction with a diaphragm-type waveguide. ZhTF, no. 4, 1972, 716-720.

Gubarev, V. Ya., N. P. Kozlov, Yu. S. Protasov, and V. I. Khvesyuk. Preelectrode potential drop in a pulsed plasma accelerator. ZhTF, no. 5, 1972, 1033-1034.

Gufel'd, I. L. Surface processes in processed electrodes, prior to breakdown in vacuum. ZhTF, no. 5, 1972, 1010-1017.

Kalashnikov, N. P., E. A. Koptelov, and M. I. Ryazanov. On the origin of orientational peaks in the bremsstrahlung spectrum of nonrelativistic electrons in a monocrystal. FTT, no. 4, 1972, 1211-1213.

Kheyfets, S. A. Separatrix of coherent phase oscillations in an accelerator, taking into account the voltage induced by the beam. PTE, no. 2, 1972, 20-23.

Khodatayev, K. V. "Mirror trap" for a high-current self-focusing relativistic electron beam in a closed trajectory. Atomnaya energiya, v. 32, no. 5, 1972, 379-382.

Kolesnikov, P. M. Elektrodinamicheskoye uskoreniye chastits. (Electrodynamic acceleration of particles.) Moskva, Atomizdat, 1971, 390 p. (RZhF, 3/72, #3G458K)

Kolyada, V. M., and V. G. Zlobin. A method for measuring lateral distribution of ion beam density. Author's certificate USSR, no. 306591, published July 21, 1971. (RZhF, 4/72, #4A488P)

Kononov, B. A. Interaction of electrons with a solid body. IN: Sbornik. Itogi issledovaniya po fizike, 1917-1967. Tomsk, Tomskiy universitet, 1971, 253-260. (RZhF, 4/72, #4Ye1235)

Konopleva, R. F., V. L. Litvinov, and N. A. Ukhin. Osobennosti radiatsionnogo povrezhdeniya poluprovodnikov chastitsami vysokikh energiy. (Characteristics of radiation damage to semiconductors by high energy particles.) Moskva, Atomizdat, 1971, 176 p. (RZhF, 4/72, #4Ye1197K)

Kovalev, V. P., V. P. Kharin, V. V. Gordeyev, and V. I. Isayev. Reflection coefficients of 12-25 Mev electrons during oblique impact on a metal surface. Atomnaya energiya, v. 32, no. 4, 1972, 342-344.

Kul'batskiy, L. D., and V. V. Supravnovich. On the problem of temperature measurements of cooling water in plasmatrons. IAN B, Seriya Fiz-ener. nauk, no. 4, 1971, 60-62. (RZhF, 4/72, #4G100)

Kulik, P. P. 10th international conference on phenomena in ionized gases. Atomnaya energiya, v. 32, no. 4, 1972, 362-364.

Kulyapin, V. M. Calculating the erosion of arc-discharge cathodes. ZhTF, no. 4, 1972, 789-794.

Kunz, W. Study of tungsten tempered and irradiated by electrons. Phys. status solidi (b), v. 48, no. 1, 1971, 387-398. (RZhF, 4/72, #4Ye1623)

Levin, V. M., I. A. Prudnikov, V. V. Rumyantsev, K. P. Rybas, and B. N. Telepayev. Effectiveness of ion focusing of short duration intense electron beams. PTE, no. 2, 1972, 146-148.

Levitskiy, S. M., and V. Z. Shapoval. Effect of beam modulation by a shf noise signal on the properties of a plasma-beam system. UFZh, no. 4, 1972, 649-651.

Lysov, G. V. Super high frequency plasmatron. Author's certificate, USSR, no. 304714, published July 7, 1971. (RZhF, 3/72, #3G205P)

Manylov, V. I. High-voltage generator of discrete nanosecond pulses into a variable load. PTE, no. 2, 1972, 91-93.

Mints, A. L. Accelerators - what are they for? UFN, v. 106, no. 4, 1972, 663-664.

Murin, B. P. Stabilizatsiya i regulirovaniye vysokochastotnykh poley v lineynykh uskoritelyakh ionov. (Stabilization and regulation of high frequency fields in linear ion accelerators.) Moscow. Atomizdat, 1971, 333 p. (Russian Book List, 1971, #884)

Pakhomov, V. I., and V. L. Sizonenko. On noncoherent excitation of plasma oscillations by a nearly monoenergetic relativistic beam. ZhTF, no. 5, 1972, 1088-1090.

Pavlovskaya, N. G., and T. V. Kudryavtseva. Tube with a needle-shaped field-emission cathode for obtaining nanosecond pulses of fast electrons. PTE, no. 2, 1972, 198-201.

Pereverzev, G. V. Ion-cyclotron instability in a plasma formed by fast ion beams. ZhTF, no. 5, 1972, 1085-1088.

Rosinskiy, S. Ye., A. A. Rukhadze, V. G. Rukhlin, and Ya. G. Epel'baum. Electron beam injection in a plasma confined by a conducting shell. ZhTF, no. 5, 1972, 929-938.

Rudakov, L. I., V. P. Smirnov and A. M. Spektor. Behavior of a high-current electron beam in a dense gas. ZhETF P, v. 15, no. 9, 1972, 540-544.

Sakharov, I. Ye., and L. D. Tsendin. Properties of a gas--discharge plasma at high ionization levels. ZhTF, no. 5, 1972, 916-920.

Stabnikov, M. V., and M. Sh. Tombak. Holograms of arc discharges excited by nanosecond electric pulses. ZhTF, no. 5, 1972, 1073-1075.

Tulinov, A. F. Physics of the interaction of fast charged particles with monocrystals. (Conference in Moscow.) VAN, no. 11, 1971, 104-105. (RZhF, 4/72, #4Ye759)

Vasserman, S. B. Function of a Rogovskiy belt in measuring currents of nanosecond pulsed beams. PTE, no. 2, 1972, 99-103.

Vaysburd, D. I., and I. N. Balychev. Destruction of a solid body by super-dense excitation of its electron subsystem. ZhETF P, v. 15, no. 9, 1972, 537-540.

Vladimirova, N. M., I. D. Kon'kov, R. Ye. Rovinskiy, and N. V. Cheburkin. Estimating the level of electron density in a high-current low-pressure discharge in argon. OiS, v. 32, no. 4, 1972, 653-654.

Yakinenko, I. T. All-Union conference on the theory of plasma. Atomnaya energiya, v. 32, no. 4, 1972, 360-362.

Yakobashvili, S. B., V. F. Khorunov, V. S. Nesmikh, and N. N. Sinitsa. Device for measuring surface tension of refractory materials. IN: Sbornik. Fizicheskaya khimiya poverkhnostnykh yavleniy v rasplavakh. Kiyev, Naukova dumka, 1971, 129-131. (RZhF, 4/72, #4Ye668)

Zagorski, Z. P., and Z. Zimek. Ustanovka dlya issledovaniya impul'snogo radioliza na baze lineynogo uskoritelya elektronov LUE 13-9. (Pulse radiolysis instrumentation for the LAE 13-9 linear electron accelerator.) Rept. inst. bad. jadr. PAN, no. 1287, 1971, 9 p. (RZhF, 4/72, #4A486)

Zaykovskaya, M. A., A. Ye. Kiv, and O. R. Niyazova. Subthreshold radiation effects in silicon. The Varley mechanism in diamond-structured semiconductors. IN: Sbornik. Metod radiatsionnykh vozdeystviy v issledovanii struktury i svoystv tverdykh tel. Tashkent, Fan, 1971, 32-52. (RZhF, 4/72, #4Ye1201)

Zubkov, I. P., A. Ya. Kislov, and A. I. Morozov. Optimizing the parameters of a high-current ion accelerator. ZhTF, no. 4, 1972, 898-900.

Zykov, V. A. Volt-ampere relationship of a point-to-disc corona discharge in air. TVT, no. 2, 1972, 248-254.

5. Miscellaneous Interest

A. Abstracts

Mandzhikov, V. F., A. P. Darmanyan, V. A. Barachevskiy, and Yu. N. Gerulaytis. Photochromism in organic compounds from the action of laser radiation. OiS, v. 32, no. 2, 1972, 412-413.

Photochromic intramolecular transformation of a spiropyran molecule was observed in the experiments with spiropyran solutions in benzene, ethanol, and polymethylmethacrylate, which were excited by a ruby laser. Output energy and pulse length were 0.4j and 3×10^{-8} sec in the experiments with a Q-switched laser, 4j and 3×10^{-4} sec in those with a free-running laser, respectively. A colored filament appeared in a colorless spiropyran solution, ranging from 8-10 mm to 40 mm long, after a laser beam was focussed on the center of the cell. Coloration vanished spontaneously in ~10 min and in a few minutes in liquid and in polymer solutions, respectively. The colored filament was not generated by ruby laser radiation in spiropyran solutions which did not absorb in the 300-400μ range, nor by neodymium glass laser in solutions of photochromic spiropyrans. The experimental plot of D versus I^2 (Fig. 1) and the absence

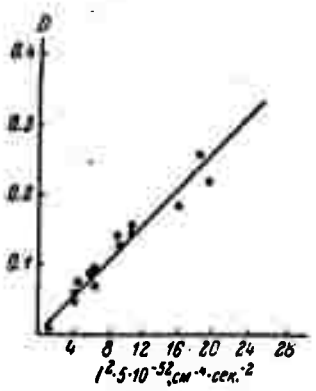

Fig. 1. Optical density D of the 8'-allyl - 6'-nitro - 1,3,3 - trimethylspiro - (2'H-1-benzopyran - 2,2'-indoline) solution in benzene versus square of intensity of exciting ruby radiation.

of electronic absorption bands at 14,400 cm^{-1} frequency in the solutions studied, indicate a two-photon mechanism of the spontaneously reversible coloration of these solutions.

Dunin, S. Z. Theory of spin waves in metals. FMiM, no. 1, 1972, 28-35.

In a contribution to the spin wave theory of a Fermi fluid with allowance for anisotropy of the Fermi surface, an electron fluid with a random Fermi surface was analyzed. It was assumed that the spin component of the interelectronic correlation function is expressed by

$$\Psi(p, p') = \Psi_0 + v_\mu(p)\alpha_{\mu\nu}v_\nu(p') \qquad (1)$$

where $\alpha_{\mu\nu} = \alpha_{\nu\mu}$ is a Landau correlation coefficient of conduction electrons. In approximation of (1), the dispersion equation

$$1 + \left[\frac{\beta_0}{1+\beta_0} + \frac{i}{\omega\tau}\right][X(\omega, k) + X_\nu(\omega, k)\alpha_{\nu\mu}L_\mu(\omega, k)] = 0 \qquad (2)$$

was derived for excitations of an electron fluid in a steady and uniform magnetic field. In (2), β_0 is another Landau correlation coefficient and τ is the pulse relaxation duration. The equation defines the spectrum of spin wave frequencies $\omega < ck$. An analysis of Eq. (2) showed that the ω spectrum of long waves including $\sim k^2$ terms depends significantly on the Landau anisotropic coefficients. A simple analysis of (2) revealed that ω of short waves propagating normally to the magnetic field is limited by $(n\Omega_{extr} \pm \Omega_0)$, where Ω_{extr} are the extremums of

$$\Omega = 2\pi\frac{eB_0}{c}\left(\frac{\partial S}{\partial \varepsilon}\right)^{-1} \qquad (3)$$

on the Fermi surface $\epsilon(p)$, and

$$\Omega_0 = 2\gamma B_0/h \qquad (4)$$

In (3) and (4), B_0 is the magnetic induction, $S(\epsilon, p_z)$ is the area of intersection of the $\epsilon(p) = \epsilon_F$ surface with the $pB_0 = \text{const}$ plane, γ is the effective momentum of a conduction electron and h is the Planck constant divided by 2π. At $n = 0$, the frequency spectrum of spin waves monotonically approaches $k \pm \Omega_0$ value. At $n \neq 0$, $\omega(\theta, k)$, where θ is the angle of the magnetic field vector with Z' crystallographic axis, oscillates around its mean $(n\Omega_{extr}(\theta) \pm \Omega_0)$ which can be determined experimentally. In principle, the Landau coefficients of the Fermi liquid can be determined from the dependence of the spectra obtained in the short wavelength range on the reciprocal orientation of magnetic field and crystallographic axes.

Kiryushchenko, A. I. and M. A. Lebedev. Development of a low-voltage arc discharge in cesium vapors. I. Development of a discharge with formation of a spherical plasma bunch. ZhTF, no. 6, 1971, 1170-1173.

In connection with the problem of direct conversion of thermal into electrical energy, electrical discharges in cesium vapors were investigated. The conditions were examined of luminous spherical plasma bunch formation in an inter-electrode gap. Discharge volt-ampere characteristics were simultaneously measured by an electrically-heated movable tungsten wire, and emission was photographed. The volt-ampere characteristic and photographs of a discharge in a 11.2 mm gap between the 18 mm diameter electrodes at 1.4×10^{-2} torr cesium vapor pressure and cathode temperature $T_c = 790^{\circ}K$ are shown (Fig. 1). Spherical plasma bunch formation and spread over the discharge gap coincide with a 1-1.5 v jump in voltage and point 6 of the v-a characteristic, respectively. Spherical bunch duration is limited by the cesium

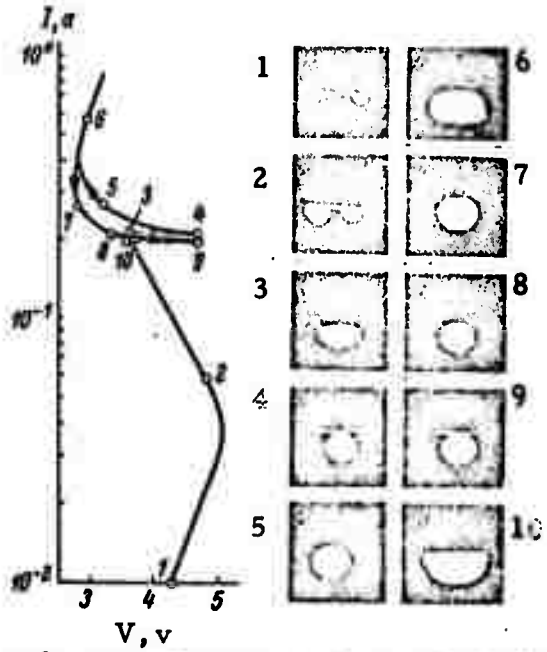

Fig. 1. Current-voltage characteristic and emission picture of a low-voltage discharge in different development phases.

vapor pressure (5×10^{-3} to 5×10^{-2} torr), the gap length ($8 \leq d \leq 18$ mm), and the electrode diameter ($8 \leq D \leq 20$ mm). The position of the bunch within the gap depends on T_c and the external magnetic field. The v-a characteristic

of a Langmuir probe shows that electron energy distribution within the spherical bunch does not obey Maxwell's law. A sharp emission boundary is observed at 4.5×10^{-2} torr cesium vapor pressure coincidentally with a change in electron concentration and potential along the spherical plasma bunch radius.

Shul'gin, B. V., A. L. Shalyapin, V. V. Ilyukhin, V. I. Rogovich, N. A. Nosyrev, F. F. Gavrilov, and N. V. Belov. Na-Oxyzirconosilicate (Na_2ZrSiO_5). Crystalline structure and optical spectra. DAN SSSR, v. 202, no. 5, 1972, 1068-1070.

A spectrographic study of Na-oxyzirconosilicate is reported, indicating its potential as a laser material. A complete analysis of spectroscopic characteristics of the Na_2ZrSiO_5-Eu^{3+} matrix, dependable characterization of the luminescence spectrum of Eu^{3+}, calculation of intensity of spectral lines and the magnitude of Stark splitting of energy levels of Eu^{3+} ion, are accordingly given. The authors discuss the crystalline structure of the matrix and possible isomorphic replacement of Zr by Eu^{3+} ions which point to the existence of two types of Eu centers; this was experimentally confirmed by observing lines in Na_2ZrSiO_5-Eu^{3+} luminescence spectrum characteristic of the two types (Eu_I and Eu_{II}) of centers. The method for identifying spectral lines corresponding to Eu_I and Eu_{II} is discussed. Inasmuch as the intensities of spectral lines and the magnitudes of Stark splitting are approximately the same for both centers, experimental and theoretical results are given only for one of these. Figure 1 shows the luminescence spectrum of Eu^{3+} in Na_2ZrSiO_5. Excitation spectra for 80°K and

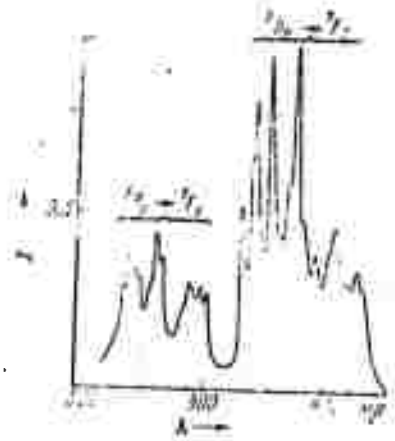

Fig. 1.

295°K were also studied. Results are presented in Figure 2, where the excitation maxima for T = 80°K are marked by the heavy black lines.

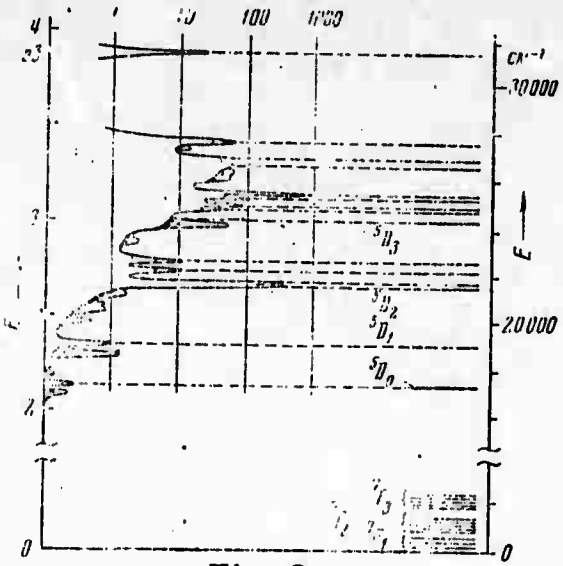

Fig. 2.

Energy levels for Eu^{3+} ion in Na_2ZrSiO_5 were computed on the basis of luminescence and excitation spectra and are shown in the right hand side of Figure 2.

Experimental and calculated magnitudes of Stark splitting of $^7F_1$ and $^7F_2$ energy levels of Eu^{3+} ion in Na_2ZrSiO_5 are given, as well as the relative intensities of emission transitions of Eu^{3+} in Na_2ZrSiO_5 crystal from the $^5D_0$ energy level. Authors also point out that the population of $^7F_2$ energy level by Eu^{3+} ion in Na_2ZrSiO_5 at room temperature is considerably smaller than in $ZrSiO_4$ or $YNbO_4$ matrices which is an important factor in considering Na_2ZrSiO_5 for a basic laser material. Judd's (B. B. Judd, Phys. Rev., 127, 750 (1962)) and Ofelt's (G. S. Ofelt, J. Chem. Phys., 37, 511 (1962)) techniques were used to calculate the crystalline field parameters in Na_2ZrSiO_5 and the relative intensity of lines in the emission spectrum of Eu^{3+}.

B. Recent Selections

Baybakov, V. I. Electromagnetic wave generation in an n-InSb Corbino disk. FTP, no. 4, 1972, 735-737.

Bazhanova, A. Ye., and V. I. Kogan. Effect of "trimmed tail" Maxwellian distribution of ion velocities on output of thermonuclear reactions in plasma. Atomnaya energiya, v. 32, no. 5, 1972, 440-441.

Belyanin, V. B. Seventeenth All-union conference on spectroscopy. Minsk, 5-9 July, 1971. OiS, v. 32, no. 4, 1972, 845-847.

Borisov, Yu. Ya., E. I. Rozenfel'd, and V. G. Smolenskiy. Effect of acoustic oscillations on a gas flare in a confined space. FGiV, no. 3, 1971, 404-411.

Bortnikov, Yu. S., V. A. Nesterov, and I. B. Rubashov. Study of characteristics of an electric gas dynamic engine. ZhPMTF, no. 6, 1971, 167-170.

Brovman, Ye. G., Yu. Kagan, and A. Kholas. Properties of metallic hydrogen under pressure. ZhETF, v. 62, no. 4, 1972, 1492-1501.

Bulyga, A. V. Evaluation of relaxation time of monatomic gases. IAN B, no. 5, 1971, 107-112. (RZhF, 3/72, #3Ye48)

Bystritskiy, V. M., V. P. Dzhelepov, N. I. Doronicheva, P. F. Yermolov, K. O. Oganesyan, M. N. Omel'yanenko, S. Yu. Porokhovoy, A. A. Rodina, V. Ye. Teplov, and V. V. Fil'chenkov. Apparatus for obtaining ultrapure gaseous hydrogen at pressures to 50 atm. PTE, no. 2, 1972, 226-227.

Fialkov, B. S., V. T. Plitsyn, Ya. I. Magun, and G. P. Senkevich. Nature of "electric noise" during combustion. FGiV, no. 3, 1971, 383-392.

Gestrina, G. N. Increasing diffraction radiation by means of plasma flow. IN: Sbornik. Radiotekhnika, no. 17, 1971, 97-98. (RZhF, 3/72, #3Zh223)

Grechikhin, L. I., and R. G. Grechikhina. Measurement of plasma parameters based on spectral brightness of transitions. IT, no. 4, 1972, 27-28.

Grishayeva, G. A., I. G. Gurevich, and V. S. Bagotskiy. Effectiveness of an electrodialysis technique for regeneration of an electrolyte as applied to fuel cells. I-FZh, v. 22, no. 5, 1972, 818-824.

Grodko, V. A., and B. N. Markar'yan. Thermodynamics of a direct chemical to electric energy conversion system. IAN Energetika i transport, no. 2, 1972, 150-159.

Gushchin, V. M. Visualization of shf radiation intensity distribution using a liquid crystal thermographic screen. Uchenyye zapiski Vladimirovskogo GPI, no. 32, 1971, 84-90. (RZhF, 3/72, #3Zh343)

Hampel, B. Liquid crystals. Laser, v. 3, no. 3, 1971, 53-56. (RZhF, 3/72, #3Ye99)

Inovenkov, I. N., D. P. Kostomarov, and O. I. Fedyanin. Diffusion decay of plasma with a density-dependent diffusion coefficient. KSpF, no. 9, 1971, 40-46. (LZhSt, 17/72, #53447)

Khokhlov, R. V. Feasibility of constructing a gamma laser using radioactive crystals. ZhETF P, v. 15, no. 9, 1972, 580-583.

Klyukin, L. M., V. I. Maksimov, B. M. Stepanov, V. A. Fabrikov, and E. N. Shevchuk. Magnetic tape recording of shf radiation structure. RiE, no. 5, 1972, 1114-1116.

Kompanets, O. N., and V. S. Letokhov. Investigation of narrow resonance during absorption saturation of SF_6 molecules by CO_2 laser radiation. ZhETF, v. 62, no. 4, 1972, 1303-1311.

Koshmarov, Yu. A., and S. B. Svirshevskiy. Heat transfer from a sphere in the transition dynamic region of a rarefied gas. MZhiG, no. 2, 1972, 170-172.

Lebedeva, N. I., and N. S. Nesmelov. Formation of luminescence centers in non-activated alkali halide crystals in very intense electric fields. FTT, no. 4, 1972, 1282-1283.

Mayorov, V. K. Measurement of excited vibrational state duration of gas molecules using a relaxation opto-acoustic sensor. IN: Sbornik. Radioelektronika opticheskogo diapazona. Moskva, 1970(1971), 67-69. (RZhF, 3/72, #3Ye47)

Petukhov, B. S., V. S. Protopopov, and V. A. Silin. Experimental investigation of deterioration of heat exchange regimes under carbon dioxide turbulent flow at ultracritical pressure. TVT, no. 2, 1972, 347-354.

Savitskaya, V. B. Nonstationary radiation from a current filament in free space. IN: Sbornik. Materialy Nauchno--tekhnicheskoy konferentsii Leningradskogo elektrotekhnicheskogo instituta svyazi. Leningrad, no. 3, 1971, 247-251. (RZhF, 3/72, #3Zh267)

Selivanov, A. S., V. M. Govorov, V. P. Chemodanov, and S. G. Ovodkova. Panoramic scan television systems for second generation lunar automatic stations. TKiT, no. 5, 1972, 43-46.

Trubnikov, B. A. Nature of ball lightning. DAN, v. 203, no. 6, 1972, 1296-1298.

Vikhrev, Yu. I., G. V. L'vov, V. P. Savchenko, and F. A. Fekhretdinov. Investigation of composite lanthanum hexaboride thermal emitters. ILEI, no. 104, 1971, 132-136. (RZhF, 4/72, #4G297)

Voloshko, A. Yu., S. I. Solodovchenko, and V. V. Chechkin. Heating a moving plasma with fast, high-amplitude whistlers. UFZh, no. 11, 1971, 1822-1828.

Zhabotinskiy, M. Ye., A. A. Izyneyev, S. L. Krayevskiy, Yu. S. Milyavskiy, and Yu. P. Rudnitskiy. Exchange interactions in energy transfer between Eu^{3+}, Sm^{3+}, Dy^{3+} and UO_2^{2+}. OiS, v. 32, no. 4, 1972, 758-763.

12 April 1972

SUBJECT: RECENT SOVIET ACTIVITIES IN UNDERSEA RESEARCH VEHICLE DEVELOPMENT

SOURCES: (1) Bezdomnyy, N. The "Odissey" puts to sea. Vokrug sveta, no. 3, 1972, 50-53.

(2) Kovadlo, M. Afalina studies the sea bottom. Bakinskiy rabochiy, 22 March 1972, p. 4, col. 1.

(3) New equipment for science and technology. Sovetskaya Moldaviya, 13 August 1971, p. 4, cols. 7-8.

One of the first concrete articles (1) on the full-configuration use of the most sophisticated Soviet undersea research vehicle (URV), the Sever-2, appeared recently and is accompanied by several photographs. The article gives a popularized account of the Sever-2's acceptance test (July 1971, in the Black Sea) with almost half its emphasis on a general description of the R/V "Odissey", the mother ship and vessel used to transport the Sever-2. The Odissey is a converted BMRT (large freezer/trawler) which has been fitted with a large "hangar" on the port side near the stern. This hangar houses the Sever-2 in a controlled environment, and large doors give access to the port side. In launching the Sever-2, the travelling crane operator, sitting in a glass enclosure over the hangar, controls the entire launch procedure, including control of ballast tanks selectively flooded to provide list to port during launching. Photographs in the article show a top view and bow view of Sever-2 being launched (or recovered), with two extendable booms. The photographs indicate that freeboard to the hangar deck is quite small (perhaps 8--10 ft.). This would indicate that the doors are watertight to protect the controlled-environment hangar against sea water entry. Sever-2's actual design is quite faithful to previously published photos of a model, with the exception of four housings on the deck. Judging from the photographs, these comprise the port and starboard

vertical-propulsion systems. The after housing consists of what appears to be either a watertight electric motor or gear box, a four-blade propeller, and a Kort nozzle mounted on a shaft. This shaft is connected to the forward housing and allows the vertical propulsion systems (port and starboard) to be swung outward 90° into their operating positions or "tucked in" over the hull during launch or recovery. It is not yet known whether this motion can be controlled from within Sever-2 or whether it is performed manually on deck by the launch/recovery team.

As Sever-2 submerged, it was tracked by the Odissey's echo sounder and graphic recorder. Aboard Sever-2, an open-mike tape system was used to record all commands and other sounds throughout the vehicle and hydroacoustic communication was used between Odissey and Sever-2.

The acceptance program was kept simple and amounted to submerging vertically to a specific depth (probably 2000 m - Sever-2's rated operating depth), measuring water parameters from the surface to the above depth, and checking the operation of the instruments and the integrity of the hull penetrations. It is interesting to note that at a depth of somewhere below 1000 m, when Sever-2 reached equilibrium in the denser water, it was decided not to risk additional ballast-tank flooding by pump. At this point, the vertical propulsion system was used to drive Sever-2 downward to the final test depth (it is mentioned that the last 50m took a half an hour). Recorders plotted current speed, water temperature, salinity, density, transparency, and other parameters. After reaching the desired depth, the Odissey was informed that Sever-2 showed no leaks or damage and was ready to ascend. During ascent, the vertical-propulsion motors were used again. At 1000m, ballast-discharge pumping began and continued to about 300m at which point Sever-2 began horizontal movement. After a brief excursion, the vertical-propulsion motors were used to bring Sever-2 to the surface.

Two principal figures associated over the years with the development and designing of the Sever-2 and other Soviet URV's were involved in the acceptance tests. The first, A. N. Dmitriyev, served as the Chairman of the State Commission for the Sever-2 tests, while the second, M. N. Diomidov, was the vehicle pilot.

Although earlier indications were that Sever-2 was to carry a crew of three, the vehicle now reportedly accomodates four crewmen.

A very brief news item (2) appearing in a March newspaper indicates that a small, relatively unknown, two-man URV, the Afalina, is presently being used for bottom mapping ("topographic surveying" in the original article) and for studying bottom flora and fauna. The Afalina was designed and built by students at the Leningrad Shipbuilding Institute and was awarded a prize at the permanently operating Exhibition of the Achievements of the National Economy in Moscow. The only previous information on Afalina appeared in an August 1971 newspaper item (3), in which it was implied that the vehicle had only been designed and produced in a small-scale model (shown in a photo) which was on show at the above exhibit. The information available on Afalina is too scant to determine when construction actually began, but if it is indeed operational, this should constitute some sort of a record for the Soviets in getting a vehicle off the drawing board and into the water. The fact that it was a "student" project, possibly not subject to conventional government red tape, may have contributed to the apparently short development time. In this regard, it is interesting to note that Sever-2, discussed above, was through its design phase (first model) in 1963 and had a projected delivery date of 1965.

6. SOURCE ABBREVIATIONS

DAN AzSSR	-	Akademiya nauk Azerbadzhanskoy SSR. Doklady
DAN BSSR	-	Akademiya nauk Belorusskoy SSR. Doklady
DAN SSSR	-	Akademiya nauk SSSR. Doklady
DAN TadzhSSR	-	Akademiya nauk Tadzhikskoy SSR. Doklady
EOM	-	Elektronnaya obrabotka materialov
FAiO	-	Akademiya nauk SSSR. Izvestiya. Fizika atmosfery i okeana
FGiV	-	Fizika goreniya i vzryva
FiKhOM	-	Fizika i khimiya obrabotka materialov
F-KhMM	-	Fiziko-khimicheskaya mekhanika materialov
FMiM	-	Fizika metallov i metallovedeniye
FTP	-	Fizika i tekhnika poluprovodnikov
FTT	-	Fizika tverdogo tela
IAN Arm	-	Akademiya nauk Armyanskoy SSR. Izvestiya
IAN Az	-	Akademiya nauk Azerbadzhanskoy SSR. Izvestiya
IAN B	-	Akademiya nauk Belorusskoy SSR. Izvestiya. Seriya fiziko-matematicheskikh nauk
IAN Energ	-	Akademiya nauk SSSR. Izvestiya. Energetika i transport
IAN Fiz	-	Akademiya nauk SSSR. Izvestiya. Seriya fizicheskaya
IAN Fizika zemli	-	Akademiya nauk SSSR. Izvestiya. Fizika zemli
IAN Metally	-	Akademiya nauk SSSR. Izvestiya. Metally
IAN UzbSSR	-	Akademiya nauk Uzbekskoy SSR. Seriya fiziko-matematicheskikh nauk

I-FZh	-	Inzhenerno-fizicheskiy zhurnal
ILEI	-	Leningradskiy elektrotekhnicheskiy institut. Izvestiya
IT	-	Izmeritel'naya tekhnika
IVUZ Fizika	-	Izvestiya vysshikh uchebnykh zavedeniy. Fizika
IVUZ Radioelektr	-	Izvestiya vysshikh uchebnykh zavedeniy. Radioelektronika
IVUZ Radiofiz	-	Izvestiya vysshikh uchebnykh zavedeniy. Radiofizika
Kristall	-	Kristallografiya
KSpF	-	Kratkiye soobshcheniya po fizike
LZhSt	-	Letopis' zhurnal'nykh statey
MP	-	Mekhanika polimerov
MTT	-	Akademiya nauk SSSR. Izvestiya. Mekhanika tverdogo tela
MZhiG	-	Akademiya nauk SSSR. Izvestiya. Mekhanika zhidkosti i gaza
NM	-	Akademiya nauk SSSR. Izvestiya. Neorganicheskiye materialy
OiS	-	Optika i spektroskopiya
Otkr izobr	-	Otkrytiya, izobreteniya, promyshlennyye obraztsy, tovarnyye znaki
Phys abs	-	Physics abstracts
PM	-	Prikladnaya mekhanika
PMM	-	Prikladnaya matematika i mekhanika
PTE	-	Pribory i tekhnika eksperimenta
RiE	-	Radiotekhnika i elektronika
RZhElektr	-	Referativnyy zhurnal. Elektronika i yeye primeneniye
RZhF	-	Referativnyy zhurnal. Fizika
RZhMekh	-	Referativnyy zhurnal. Mekhanika

RZhMetrolog	-	Referativnyy zhurnal. Metrologiya i izmeritel'naya tekhnika
RZhRadiot	-	Referativnyy zhurnal. Radiotekhnika
TKiT	-	Tekhnika kina i televideniya
TMF	-	Teoreticheskaya i matematicheskaya fizika
TVT	-	Teplofizika vysokikh temperatur
UFN	-	Uspekhi fizicheskikh nauk
UFZh	-	Ukrainskiy fizicheskiy zhurnal
VAN	-	Akademiya nauk SSSR. Vestnik
VLU	-	Leningradskiy universitet. Vestnik. Fizika, khimiya
VMU	-	Moskovskiy universitet. Vestnik. Seriya fizika, astronomiya
ZhETF	-	Zhurnal eksperimental'noy i teoreticheskoy fiziki
ZhETF P	-	Pis'ma v Zhurnal eksperimental'noy i teoreticheskoy fiziki
ZhFKh	-	Zhurnal fizicheskoy khimii
ZhPMTF	-	Zhurnal prikladnoy mekhaniki i teoreticheskoy fiziki
ZhPS	-	Zhurnal prikladnoy spektroskopii
ZhTF	-	Zhurnal tekhnicheskoy fiziki
ZhVMMF	-	Zhurnal vychislitel'noy matematiki i matematicheskoy fiziki

7. AUTHOR INDEX